ECMWF Newsletter

Number 156 – Summer 2018

European Centre for Medium-Range Weather Forecasts
Europäisches Zentrum für mittelfristige Wettervorhersage
Centre européen pour les prévisions météorologiques à moyen terme

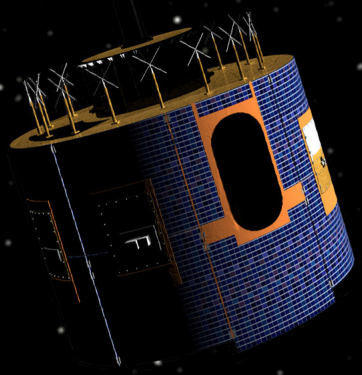

www.ecmwf.int/en/about/news-centre/media-resources

CONTENTS

PUBLICATION POLICY

The *ECMWF Newsletter* is published quarterly. Its purpose is to make users of ECMWF products, collaborators with ECMWF and the wider meteorological community aware of new developments at ECMWF and the use that can be made of ECMWF products. Most articles are prepared by staff at ECMWF, but articles are also welcome from people working elsewhere, especially those from Member States and Co-operating States. The *ECMWF Newsletter* is not peer-reviewed.

Editor: Georg Lentze

Typesetting and Graphics: Anabel Bowen with the assistance of Simon Witter

Cover image: Montage based on a Meteosat-8 satellite image 1 February 2017 (*copyright: EUMETSAT*) and an image showing a Meteosat Second Generation satellite (*copyright: EUMETSAT*)

Any queries about the content or distribution of the *ECMWF Newsletter* should be sent to Georg.Lentze@ecmwf.int.

Guidance about submitting an article is available at www.ecmwf.int/en/about/news-centre/media-resources.

CONTACTING ECMWF

Shinfield Park, Reading, Berkshire RG2 9AX, UK

Telephone:	National	0118 949 9000
	International	+44 118 949 9000
ECMWF website:		www.ecmwf.int

In the cloud

The past quarter has been rich in important developments at ECMWF, first among them the successful implementation of the latest upgrade of the Integrated Forecasting System (IFS). IFS Cycle 45r1 improves analyses, notably through a better use of radiosondes, and forecasts, for example by addressing systematic short-wave radiation biases in the storm tracks and over the southern oceans as well as longstanding precipitation issues along coastlines. Users have also welcomed the introduction of lightning flash density predictions.

In research, work is under way to develop 'continuous data assimilation'. Experimental results show consistent improvements translating into a 2- to 3-hour gain in forecast skill. We are expecting to be able to make this new process operational in the near future.

With new products constantly being developed or improved, it was important to ensure that our Forecast User Guide is up to date. This is now the case, with a revised version of the guide published online on 14 May. The guide provides all the tools needed for the correct interpretation and use of ECMWF's products.

On the Copernicus front, our Atmosphere Monitoring Service will be releasing a new massive open online course (MOOC), developed jointly with our sister organisation EUMETSAT. This will offer a great opportunity to learn how atmospheric composition can be monitored from space and how this can be combined with in situ data and numerical models to provide information and forecasts. Still on Copernicus, in June our Climate Change Service launched the long-awaited Climate Data Store, and two months earlier it published its first European State of the Climate report.

The extensive work between ECMWF and Emilia-Romagna teams enabled the building tender for ECMWF's new data centre in Bologna to be released in mid-May, with a prospective start of building work around mid-November.

Whilst the supercomputers to be hosted in our new data centre in Italy will enable more scientific developments, the challenges created by the dissemination of all this data are likely to be addressed by cloud options. In June, an event organised by the European Commission in Baveno commemorated the 20th anniversary of the Baveno Manifesto, the document which gave birth to the Copernicus programme (known as GMES at the time). This was a great opportunity to showcase the WEkEO service we are jointly developing with our colleagues from EUMETSAT and Mercator. WEkEO is a reference portal for environmental data, virtual environments for data processing and skilled user support. At the same time, we are working with our key partners to develop a European Weather Cloud. Watch this space.

Florence Rabier
Director-General

Forecasting convective rain events in late May

LINUS MAGNUSSON, IVAN TSONEVSKY, TIM HEWSON

During most of May 2018, northern Europe experienced a heat wave. The intensity and spatial extent of the event are evident in the monthly mean air temperature summary maps provided by the Copernius Climate Change Service implemeted by ECMWF (https://climate.copernicus.eu/). Many records for May average temperature were broken. For Stockholm, where temperature records go back to 1759, the monthly average temperature reached 16.1°C, which is 2.2°C higher than the previous record of 13.9°C, the Swedish national meteorological service reported. The hottest days were at the end of May and continued into the first days of June. In the warm and humid air and with generally weak synoptic-scale forcing over north-western Europe, severe convective systems developed during these days. Global forecasting systems can struggle to capture such relatively small-scale systems. Here we look at the usefulness of different ECMWF products for this type of event. We will focus on 29 May, when extreme rain and flash floods affected parts of Germany, the Netherlands, Belgium and France, where Paris was hit by intense rainfall. Severe thunderstorms were accompanied by other convective hazards, including large hail, strong winds and lightning.

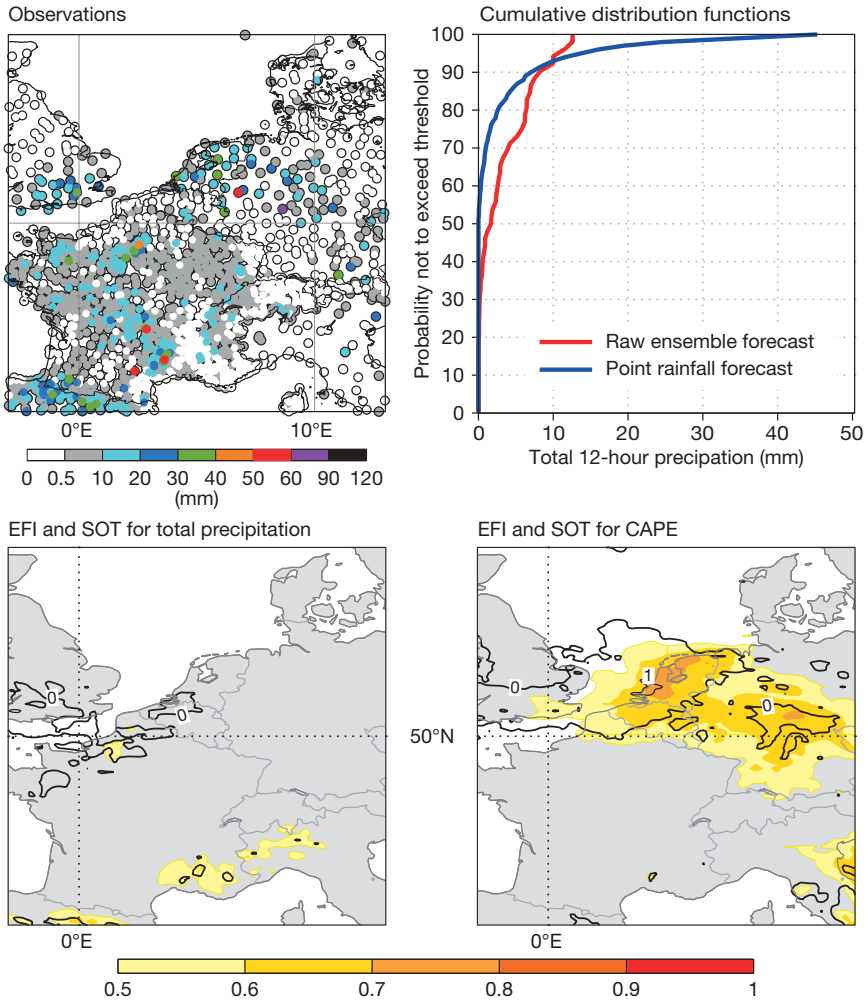

Rainfall and CAPE predictions. The plots show 24-hour observed precipitation between 29 May 06 UTC and 30 May 06 UTC (top left); cumulative distribution functions for raw ensemble and ecPoint-Rainfall forecasts over Paris starting at 00 UTC on 25 May for 12 UTC on 29 May to 00 UTC on 30 May (top right); EFI and SOT of total precipitation for 29 May in the forecast from 25 May 00 UTC (bottom left); and EFI and SOT for CAPE for 29 May in the forecast from 25 May 00 UTC (bottom right).

In global forecasting systems, heavy convective rain events are usually associated with low forecast probabilities due to the high spatial variability of precipitation and uncertainties in convective initiation. As a result, the total precipitation Extreme Forecast Index (EFI) generally provides weak signals of extreme rain even in short-range forecasts in such situations. This was the case with the forecasts for 29 May over Germany. The predictability of heavy rain events in Belgium and the Netherlands was higher, with positive Shift of Tails (SOT) in the medium range, indicating that at least 10% of ensemble members were predicting extreme rainfall. On the other hand, the model is usually quite good at predicting the favourable environment for deep moist convection well in advance. In the case presented here, the CAPE EFI, for example, gave a much stronger signal for convective hazards throughout the short and medium range than the EFI for total precipitation.

ECMWF's recently developed ecPoint-Rainfall product uses an innovative post-processing method to account for sub-grid variability and weather-dependent biases in rainfall totals (Newsletter No. 153, autumn 2017). For cases of severe convection, this product should increase probabilities for extreme rainfall and also for no rainfall, compared to the grid-box average probabilities provided by raw model output. In the case of Paris on 29 May, observations of 24-hour rainfall ranged from less than 5 mm to more than 30 mm within the metropolitan area, most of which fell during the afternoon. The raw ensemble from 5 days before (25 May) indicated a maximum possible value of 13 mm/12 hours (as a grid-box average), while the post-processed ecPoint product indicated that point

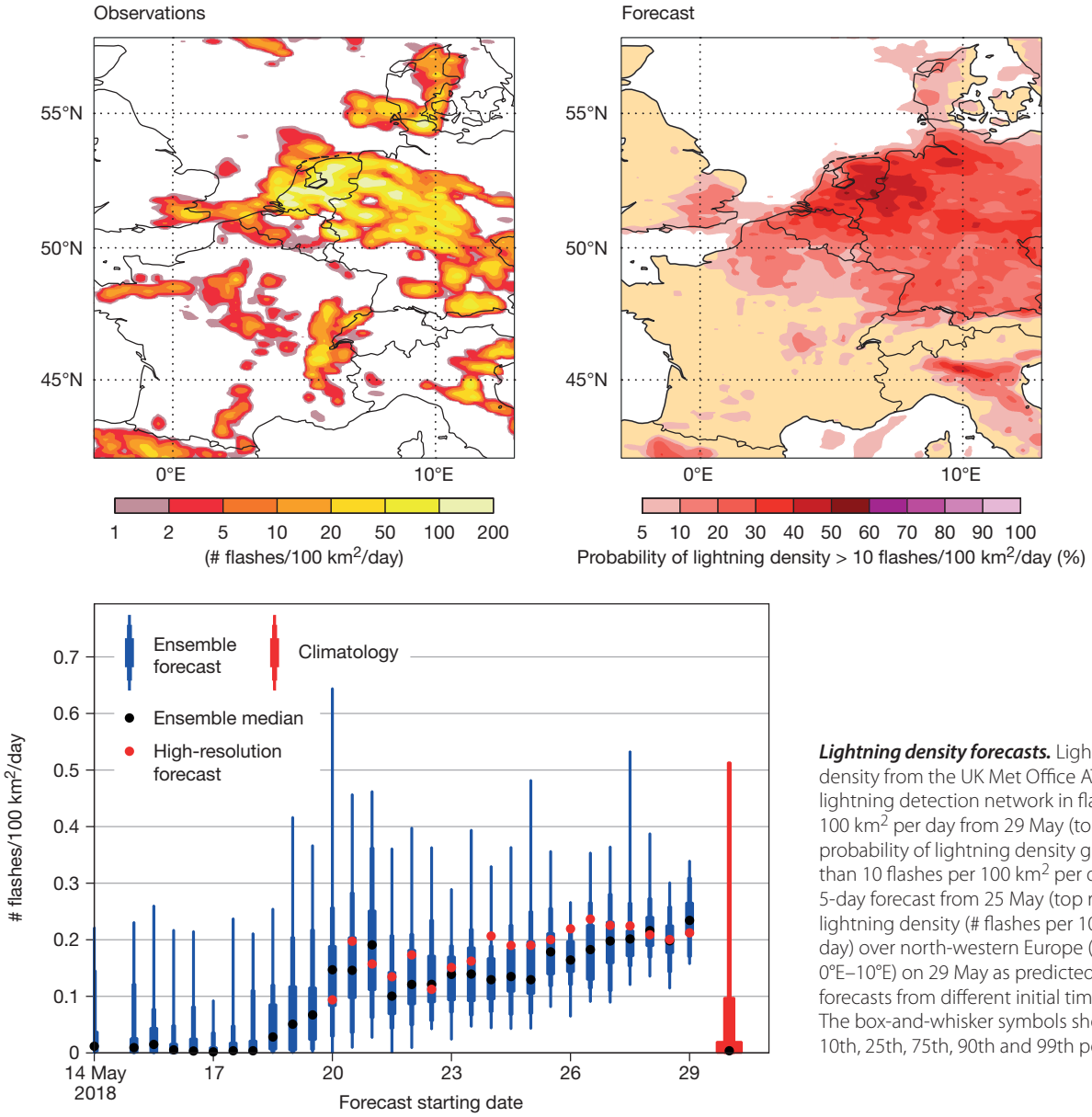

Lightning density forecasts. Lightning density from the UK Met Office ATDnet lightning detection network in flashes per 100 km^2 per day from 29 May (top left); probability of lightning density greater than 10 flashes per 100 km^2 per day in the 5-day forecast from 25 May (top right); and lightning density (# flashes per 100 km^2 per day) over north-western Europe (45°N–55°N, 0°E–10°E) on 29 May as predicted by forecasts from different initial times (bottom). The box-and-whisker symbols show the 1st, 10th, 25th, 75th, 90th and 99th percentiles.

rainfall above 30 mm/12 hours was possible (forecasts valid for 12 UTC on 29 May to 00 UTC on 30 May).

The convection over north-western Europe on 29 May was also associated with intense lightning activity. ECMWF has recently implemented a new parametrization of lightning density (Newsletter No. 155, spring 2018). For the case of 29 May, probabilities of intense lightning in the 5-day forecast from 25 May highlighted the risk over Belgium, Germany and the Netherlands. Note that ATDnet (used here for verification) detection efficiency is much higher for cloud-to-ground (CG) flashes than for intracloud (IC) flashes, whilst the forecast lightning density accounts for both CG and IC discharges, hence we do not expect a perfect match between predicted and observed quantities. Summarising all lightning forecasts valid for 29 May over western Europe (45°N–55°N, 0°E–10°E) in one plot, we find that as early as 10 days before the event the ensemble had a clear signal, with the ensemble median above the 90th percentile of the model climate, and the signal was consistent in all subsequent ensembles.

In summary, ECMWF forecasts captured the risk of thunderstorms in western Europe more than a week in advance. The high predictability was linked to the ability to predict the large-scale environment in which the convective storms developed. Indices such as CAPE and lightning density forecasts are expected to give good guidance on regions likely to be affected by convective hazards. By contrast, there is low predictability for the location and timing of individual convective cells and associated precipitation, although the point rainfall product can better reflect the range of probabilities at particular points than the raw ensemble.

Improved precipitation forecasts in IFS Cycle 45r1

RICHARD FORBES

Cloud and precipitation processes are represented in the Integrated Forecasting System (IFS) with parametrizations that capture the gridscale effects of water and ice particle microphysics in the atmosphere. This includes the formation of particles, phase changes and collisions between particles as they fall. The representation of these processes in the IFS has improved significantly in recent years. In the latest upgrade, implemented in IFS Cycle 45r1 operational from 5 June 2018, changes to the parametrized processes for liquid-phase microphysics were made to address a long-standing problem of precipitation maxima just off the coastline and over lakes. This occurred in situations where the warm-rain generation process was active over a prolonged period. The results show significant improvements to the spatial pattern of rainfall and quantitative precipitation forecasts near coastlines and over lakes in these specific situations.

Warm-rain cloud and precipitation processes

Warm rain refers to the process of precipitation production through the collision and coalescence of liquid particles (cloud droplets, drizzle drops and raindrops). In the model, just less than half of the global stratiform rainfall is produced via the warm-rain process, with the rest produced via melting snow particles as they fall through the 0°C level in deeper cloud systems. The warm-rain process dominates in clouds with shallow to mid-level tops, particularly in the warmer seasons when the melting level is high.

Whether a cloud generates rain and the intensity of generated rainfall depends on many factors, including the strength of updraughts in the cloud, the size of the cloud particles, and the lifetime and depth of the cloud. To capture the wide range of observed conditions (from cloud with no rain at the surface, to drizzling stratocumulus, to widespread moderate rain, to heavily precipitating events), the model must capture the appropriate non-linearity of the warm-rain process and all factors that affect the rain generation, particle size distribution, fall of raindrops and evaporation in the sub-cloud layer.

Microphysics upgrade

The focus of the warm-rain microphysics upgrade in IFS Cycle 45r1 is on improved numerics of autoconversion (cloud droplets coalescing to form larger raindrops), accretion (raindrops colliding and coalescing with cloud droplets to form larger raindrops), fall speed and rain evaporation processes to reduce the dependence on threshold values and to make the microphysics parametrization more robust to timestep. Specific changes in 45r1 include:

- The critical threshold for activation of the warm-rain process is removed. As the threshold was previously different over land points and open water points (sea and gridscale lakes), this change removes the discontinuity in the warm-rain process at the land/water boundary.
- The numerical formulation of the sedimentation process (fall due to gravity) is modified to allow a change of the terminal fall speed for raindrops from a fixed 4 m/s to a realistic drop size dependence. As observed, larger drops can fall faster than smaller drops, leading to an improved representation of the rain accretion and sub-cloud evaporation processes.
- The formulation of the warm-rain processes was made more robust to timestep, which allows the model to give similar results across the full range of timesteps used in different IFS configurations without changes in computational cost.

Impact on forecasts

The impacts of the changes in Cycle 45r1 are evident in the frequency distribution of rainfall rates and accumulations, with fewer occurrences of light rain and increased occurrence of heavier rain, generally closer to the observed distribution. However, the most noticeable change for users is in the spatial distribution of rainfall near coastlines and over lakes (resolved by the model grid) in meteorological situations dominated by the warm-rain process and persistent for several hours. The unrealistic rainfall over the water is removed or moves downwind over the land in closer agreement with observed rainfall patterns throughout the forecast range.

Ongoing research is looking at further developments to the representation of both stratiform and convective cloud and precipitation processes in the IFS for further improvements to quantitative precipitation forecasting in the future.

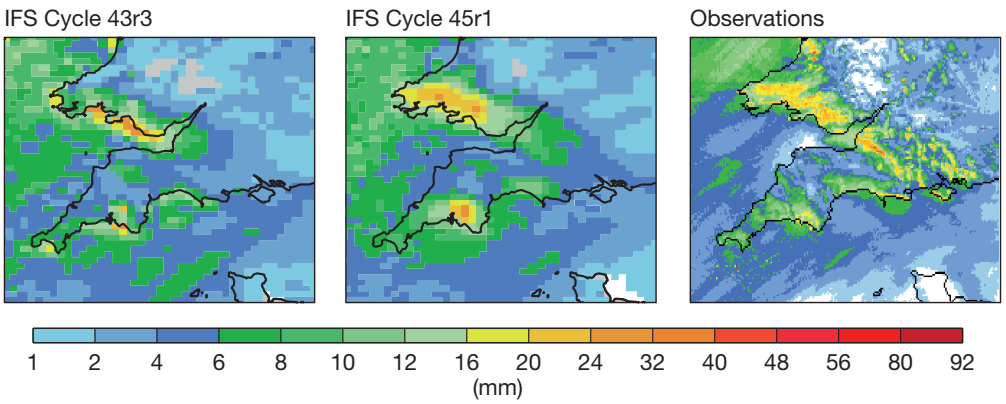

Example of changes to near-coastline precipitation. 24-hour accumulated precipitation (mm) on 15 May 2017 from a 00 UTC 14 May 2017 forecast in a warm-rain dominated south-westerly flow over the UK for IFS Cycle 43r3 (left), IFS Cycle 45r1 (middle) and the radar observations (right).

European State of the Climate 2017

FREJA VAMBORG

The Copernicus Climate Change Service (C3S) and Copernicus Atmosphere Monitoring Service (CAMS), both implemented by ECMWF, presented their first European State of the Climate report at the European Parliament in Brussels on 10 April. The event was co-hosted by Members of the EU Parliament Flavio Zanonato and Klaus Buchner.

The presentation showcased the benefits of freely accessible environmental data and information for a better understanding of our planet and informed decision-making. It also showed how Copernicus, the European Union's flagship programme to monitor the Earth's environment, helps European businesses to adapt to an evolving environment.

To address the challenges of climate change, the Copernicus services monitor data on a global scale, including surface air temperature, precipitation, sea ice area and atmospheric greenhouse gases. The report's findings are based on measurements from satellites and ground stations, and on data from global reanalysis – a consistent combination of computer modelling and multiple data sources.

The European State of the Climate 2017 covers two main themes: the climate in 2017 and headline climate indicators. The former compares the annual and seasonal climate from 2017 with the reference period 1981–2010, focusing mostly on Europe. The section on headline climate indicators deals with long-term key indicators for global and regional climate change.

The climate in 2017 findings highlight two regions: the European sector of the Arctic and the southwest of Europe, focusing on the 'Lucifer' heat wave. The report found that:

- the European average temperature in 2017 overall was 0.8°C higher than the 1981–2010 average, making the year the fifth or sixth warmest on record, depending on the dataset considered;
- during the final months of 2017, some land areas of the north Atlantic Arctic experienced monthly temperatures more than 6°C above the 1981–2010 average;
- in the European sector of the Arctic, sea ice cover was much lower than average during the first three months of the year, and January showed the largest negative anomaly on record;
- in southwestern Europe, spring was one of the warmest on record at close to 1.7°C above the 1981–2010 average;
- annual temperatures in the region were the highest on record and soil moisture was the lowest, with heat waves gripping Portugal and Spain during the summer and drought persisting in southern and central Italy throughout the year.

The headline climate indicators show the long-term evolution of several key climate variables. These can be summarised as follows:

- Global temperatures have risen by about 1.1°C since the start of the industrial era and by about 1.8°C in Europe since the latter half of the 19th century;
- The net surface fluxes into the atmosphere of the greenhouse gases carbon dioxide, methane and nitrous oxide have been increasing in recent decades;
- Arctic sea ice area is in a downward trend, especially since the year 2000, while glaciers both globally and in Europe have seen a strong and continued ice mass loss since about 2000;
- The global mean sea level has risen by about 8 centimetres in the past 25 years and the mean sea level has increased by 1 to 2 mm per year in most European coastal areas.

The 2015 Paris Agreement aims to limit global temperature rises to well below 2°C compared with the pre-industrial era, and to pursue efforts to restrict it to 1.5°C. The latest five-year average global temperature is the highest on record. Copernicus is the world's third-largest data provider, and its services are part of a broader effort to support the Paris Agreement.

The European State of the Climate 2017 report is available online at:

climate.copernicus.eu/CopernicusESC

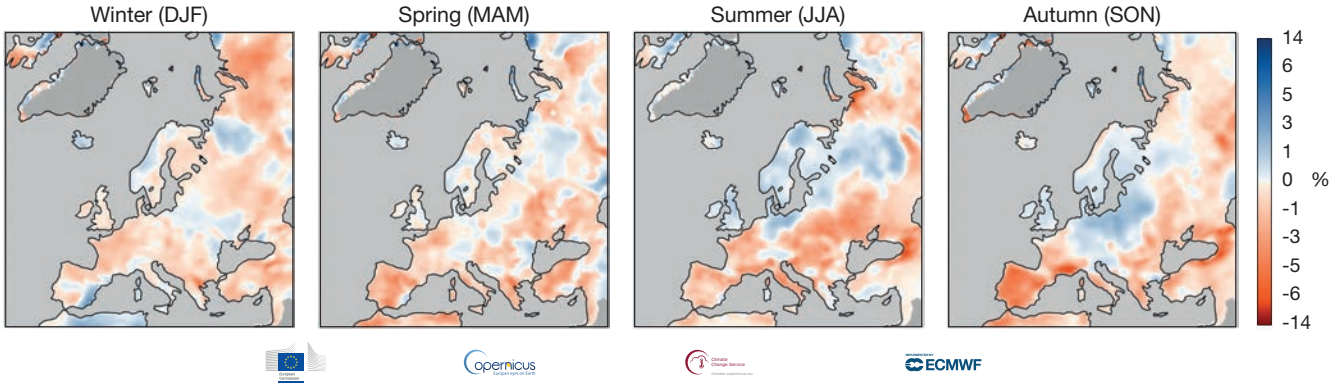

Soil moisture anomalies. The figure shows seasonal soil moisture anomalies for winter, spring, summer and autumn 2017 relative to the respective seasonal average for the period 1981–2010. Southwest Europe experienced a year of large negative soil moisture anomalies, especially during spring and autumn, whereas Scandinavia and the Baltic region saw large positive anomalies during both summer and autumn. Data Source: ERA-Interim reanalysis. Credit: Copernicus Climate Change Service/ECMWF.

Effects of ocean coupling on weather forecasts

KRISTIAN S. MOGENSEN, TIM HEWSON, SARAH KEELEY, LINUS MAGNUSSON

Experiments have shown that using interactive ocean and sea ice components in ECMWF's Integrated Forecasting System (IFS) can significantly improve sea-surface temperature predictions in Europe and, as a result, predictions of near-surface air temperature.

With the operational implementation of IFS Cycle 45r1 on 5 June 2018, all forecasts issued by ECMWF are based on a coupled model with interactive ocean and sea-ice components. This coupled model exchanges data from the atmospheric model with the ocean/sea-ice models and receives back information about the dynamic evolution of the sea-surface temperature (SST) and sea-ice concentration. A recent ECMWF Newsletter article (No. 154, winter 2017/18 issue) showed that SST coupling is important for the prediction of large-scale tropical cyclones, but there are other situations where this coupling also matters. Here we show two examples of how coupling can improve the prediction of SST in the seas surrounding Europe, and we present the repercussions on atmospheric variables. All results shown here are from research done in preparation for the introduction of coupling in ECMWF's high-resolution forecasts (HRES) in 45r1.

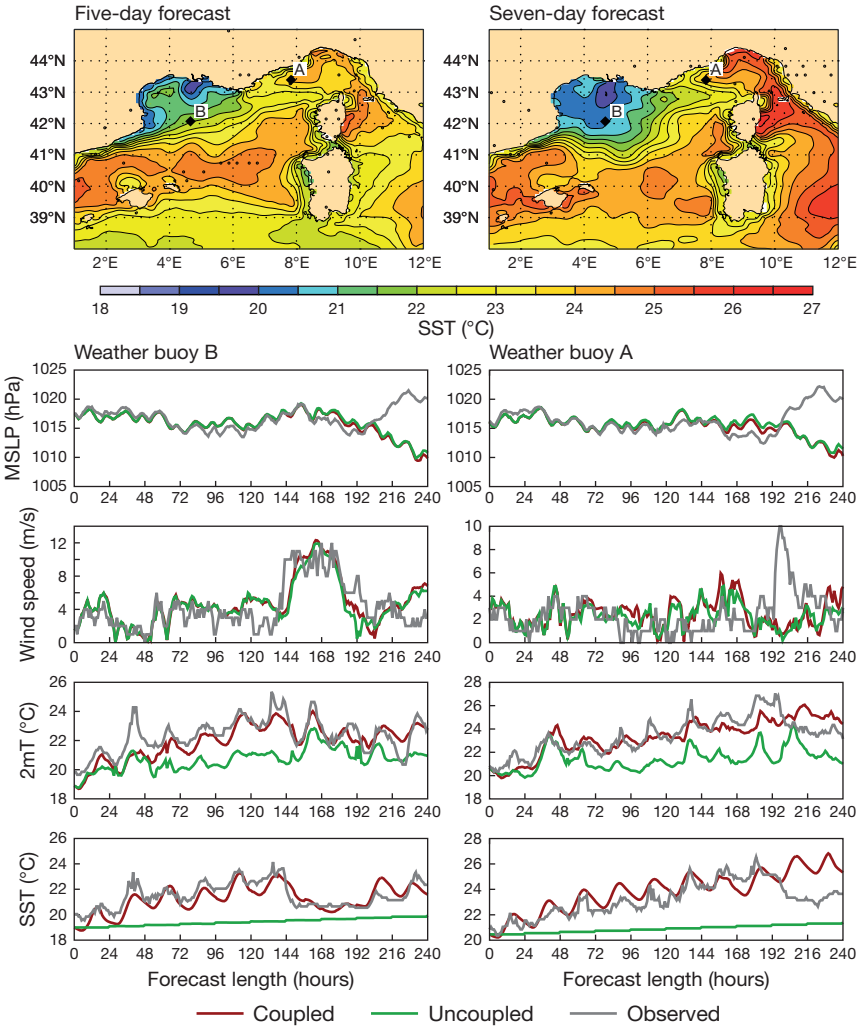

Mistral case. Predicted SST from experimental runs with ECMWF's coupled model starting from 00 UTC on 10 June 2017 valid at 00 UTC on 15 June (top left) and at 00 UTC on 17 June 2017 (top right). The other panels show the observed and predicted mean sea level pressure, wind speed, 2-metre temperature (2mT) and SST at the location of two buoys marked A and B in the top panels.

Physical mechanisms

Aside from advection of sea water, there are multiple physical mechanisms that can cause substantial in situ changes to SST:

1. Cooling via an upward sensible and/or latent heat flux. This cooling is enhanced when the overlying air is, in relative terms, very cold and/or very dry, and also when winds are strong.
2. Heating via insolation. This is enhanced when winds are light, because there is a reduction in mechanical mixing, allowing heating to be confined to the upper ocean layers.
3. Cooling by mechanical mixing. This is particularly effective when a very shallow layer of relatively warm water at the top of the ocean overlies much cooler water below (e.g. following an insolation-related heating episode as in 2). The converse, heating by mixing, tends not to occur because it requires, beforehand, a stratification with cold water above warm water, which is generally unrealistic as it is unstable (although salinity variations can complicate the picture).

The most powerful of these processes is probably (3), with changes of as much as 10°C in 24 hours having been recorded in the Adriatic during a Bora wind event. The coupled model should be able to represent all of the above processes, although the depth of the uppermost ocean model layer, 1 m, could be a limiting factor. The first example below illustrates processes (2) and (3) whilst the second example illustrates process (1).

Effect of summer insolation and Mistral on SST

During June 2017, there were long periods of warm weather over the Gulf of Lion interspersed with several Mistral

events (strong cold winds blowing from the south of France into the Gulf of Lion). An example of a simulation with the new coupled HRES configuration can be found in the first figure. After the onset of the Mistral, predicted SST is reduced by about 2ºC in large parts of the Gulf of Lion. To get a feel for how realistic the simulation is, we have compared it with measurements from two moored buoys deployed by Météo-France (black diamonds in the top panels). The agreement between the predicted SST and the observed SST is remarkably good up to 8 days for the eastern buoy (marked 'A' in the map) and even better for the western buoy (marked 'B' in the map). It is worth noting that during the first five days of the forecast the SST at buoy B is steadily increasing (with a diurnal cycle superimposed), but as soon as the wind starts to pick up the SST drops rapidly, for a period of 48 hours, before increasing again. Buoy A shows a similar steady increase in SST during the first 8 days, but the model fails to capture the rapid increase in wind from day 8 to day 9, and because of this it also fails to predict the concurrent decrease in SST.

Comparing the coupled simulation with an uncoupled simulation (bottom panels), we see that mean sea level pressure (MSLP) and wind speed are similar, but the predicted 2-metre temperature is quite different. Observations agree much better with the coupled model output. It is worth bearing in mind that the uncoupled simulation only changes the SST in accordance with date-based climatological trends, so it is not surprising that it fails to capture changes in 2-metre temperature originating from changes to SST.

Cooling of North Sea SST

During the winter of 2018, there was an extended period when exceptionally cold air blew in from the east across the North Sea. The second figure shows an example of the predicted SST at day 8 from a coupled HRES simulation (top left) together with an uncoupled simulation (top right) and the corresponding analysis (bottom left). In this case the coupled simulation predicts the cooling in the German Bight quite well, whereas the cooling in the Skagerrak between south Norway and Denmark is too large. If we compare with observations from a moored buoy (bottom right, diamond in maps), we can see that the predictions for the German Bight are in remarkable agreement with the observations.

Conclusions

The two examples presented here both show that the SST reacts to meteorological fields in physically sound ways. The Mistral case also shows that this can lead to improvements in the prediction of 2-metre temperature. Work will continue to improve the understanding of the processes involved in interactions between the atmosphere and the ocean (including sea ice) to further improve our coupled modelling capabilities in accordance with ECMWF's Strategy.

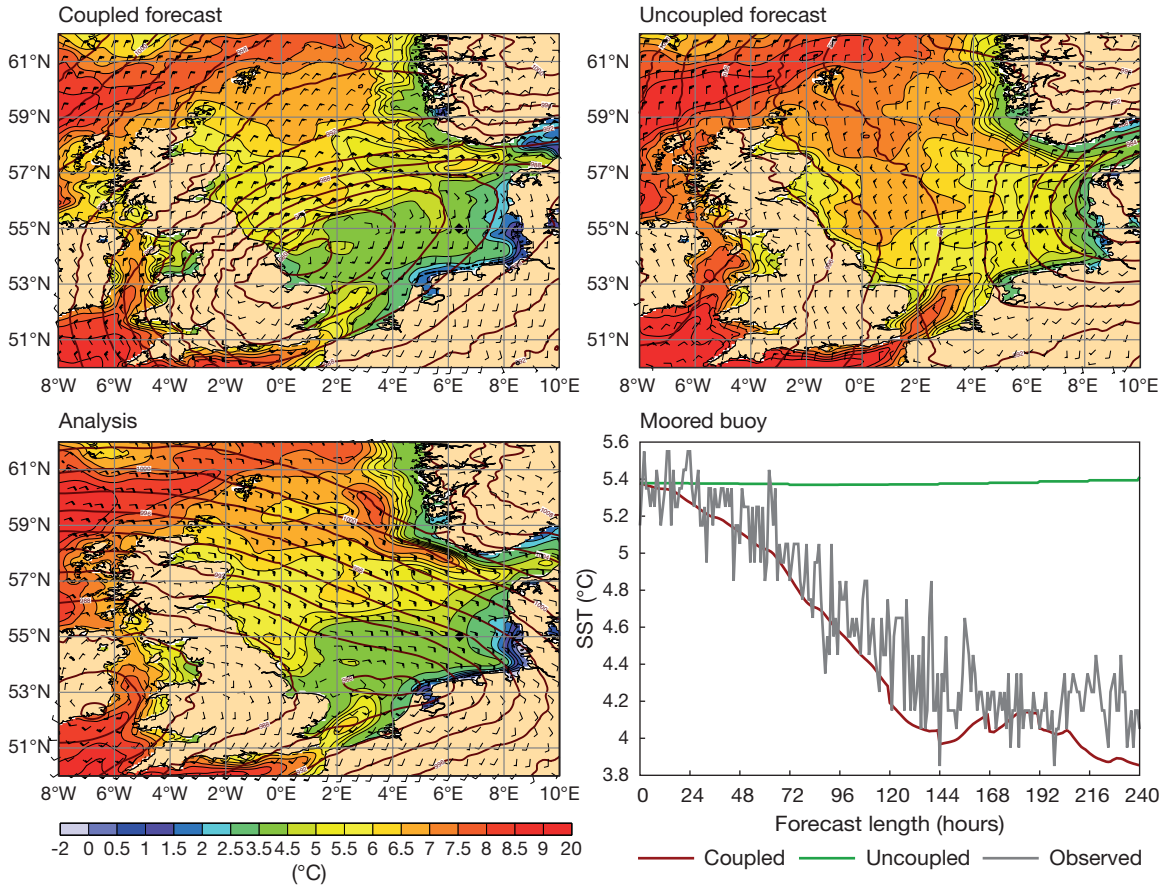

North Sea case. Predicted SST with mean sea level pressure (contours) and wind (barbs) for 8-day coupled (top left) and uncoupled (top right) forecasts with corresponding analysis (bottom left). The bottom-right panel shows the SST evolution of the coupled and uncoupled forecast at the location of a moored buoy (marked with a diamond in the other plots) together with the observed SST.

NOAA satellite launch in 1998 opened new era

NIELS BORMANN, STEPHEN ENGLISH, ANTHONY MCNALLY

The meteorological satellite sounding community recently celebrated the 20th anniversary of the start of a new era in meteorological satellite observations: on 13 May 1998, the US NOAA-15 satellite was launched, beginning the Advanced TIROS Operational Vertical Sounder (ATOVS) series of satellite observations that has been hugely influential for numerical weather prediction (NWP) and continues to this day.

ATOVS was the first major enhancement in polar satellite instrument observing capability since the first operational system was launched 20 years earlier in 1978. For the first time, the microwave sounding capability provided information not just on temperature but also on humidity, and the vertical resolution of the temperature information was significantly improved. Previously the infrared sounder was the primary sounding instrument, but this was restricted to cloud-free areas. The new microwave sounders provided data of comparable quality, but in clear and cloudy regions. ATOVS suites were subsequently launched on many other satellites, including NOAA-16 through to 19 and the European Metop satellites, and they inspired similar instruments on other US, Chinese, and Russian satellites.

Making the most of the data

ATOVS was launched shortly after the introduction of 4D-Var at ECMWF in November 1997. One of the motivations for developing 4D-Var was that it makes better use of satellite radiance data. ATOVS in many ways showcased the value of this strategic development. A year after launch, on 5 May 1999, ECMWF started the direct assimilation of these new observations as raw radiances, resulting in very significant improvements in forecast skill.

The start of assimilating ATOVS data was also the start of learning how to make best use of these observations. We can now treat random and systematic uncertainties better and have extended the data usage over land. The development of the all-sky assimilation approach made it possible to better extract dynamical information from the humidity and cloud information contained in the data. All this means that we are now extracting more information from these observations than when they first arrived 20 years ago, ensuring that ATOVS data remain leading contributors to forecast skill.

Benefits of a long life span

NOAA-15 not only carries the first in a major new generation of instruments but has also proven one of the most durable satellites. Indeed, ECMWF is still assimilating data from NOAA-15 20 years on – a remarkable feat given the satellite was originally planned to have a life span of only five years. The observations give us a unique view of the evolution of ECMWF's operational system, not least owing to the observations' stable noise characteristics. Comparisons between observations and model equivalents calculated from short-range forecasts show a gradual reduction in standard deviation, reflecting the various improvements in ECMWF's Integrated Forecasting System over the years (not only in terms of the use of the NOAA-15 observations, but also in terms of other aspects of the forecasting system). Similarly, our reanalysis activities benefit immensely from this longevity and stability. Since in reanalyses the assimilation system is fixed, standard deviations of differences between observations and short-range forecast equivalents are a lot more stable over time, with only a small reduction due to general improvements of the observing system in the last two decades. The ATOVS suite is one of the backbones of any satellite-era reanalysis.

Still a crucial observing system

Even today, the microwave sensors of the ATOVS suite continue to be leading contributors to forecast skill in ECMWF's operational assimilation system. At the time of writing, ECMWF assimilates data from six microwave temperature sounders and four

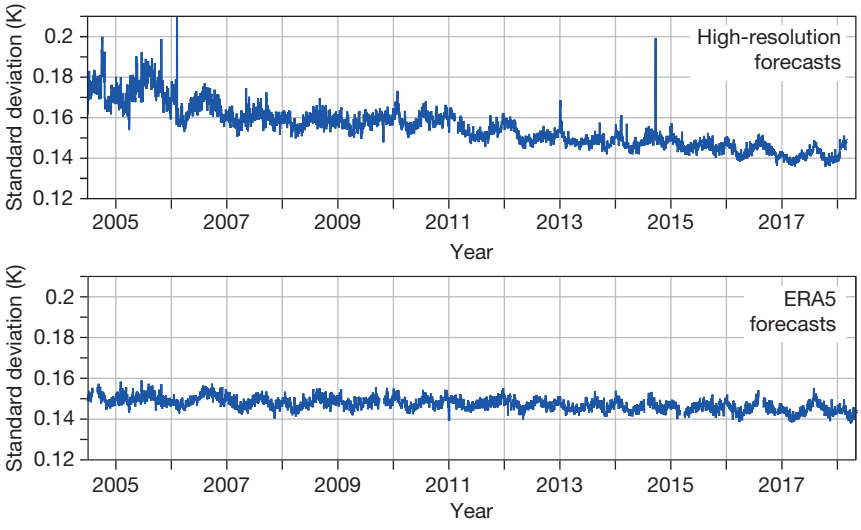

Improvements in forecasts and reanalyses as seen by NOAA-15. The plots show standard deviations of differences between observations and short-range forecasts from the high-resolution operational system (top) and from the ERA5 reanalysis (bottom) for radiances from channel 8 of AMSU-A on the NOAA-15 satellite. This is a microwave temperature-sounding channel peaking around the tropopause. The standard deviations show a combination of errors related to the observations as well as the short-range forecasts. One main contributor from the observations is the instrument noise, which independent monitoring shows has been stable at around 0.13 K throughout the entire period. The gradual reduction in standard deviation reflects improvements in the short-range forecasts and also improved processing of the observations in the ECMWF system.

humidity sounders of the ATOVS family from several satellites. We expect to add one further instrument for each type later this year after EUMETSAT's Metop-C is launched, carrying the last flight models of this successful suite of instruments. Since ATOVS there has been an acceleration of new satellite capabilities, for example the hyperspectral infrared sounders with much better vertical resolution, and refined ATOVS-inspired microwave sensors on US, Chinese and Russian satellites.

Twenty years ago, the use of satellite data in NWP stepped up a gear through the technological advances provided by ATOVS. This is certainly a reason to celebrate. Happy birthday NOAA-15 – and happy birthday ATOVS!

Massive open online course on monitoring atmospheric composition

MARK PARRINGTON

The ECMWF-run Copernicus Atmosphere Monitoring Service (CAMS) is joining forces with the European Organisation for the Exploitation of Meteorological Satellites (EUMETSAT) to produce a free online course that will help the public to better understand the chemical composition of the Earth's atmosphere.

Starting in the week beginning 22 October, anyone who is interested in the topic will be able to participate in the massive open online course (MOOC), which is being developed by the London-based media company Imperative Space. The Monitoring Atmospheric Composition MOOC will run for five weeks and will feature several hours of online learning per week through educational videos, interviews with experts in the field of atmospheric science, knowledge-based quizzes and interactive content. The author (CAMS ECMWF) and Rosemary Munro (EUMETSAT) are the lead educators on the course, which will be presented by physicist and BBC broadcaster Helen Czerski from University College London.

At the end of each week, one of the lead educators will address questions that are posted on the MOOC forum, relating to the subject matter for that week. A short video addressing some of the more interesting questions will be filmed and put on the MOOC platform.

The weekly topics will focus on 'Earth's atmosphere and the challenges we face' (Week 1); 'pollution, air quality and health' (Week 2); 'large-scale changes in ozone and greenhouse gases' (Week 3); 'long-range transport of air pollutants' (Week 4); and 'policies to maintain our life-support system in the future' (Week 5). ECMWF experts appearing in the videos include Vincent-Henri Peuch, Head of CAMS; Richard Engelen, Deputy Head of CAMS; CAMS scientists Melanie Ades, Anna Agusti-Panareda and Johannes Flemming; and ECMWF service shift manager Antonio Mariano.

Other institutions involved in the filming of interviews include the University of Leicester, King's College London, Météo-France, the French National Center for Scientific Research (CNRS), the University of Bremen, the Finnish Meteorological Institute and NASA's Jet Propulsion Laboratory.

The aim of the course is to provide information and educational materials that are easily accessible to people so they can understand the air that we breathe and how we monitor it. The material should be of interest to a broad audience, from high-school pupils, teachers and undergraduates to interested professionals and anyone interested in learning about atmospheric composition.

Monitoring Atmospheric Composition will be the second MOOC arranged between EUMETSAT and Copernicus, the EU's Earth observation programme. In 2016, more than 5,000 people participated in the first open online course on monitoring the oceans from space.

MOOC interview. Helen Czerski (left) interviewed Melanie Ades about the red skies over western Europe associated with ex-hurricane Ophelia in October 2017.

Climate Data Store open for business!

CEDRIC BERGERON, BAUDOUIN RAOULT, KEVIN MARSH, CARLO BUONTEMPO

The Climate Data Store (CDS) was launched online on 14 June by the Copernicus Climate Change Service (C3S) operated by ECMWF. It is set to revolutionise user access to a vast treasure of climate data, presenting new opportunities to all those who require authoritative information on climate change. A quick 'click-and-go' experience via a simple, uniform user interface offers easy online access to a wealth of climate data that anyone can freely browse and download after a simple registration process. The CDS is able to handle several hundred thousand user requests per day, and this can be increased in line with demand. As well as discovering and browsing datasets, developers can build their own data processing workflows to work within the environment of the CDS, and large data requests can be fulfilled via the CDS application programming interface.

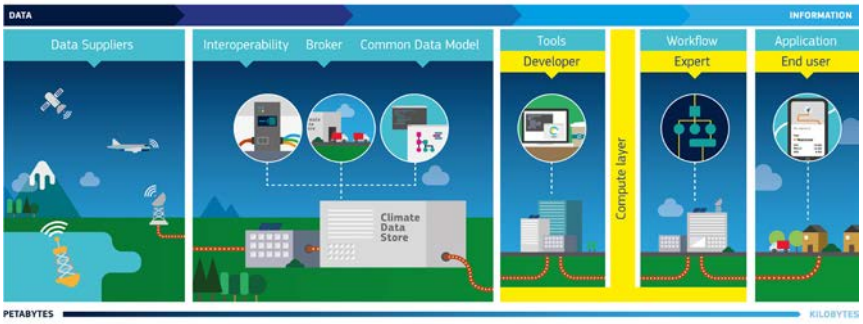

CDS data flow. The CDS includes tools that enable climate data to be transformed into information relevant to different sets of users.

About the CDS

Developed by C3S, the Climate Data Store provides access to petabytes of open climate data from the European Commission's Copernicus Programme via a straightforward web interface. These climate-related data include observations, reanalyses (obtained by combining observations with numerical models), seasonal forecasts and climate projections. The variety and volume of the data made available will increase rapidly over the coming years. The Climate Data Store is a game changer because it provides policy-makers, businesses, scientists and other users with seamless access to data collections distributed over multiple data suppliers.

Toolbox feature

A major feature of the CDS is its integrated toolbox, which allows developers to create web-based applications that can utilise CDS data. On the face of it, the variety of CDS data types, formats and volumes makes their combined use challenging. The CDS toolbox removes this complexity and allows application developers to focus on algorithms to process data and create knowledge. The toolbox provides a series of tools that allow users to perform basic operations and statistical computations on the datasets; these tools can then be combined into more elaborate workflows, the results of which can be graphically presented on the screen. Such workflows can be used to analyse, monitor and predict the patterns of both climate drivers and impacts on specific business sectors, such as energy, water management, and agriculture.

A recent ECMWF Copernicus hackathon event (#OpenDataHack2018) held in Reading, UK, on 9 and 10 June inspired developers, designers, and entrepreneurs to see what could be achieved with the CDS, with great results. In addition, training sessions on using the CDS and toolbox are available to developers.

Use case examples

Whilst the CDS is open to everyone, many users are likely to be 'intermediaries' who have the technical capability to develop Python workflows which transform the data into climate-related information. They can function as the interface between the CDS and end users of the information, for whom they develop specific applications.

Over the last two years, C3S has developed example applications that illustrate how the data can be made relevant to specific sectors. For instance, before providing funding for a new wind farm, investors would require information on the profit such a wind farm is likely to generate. This in turn depends on possible future variations in wind resources, which could be influenced by events such as El Niño or by climate change. By combining historical data with climate projections, CDS users could derive information able to guide an investment made in a specific wind farm.

ECMWF's next major development in the context of Copernicus will be the implementation of a DIAS (Data and Information Access Services) platform called WEkEO (https://www.wekeo.eu), in partnership with EUMETSAT and Mercator Ocean. ECMWF will bring its experience in data management and tools to this endeavour. WEkEO is a natural extension of the CDS and will allow users to allocate their own compute resources to process not only the data provided by the partners, but all the data made available by the Copernicus programme. This project will be described in detail in a future Newsletter article.

Useful links

Access to the Climate Data Store: https://cds.climate.copernicus.eu

ECMWF Newsletter article (spring 2017) on the design of the CDS: https://www.ecmwf.int/en/newsletter/151/meteorology/climate-service-develops-user-friendly-data-store

Wind power use cases: http://clim4energy.climate.copernicus.eu/wind-power

Ocean experts discuss use of observations in NWP

MAGDALENA A. BALMASEDA

More than 50 ocean and data assimilation experts came together at ECMWF from 22 to 25 January 2018 to discuss the way forward for the use of observations of sea-surface temperature (SST) and sea ice in numerical weather prediction (NWP) and climate reanalysis applications, and to advise ECMWF on how best to exploit the observational information.

The workshop was intended to bring together experts in all aspects of the field, including the processing of ocean surface observations (both satellite and in situ), data assimilation techniques and modelling. Three days of presentations were followed by working group meetings, which tried to assess the current state of the art and identify areas where significant improvements and progress can be made.

Wide range of expertise. More than 50 experts including 24 speakers attended the workshop.

Outcomes

The main recommendations can be summarised as follows:

1. ECMWF was encouraged to gradually move towards the assimilation of radiances to constrain SST and sea ice in the context of running fully coupled systems. This will require extensive collaboration with space agencies and experts outside ECMWF.
2. While there are exciting synergies between assimilating ocean-surface sensitive radiances and coupled data assimilation, no blocking inter-dependencies are foreseen, so the two developments can proceed largely in parallel exploiting available resources and expertise.
3. In the spirit of moving towards coupled data assimilation, the quality of the individual ocean and sea ice components – both model and data assimilation – should receive adequate attention.
4. There is generally good guaranteed future provision of operational satellite data to support these activities, with the possible exception of gaps with respect to low-frequency passive microwave data. This should be matched by an adequate level of support and governance for the in situ component.
5. International coordination is also required to optimise the use of SST and sea ice information in Earth system reanalyses.

Motivation and background

An accurate characterisation of the ocean in terms of its surface temperature and sea ice coverage is vital for weather forecasts a few days in advance out to the seasonal range. The landscape of users and applications of SST and sea ice information has changed considerably over the past few years. Observations, applications and methodologies are undergoing a major shift. In the case of SST and sea ice, the paradigm of Earth system forecasting systems has brought together activities and communities traditionally separated, such as the weather and marine communities, and the weather and climate communities. There is a pressing need to revisit standard practices in view of current and potential future deficiencies, to provide guidelines for future directions, and to prepare the ground for institutional collaboration at international level.

The workshop was timely for ECMWF, which is embarking on an ambitious programme to develop Earth system analyses and forecasts as part of its ten-year Strategy. This workshop provided an opportunity to discuss with experts how best to proceed in this area.

Topics discussed

Twenty-four speakers explored a wide range of topics, from observation operators for SST to the latest research on data assimilation systems in which the ocean and the atmosphere are coupled. The workshop revolved around four central themes: observations of SST and sea ice; processing chains (e.g. retrievals, gap filling, product delivery); applications; and new methods.

The presentations were followed by working group discussions focusing on (1) sea ice, (2) applications and (3) SST. The working groups were asked to address the following questions:

- What are possible visions for SST and sea ice information at ECMWF in the time range of ten years?
- What are the current deficiencies and gaps and future barriers (observations, forward models, methods)?
- What should be the next steps for ECMWF to improve SST and sea ice in NWP and reanalysis?
- What recommendations would you make to space/observation agencies?
- Which observations and processing level should drive the evolution of our systems?

The full workshop report as well as presentations and working group recommendations can be found at: https://www.ecmwf.int/en/learning/workshops/workshop-observations-and-analysis-sea-surface-temperature-and-sea-ice-nwp-and-climate

ECMWF meets its users: UEF 2018

ANNA GHELLI

This year's Using ECMWF's Forecasts meeting (UEF) was attended by a record 120 participants. It took place at the Centre from 5 to 8 June. The UEF offers an opportunity to learn about ECMWF's plans and new products and services. It also fosters networking and experience-sharing among participants. As in previous years, a dedicated session provided an opportunity to give feedback on ECMWF data and products.

The meeting included presentations, posters and demonstrations. Participants showed and tried out software or services developed at institutions in ECMWF's Member and Co-operating States and at ECMWF, including the Copernicus services implemented by the Centre.

The only limit is your imagination

Weather data must be transformed into relevant information to be used in decision-making processes. The theme of this year's UEF was that 'the only limit is your imagination' when turning weather data into useful information. For example, indices highlighting favourable conditions for flu outbreaks can help people to make informed decisions regarding their health and well-being; probabilities of winds being above or below specified thresholds are useful in wind farm management; and probabilities of occurrence of specified weather scenarios can help farmers to minimise damage due to mildew on vineyards. These are just a few of the applications that were presented during the UEF. The meeting also looked at how experiencing a severe weather event in virtual reality could support decision-making and how infographics can be used to communicate forecast confidence. The overall focus was on two thematic areas: processing model outputs and impact forecasting.

Meeting highlights

ECMWF Director of Forecasts Florian Pappenberger presented recent developments in physical parametrization, data assimilation and ocean–atmosphere coupling. He also mentioned improvements in Copernicus Climate Change Service (C3S) and Copernicus Atmosphere Monitoring Service (CAMS) open-data forecast products, the availability of global hydrological forecasts (Global Flood Awareness System - GloFAS) and the newly set up service to provide fire danger indices.

Poster session. The UEF 2018 meeting provided many opportunities for forecast users to exchange information and seek new collaborations.

A talk on ECMWF forecast product development presented among other things the Centre's new lightning density products and a new product to show the vertical structure of the atmosphere at a point. Irina Sandu (ECMWF) presented the 'Understanding uncertainties in the surface–atmosphere exchange' (USURF) project, which aims to better understand the causes of the observed biases in near-surface parameters. Laura Ferranti (ECMWF) showed a set of new products which are being developed to monitor the quality of predictions of seasonal transitions in the medium and extended ranges.

Applications of ECMWF data presented by weather companies included supporting African farmers by providing them with local weather forecasts,

Poster sessions

Posters sessions have become a central part of the UEF, with an increasing number of interesting contributions submitted for the meeting. Posters provide an opportunity to engage with other participants who have similar areas of interest and to seek future collaborations.

This year a record number of posters were shown in two sessions. Topics covered included the use of ECMWF's ensemble forecasts (ENS) for applications in the developing world (Bangladesh, Uganda) to increase resilience and mitigate natural disasters. The quantification of uncertainty by the ENS boosts the value of the forecasts.

There is growing interest in the aviation sector in the use of ECMWF model outputs and products to manage operations at airports and provide flight-specific turbulence forecasts for commercial routes.

A number of posters presented performance assessments of ECMWF forecasts in the medium and extended ranges.

There is a growing number of applications using extended-range forecasts in ECMWF's Member and Co-operating States. MeteoSwiss presented an application in support of the European HEAT-SHIELD project, which aims to support European workers by providing heat-stress indicators for an early-warning system.

and coupling an eddy-resolving model with ECMWF data to resolve small-scale phenomena like turbulence for applications such as wind turbine planning and management.

A variety of talks showed the use of ECMWF data to support forecasters at national meteorological services in Member and Co-operating States in their duties. Examples of the use of ensemble forecasts to initialise limited-area models and storm surge models were also shown.

Tim Scheitlin from NCAR in the US led a workshop on visualising geoscience data using virtual and augmented reality. Virtual reality (VR) allows the user to be fully immersed in a virtual environment, while augmented reality (AR) enhances the real world with virtual objects. Tim suggested that VR could be used by decision-makers to experience severe weather and understand how their decisions may affect people. UEF participants were able to gain first-hand experience with VR and AR using ECMWF snowfall and snow accumulation products.

Computing Representatives give useful feedback

UMBERTO MODIGLIANI

The 30th Computing Representatives' meeting took place at the Centre from Wednesday 16 to Friday 18 May 2018. The meeting enabled the Representatives and ECMWF staff to exchange their experiences and provided ECMWF with very useful feedback on the services provided.

ECMWF has over 3,000 registered external users with access to its high-performance computing facility and ecgate (see box). It has many more web-only users, 10,000 of whom are from our Member and Co-operating States. Each Member State and Co-operating State is asked to appoint a 'Computing Representative' to represent users in their countries on day-to-day matters relating to the use of ECMWF's computing and archiving service. Representatives also help people to access ECMWF's facilities, and they provide some support for users in their organisation. To support the work of the Computing Representatives, ECMWF organises meetings with them, typically every 12 to 18 months. This year's event was attended by 26 external participants from 23 organisations. The meeting provides a forum for ECMWF and the Member and Co-operating States to exchange views and experiences. Representatives usually give an update on their computing environment and on their use of ECMWF's computing and archiving systems. The first such meeting took place in 1980.

This year, ECMWF gave a series of reports on the latest changes in its services, including the new Copernicus Climate Data Store and cloud-related services. ECMWF also presented Metview's new Python interface and the new Meteorological Interpolation and Regridding package (MIR). The Member and Co-operating States gave presentations on:

- their experiences of significant IT transformation exercises (e.g. creation of new IT services, significant changes in IT services, move of their data centre, lessons learnt in doing this)
- their experiences in providing remote access to their IT services (e.g. what sort of access they provide, whether they use Virtual Desktop Infrastructure, and whether access differs by type of user).

All presentations are available to registered users on the ECMWF website at:

www.ecmwf.int/en/about/who-we-are/representatives/computing-representatives-meeting-2018

Computing representatives meet ECMWF staff. The meeting was attended by 26 external participants from 23 organisations, including EUMESAT and the Preparatory Commission for the Comprehensive Nuclear-Test-Ban Treaty Organization (CTBTO).

ecgate

ecgate is a Linux cluster available to registered users from ECMWF's Member and Co-operating States. This general-purpose computing facility can among other things be used to carry out pre- and post-processing work that is not suitable for the supercomputer; to access the Data Handling System; and to transfer data to and from external sites.

New forecast evaluation tool for OpenIFS

GABRIELLA SZÉPSZÓ, GLENN CARVER

The OpenIFS team at ECMWF has released a new tool for users of OpenIFS to test the performance of this easy-to-use version of the Centre's Integrated Forecasting System (IFS). The tool is based on two case studies. Input data, the Metview visualisation programs with detailed guidance and output figures are available for download.

Until now, OpenIFS users could only check their model installation with a short acceptance test at the lowest model resolution (T21). Our aim with the new tool is to provide benchmark forecasts for two weather events, which users can repeat with their OpenIFS version on their computing facility. They can then compare their results to the ones produced using OpenIFS at ECMWF. We also plan to use the package internally.

The meteorological performance of the IFS is extensively assessed before each model upgrade. However, the IFS evaluation system is too complex to be made available with OpenIFS. This is why a similar suite was designed to explore new OpenIFS cycles before their release. The evaluation programs have for the first time been made available together with OpenIFS 40r1v2. The input data and the figures can be retrieved from the ECMWF download server and a comprehensive description with a user guide can be found on the OpenIFS home page (see the links at the end of this article).

We selected storm events with severe impacts over Europe and governed by large-scale dynamics: Xaver and Desmond. Storm Xaver hit the North Sea region and several adjacent countries on 5 December 2013. The cyclone developed on 4 December northeast of Newfoundland and was situated between converging northerly and southerly airstreams. The operational IFS forecast predicted the cyclone eight to nine days ahead and the very strong wind gusts three to four days in advance. The orographically driven precipitation of storm Desmond caused severe flooding across northern England, parts of Scotland and Ireland on 5 December 2015 and broke the United Kingdom's 24-hour rainfall record. Although the IFS forecast the high rainfall amounts well, it underestimated the peak values and overestimated the precipitation in the lee of hills.

OpenIFS was run several times for both cases to test the effect of forecast length, initial conditions and spatial resolution on forecast quality. We initialised the experiments from the ERA-Interim and ERA5 reanalyses one to five days before the high-impact events using three different resolutions: T255L91, T639L137 and T1279L137 (approximately 80, 32 and 16 km grid spacing with 91 and 137 vertical levels, respectively). The evaluation pages on the OpenIFS website guide the users step by step through post-processing the model outputs and plotting them with Metview.

We prepared Metview macros to analyse the initial conditions, the forecast results and the reference data. Our focus was on the evolution of mean sea level pressure, 2-metre temperature, 24-hour precipitation, 3-hourly maximum 10-metre wind gusts, 850 hPa temperature, 700 hPa relative humidity, 500 hPa geopotential, and 250 hPa and 100 hPa wind fields

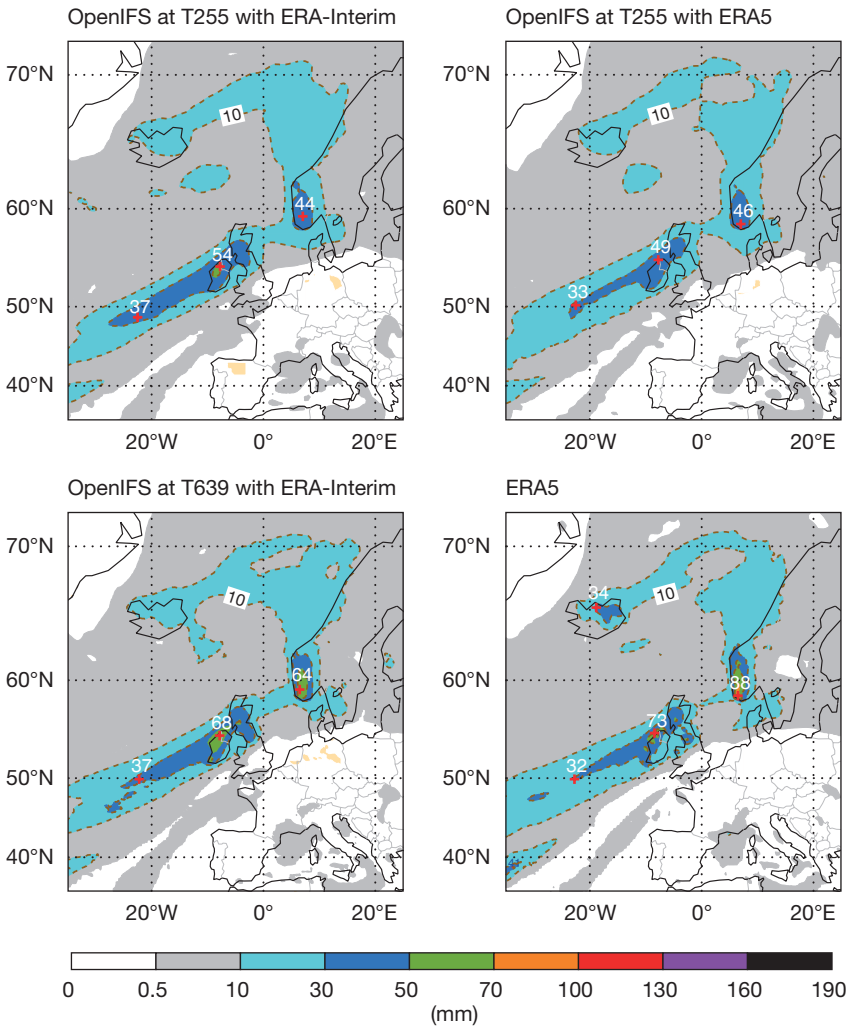

Twenty-four hour precipitation experiments. The plots show 48-hour forecasts of 24-hour precipitation on 6 December 2015 in T255 resolution experiments initialised from ERA-Interim (top left) and ERA5 (top right) and in a T639 resolution experiment initialised from ERA-Interim (bottom left), and 24-hour precipitation in ERA5 (bottom right). More realistic precipitation patterns are produced at the higher resolution, while the difference between initialising from ERA-Interim and ERA5 at lower resolution is less pronounced.

on 5 December. As a reference, we used ERA-Interim and ERA5, which are the fourth and fifth generations of ECMWF atmospheric reanalyses. ERA5 uses a newer model version with higher resolution than ERA-Interim and includes newly reprocessed observational data.

For an overview of the large number of figures produced by the Metview macros, an album can be prepared containing all plots for each selected variable and a given investigation aspect (e.g. to study the impact of resolution changes in the forecast) in a concise format. We provide two methods for users, Microsoft Word macros and html templates, to quickly generate such an album.

The package has already been tested by students at the Eötvös Loránd University in Budapest. We encourage other OpenIFS users to implement the evaluation package and to provide feedback on their experiences.

ECMWF download server: http://download.ecmwf.int/test-data/openifs/reference_casestudies

OpenIFS Meteorological Evaluation: https://software.ecmwf.int/wiki/x/jxwXBQ

The APPLICATE Polar Prediction School

JONATHAN DAY, LINUS MAGNUSSON (both ECMWF), **FIONA TUMMON** (Arctic University of Norway & APECS), **GUNILLA SVENSSON** (Stockholm University)

As part of ECMWF's contribution to the EU Horizon 2020-funded APPLICATE project and to the World Meteorological Organization's Year of Polar Prediction (YOPP), ECMWF scientists played a leading role in the Polar Prediction School held at the Abisko Scientific Research Station in northern Sweden from 17 to 27 April 2018. The event was an international effort involving many partners from within the APPLICATE consortium and beyond, led by the Association of Polar Early Career Scientists (APECS).

Both the climate and weather patterns of the polar regions are changing faster than anywhere else on Earth. These changes are opening up new opportunities for shipping, energy extraction, and tourism, but they are also exposing these sensitive regions to increasing environmental hazards and posing major challenges to local communities. Our ability to predict polar weather and climate change on scales from days to decades is still limited, hampering effective decision-making. The 10-day course was designed to provide 30 early career scientists with the tools needed to address these limitations in the coming years.

The course included lectures, practical exercises, fieldwork, and a dedicated science communication programme. It covered a wide range of topics: satellite and conventional observation techniques; numerical modelling of the polar atmosphere, sea ice and ocean; data assimilation; and model evaluation. Each of these is a crucial aspect of the prediction problem.

Outside the Abisko Scientific Research Station. Students and lecturers pose for a photo.

Linus Magnusson lectured on numerical weather prediction (NWP) and evaluation, and Jonny Day on sea ice prediction. Jonny was also one of the school's organisers, leading the design of the school's scientific programme. In addition to the teaching, ECMWF contributed to the school by providing forecast products, which were used in the production of daily weather briefings prepared by the students. This supported evaluation activities in the field as well as training in the use of ECMWF charts and other products. Field data from a micrometeorological mast on site helped to evaluate ECMWF forecasts, producing a dataset which can also be used for evaluation purposes at the Centre.

Micrometeorological observations and daily radiosoundings provided hands-on training opportunities. These data were directly used in the practical exercises, allowing the students to investigate the topics discussed in the theoretical lectures more thoroughly. They were also used in the daily weather briefings – exercises which encouraged the students to interpret and evaluate the output of forecast models for a mountainous polar area. The science communication sessions complemented the scientific programme and led to the production of brief informative videos aimed at the general public.

Fieldwork on a frozen lake. Micrometeorological mast installed on Lake Torneträsk.

The school provided an excellent opportunity to advertise different output from ECMWF forecasts and introduce the students to some of the interesting scientific problems related to NWP in the polar regions.

ECMWF improves web user experience

HELEN SETCHELL

ECMWF has continued to enhance its web presence over the last year by refreshing its home page and other interfaces, publishing a directory of staff profiles, improving its eLibrary and web charts, and introducing eLearning. These changes are accompanied by other, less visible changes to improve web service delivery for our users.

Most users will have seen that we now have a consistent look and feel across the whole ECMWF web presence. This started with a refreshed home page incorporating both a live chart of the high-resolution mean sea level pressure and ensemble spread and more updates on our activities.

Some of these home page updates are publicised through integration with our new social media channels, Twitter and LinkedIn. ECMWF also now publishes a regular science blog written by ECMWF experts.

To make it easier to find and collaborate with ECMWF experts, we now have a directory of staff profiles on our website. Each profile provides information about that person's expertise and outputs, linked to their publications in our eLibrary.

This summer, we are implementing a refresh of the eLibrary. A great deal of work has gone into reviewing and improving the catalogue in the background and the search interface at the front end, based on feedback from users. We are rolling out digital object identifiers (DOIs) and ORCID iDs to make it easier to find and share ECMWF publications, credit our authors, and manage and report on our publications.

As part of this work we have made ECMWF Newsletter feature articles available as stand-alone publications and provided access to eLearning materials. We will continue to develop and add new eLearning modules, which give learners flexibility in terms of when, where and how they want to learn to make the most of our products and services.

Chart products are continually being added to and improved based on user requests. ecCharts has seen many improvements: new layers, meteograms and styles have been added, as have new products, including ecPoint-Rainfall; lightning flash density; and charts that show the vertical structure of the atmosphere at a point.

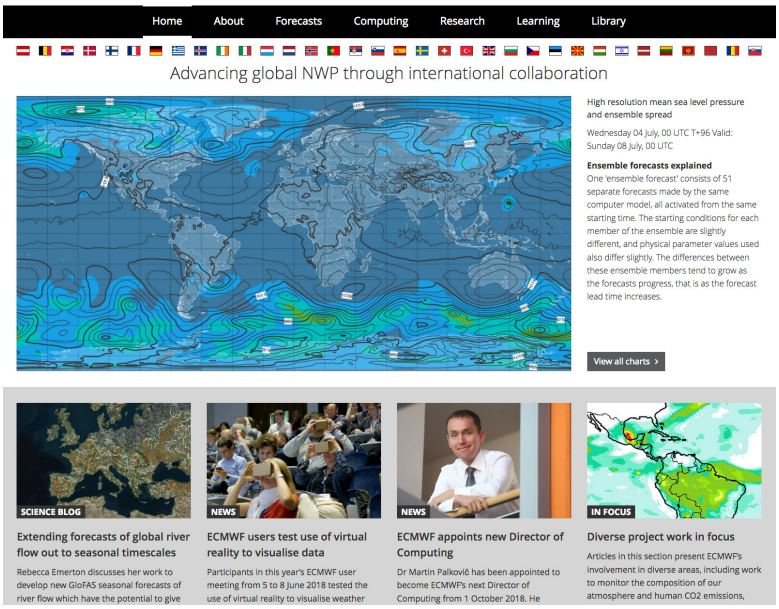

Website home page. The refreshed home page provides a live chart of the high-resolution mean sea level pressure and ensemble spread and more updates on our activities.

Continued focus on the user

To help us decide where to focus these continuing web improvement efforts, we have been studying the most-used content across the ECMWF websites.

Nearly three in four page views are of pages which provide access to data (33%), the chart pages (22%), and documentation and support (17%).

Nearly all the remaining views (23%) are of pages which link users to what they are looking for, such as the 'Forecasts' landing page. However, users spend the least time on these navigation pages. This suggests we need to look closely at site navigation over the coming year to see if we can get users of our charts, data, and documentation and support to where they want to be in fewer clicks.

Looking at the time users spend on each page, chart pages are top of the list. This is likely due to the high level of interactivity on each chart page, something we are continually working to improve in terms of response times and features. Documentation and support come in second place, which coupled with the high hits tells us that it would be worthwhile focusing on making this content as quick and easy to use as possible, as well as improving the technical architecture to increase performance and reliability. Third place is held jointly by the pages which provide access to data – so we will be looking at improving how users discover and access data – and those which provide event and learning content.

If you have feedback about any of the above, or ideas about improving the ECMWF web presence, please contact servicedesk@ecmwf.int.

Useful links

eLibrary: https://www.ecmwf.int/search/elibrary

Staff profile directory: https://www.ecmwf.int/en/about/who-we-are/staff-profiles

eLearning materials: https://www.ecmwf.int/en/learning/education-material/elearning-online-resources

Science blog: https://www.ecmwf.int/en/about/media-centre/science-blog

Twitter: https://twitter.com/ecmwf

New ECMWF Forecast User Guide launched

BOB OWENS, TIM HEWSON

A new and extensively updated edition of ECMWF's user guide was made available online in May this year. The ECMWF Forecast User Guide helps forecasters and other meteorologists to make the best use of the Centre's forecast products. It provides all the tools needed for the correct interpretation of these products, enabling users to deliver a high-quality service to their own customers. It also encourages users to employ new or previously overlooked forecast techniques.

The guide focuses on the medium range but also covers the increasingly important monthly and seasonal output. The correct use of probabilistic information and of departures from worldwide model climatologies is stressed throughout. While the emphasis is on ECMWF's own web-based products, including ecCharts output, the content is also relevant to users who reference gridded data imported onto their own dedicated forecaster workstations.

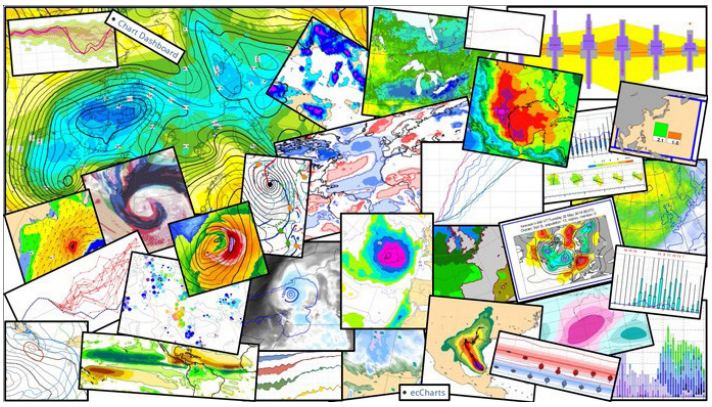

The guide explains how ECMWF's Integrated Forecasting System (IFS) works, what recent changes there have been and what these mean for forecast quality. It also details how physical processes are represented in the IFS, and it describes the ways in which observation usage is optimised. The many new products that have been added in recent years are comprehensively discussed, with strengths and weaknesses highlighted. Knowledge of these various aspects allows users to better adapt ECMWF forecast output for their own local purposes.

Until May 2018, the user guide was available to download from ECMWF's website as a PDF document. Now in web-based format, this new edition will be updated swiftly as the IFS, the products and our understanding evolve. In future, we are aiming for the web platform to allow comments and discussions.

The ECMWF Forecast User Guide can be accessed at:

https://software.ecmwf.int/wiki/display/FUG/Forecast+User+Guide

New observations since January 2018

The following new observations have been activated in the high-resolution ECMWF assimilation system since the beginning of 2018:

Observations	Main impact	Activation date
Atmospheric Motion Vectors and All-Sky Radiances from Meteosat-11 (replacing Meteosat-10, which has been excluded since 7 February 2018)	Tropospheric wind and humidity	20 February 2018
Radio occultation bending angles from GNOS on FY-3C	Temperature in upper troposphere/lower stratosphere	6 March 2018
Radiances from ATMS on NOAA-20	Temperature, humidity, dynamics	22 May 2018
Atmospheric Motion Vectors from GOES-16 (replacing GOES-13, which has been excluded since 2 January 2018)	Tropospheric wind	22 May 2018
Significant wave height from JASON-3 and Sentinel-3A altimeters	Ocean waves	5 June 2018

doi:10.21957/729r3bdsx6

IFS upgrade brings more seamless coupled forecasts

ROBERTO BUIZZA, GIANPAOLO BALSAMO, THOMAS HAIDEN

On 5 June 2018, ECMWF implemented a substantial upgrade of its Integrated Forecasting System (IFS). IFS Cycle 45r1 brings coupling to all ECMWF forecasts, from forecast day 1 to one year, by including the three-dimensional ocean and sea-ice model in the single high-resolution forecast (HRES). This is a further step towards the implementation of the 2016–2025 Strategy, whose goals include a more complete and seamless description of the Earth system across all ECMWF configurations.

Since 2013, a coupled model configuration with the community ocean model NEMO (the Nucleus for European Modelling of the Ocean, *http://www.nemo-ocean.eu/*) has been used in the medium-range/monthly ensemble (ENS) from day 0, and in 2016 coupling with the LIM2 Louvain-la-Neuve sea ice model developed at the Belgian Université de Louvain was introduced in ENS (*Buizza et al.*, 2017b). The introduction of ocean and sea ice coupling in the HRES enables rapidly interacting processes (e.g. during tropical cyclones) to be better described. In line with increased ocean–atmosphere coupling, the sea-ice product used by the atmospheric analysis in IFS Cycle 45r1 is provided by ECMWF's ocean analysis (OCEAN5). The upgrade introduces full ocean coupling in the tropics for both HRES and ENS, but it retains partial coupling in the extratropics. Partial coupling, as implemented in ENS in 2013, couples the sea-surface temperature tendencies rather than the actual sea-surface temperature field from the ocean model during the first four days of the forecast.

With IFS Cycle 45r1, an increased number of observations are assimilated, and the latest radiative transfer model (RTTOV-12) is used in the assimilation of all satellite radiance data. A better use of radiosondes, accounting for the drift during ascent, and improved aircraft bias correction lead to better analyses. Changes in the cloud microphysics and convection address longstanding systematic shortwave radiation biases (due to supercooled liquid water) in the storm tracks and over the southern oceans, as well as precipitation issues along coastlines. Modifications to the tangent-linear physics substantially improve the overall stability of the data assimilation.

In IFS Cycle 45r1, the model uncertainty scheme SPPT (Stochastically Perturbed Parametrization Tendencies) is revised, and the SKEB (Stochastic Kinetic Energy Backscatter) scheme is deactivated, bringing computing time savings of about 2.5%. The changes to SPPT make the Ensemble of Data Assimilations (EDA) more reliable and consistent with ENS. They have a positive impact on extended-range forecasts, e.g. in predicting the organised convection associated with the Madden-Julian Oscillation (MJO). Cost savings in the post-processing and changes to the software infrastructure enabled the introduction of the ocean model at essentially no extra cost. With IFS Cycle 45r1, for the first time lightning products will become available. See *Lopez* (2018) for details on the lightning parametrization and forecast performance.

The impact of the upgrade on forecast scores is positive over the tropics for both HRES and ENS. Over the extratropics, the impact is positive to neutral: overall slightly positive for HRES and mixed for ENS.

Summary of main changes

IFS Cycle 45r1 brings major changes in many areas of modelling, observation handling and data assimilation, and forecast infrastructure. These changes include:

- **Forecast model:** Introduction of coupling of HRES to the 3-dimensional ocean model NEMO, with a 0.25 degree resolution and 75 layers, and LIM2 sea ice model (as in ENS, see the article by *Keeley & Mogensen* in this issue); improved numerics for warm-rain cloud microphysics and the vertical extrapolation for semi-Lagrangian trajectories; improved representation of supercooled liquid water in convective clouds (*Forbes et al.*, 2016); improved representation of mid- to upper-stratospheric water vapour; new output parameters including maximum CAPE and CAPE-shear in the last 6 hours of the forecast and lightning flash density; new bathymetry (water depth) in the wave model, mainly affecting wave fields in coastal areas.
- **Data assimilation:** For the first time, the atmospheric assimilation makes use of the OCEAN5 sea-ice analysis in the surface analysis of the high-resolution and EDA analyses. This enhances the coupling between the ocean and atmosphere. OCEAN5 makes use of LIM2 and assimilates the UK Met Office's OSTIA product instead of using it directly to define the sea ice initial conditions. Relative humidity increments are calculated using temperature instead of virtual temperature. The weak constraint model error forcing is applied at every time step instead of every hour to avoid shocks in the model integration. Changes to the tangent-linear (TL) and adjoint (AD) physics have led to a dramatic reduction in the number of spuriously large analysis increments in both the EDA and the high-resolution 4D-Var analysis.
- **Observations:** Assimilation of non-surface-sensitive infrared (IR) channels over land; assimilation of all-sky microwave (MW) sounding channels over coasts; introduction of RTTOV-12 and new microwave instrument coefficients; retuning of the radiosonde observation error, and introduction of a scheme to account for radiosonde drift *(Ingleby et al.*, 2018); assimilation of wave height data from JASON-3 and Sentinel-3A altimeters; use of BUFR SYNOP observations in the surface analysis, with more than 200 additional snow depth observations in China.
- **Model uncertainties (EDA, ENS):** Improved flow-dependent error representation in the SPPT scheme via

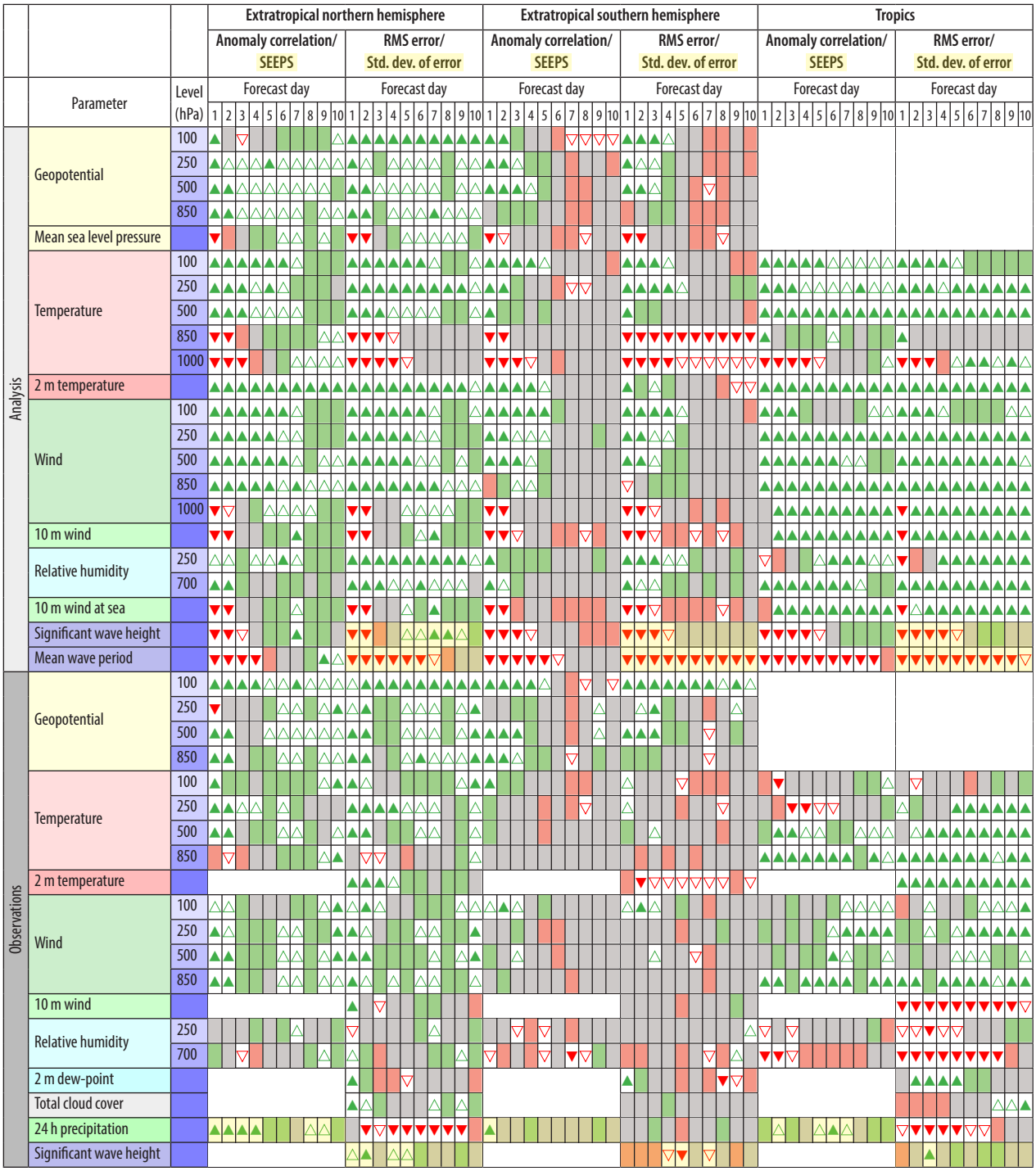

Symbol legend: for a given forecast step...

- ▲ 45r1 better than 43r3 statistically significant with 99.7% confidence
- △ 45r1 better than 43r3 statistically significant with 95% confidence
- 45r1 better than 43r3 statistically significant with 68% confidence
- no significant difference between 43r3 and 45r1
- 45r1 worse than 43r3 statistically significant with 68% confidence
- ▽ 45r1 worse than 43r3 statistically significant with 95% confidence
- ▼ 45r1 worse than 43r3 statistically significant with 99.7% confidence

Figure 1 HRES scorecard of IFS Cycle 45r1 versus IFS Cycle 43r3, verified by the respective analyses and observations at 00 and 12 UTC, based on 855 forecast runs in the period December 2016 to June 2018. See Box A for a discussion of how scores computed against analyses have been affected by changes to the analysis in IFS Cycle 45r1.

reduced spread in clear-sky regions (due to unperturbed radiative tendency in clear sky), the activation of tendency perturbations in the stratosphere, and weaker tapering of perturbations in the boundary layer; a reduction in the amplitude of the SPPT perturbation patterns (by 20%); introduction of the cycling of stochastic physics random fields in the EDA, and adoption of the same SPPT configuration in EDA as in ENS; deactivation of the stochastic backscatter (SKEB) scheme due to improved model error representation by the SPPT scheme (see above), leading to a 2.5% cost saving in ENS.

- **Software infrastructure:** the *ecBuild* system is incorporated into the IFS source repository, which enables a standalone build of the IFS to be created on a workstation, with all required dependencies resolved automatically, and a small quality assurance test suite to be run. This will help to develop and test future code changes more efficiently.

Impacts

A comparison of parallel runs of the previous operational cycle (43r3) and the new cycle (45r1) indicates an overall positive impact in the tropics for both HRES and ENS (Figures 1 and 2). For the extratropics, results are mixed, with an overall slightly positive impact on the HRES scores, while for the ENS the sign of the impact depends on the geographical region and the variable.

Upper-air fields

The new cycle leads to improvements in HRES upper-air fields. When these fields are verified against the

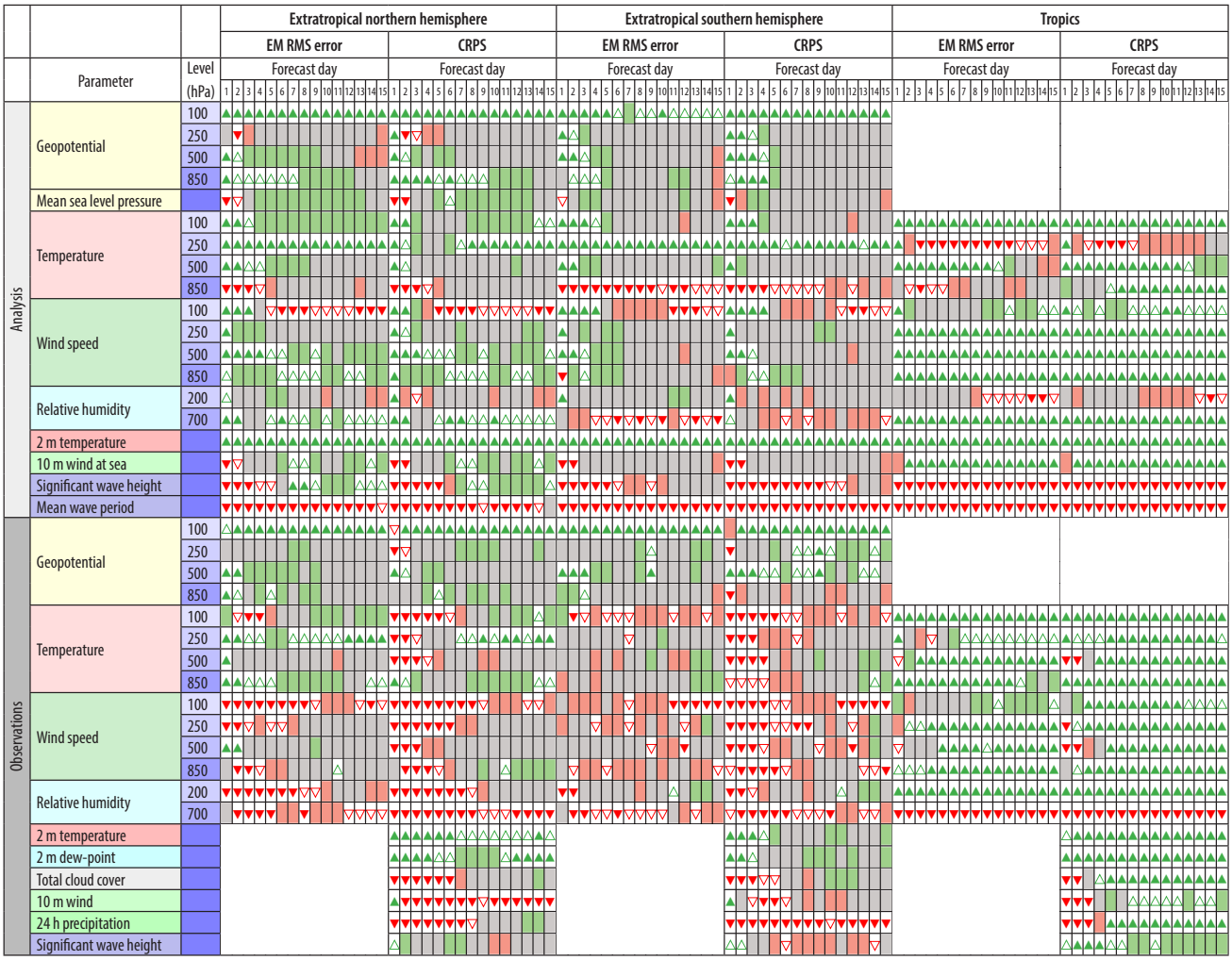

Symbol legend: for a given forecast step...

- ▲ 45r1 better than 43r3 statistically significant with 99.7% confidence
- △ 45r1 better than 43r3 statistically significant with 95% confidence
- 45r1 better than 43r3 statistically significant with 68% confidence
- no significant difference between 43r3 and 45r1
- 45r1 worse than 43r3 statistically significant with 68% confidence
- ▽ 45r1 worse than 43r3 statistically significant with 95% confidence
- ▼ 45r1 worse than 43r3 statistically significant with 99.7% confidence

Figure 2 ENS scorecard of IFS Cycle 45r1 versus IFS Cycle 43r3 for medium-range/monthly forecasts up to forecast day 15, verified by the respective analyses and observations at 00 and 12 UTC, based on 408 ENS forecast runs in the period December 2016 to June 2018. See Box A for a discussion of how scores computed against analyses have been affected by changes to the analysis in IFS Cycle 45r1.

model analysis, a positive signal is seen throughout the troposphere for most parameters, except temperature in the lower troposphere at shorter ranges. The latter is mainly a result of changes to the analysis, linked to changes in the stochastic scheme used in the EDA (see Box A). Forecast verification against observations shows a neutral impact. Upper-air improvements are more pronounced in the tropics, especially for wind and temperature. When verified against observations, upper-air changes are overall positive in the tropics except for relative humidity, and neutral to slightly positive in the extratropics. Upper-air results for ENS verified against the analysis are mostly positive in the tropics but more neutral in the extratropics. The negative signal for temperature in the lower troposphere at shorter lead times is again mainly due to changes in the analysis. Against observations, results are mostly negative in the extratropics at short lead times and significantly positive in the tropics, with the exception of relative humidity at 700 hPa. The negative impact in the extratropics is partly due to a slight reduction in ensemble spread associated with the transition to a physically more realistic SPPT scheme. Whether or not this reduced spread is genuinely detrimental depends on how significant the impact of observation errors is in the verification; this has not been routinely taken into account so far. Experimental verification against radiosonde data that takes observation error into account indicates that a large fraction of the negative ENS results disappear or become statistically insignificant.

Weather parameters and waves

There is an overall improvement in 2-metre temperature both in the HRES and ENS, particularly for Europe. The impact on 2-metre humidity is largely neutral for HRES and positive for ENS, particularly in the tropics, while for 10-metre wind speed the impact is largely neutral in the HRES but slightly negative in the ENS. Precipitation in the HRES is improved in terms of categorical verification (e.g. the SEEPS score), and near-coastal precipitation in warm-rain dominated situations is significantly improved due to changes in the cloud physics. However, the model changes lead to more activity at higher precipitation rates in active regions such as the East Asian monsoon, and as a result error measures such as RMSE or CRPS (for the ENS) are increased. The negative signal for significant wave height against analysis is a result of changes to the analysis resulting from a large increase in observation usage.

Verification against analyses or observations?

A

During the testing and evaluation of IFS Cycle 45r1, a lot of effort was put into clarifying the relative role of verification against analyses and observations, and into upgrading the evaluation tools applied to assess the impact of the upgrade on forecast performance.

The analysis is the result of combining observations with a short-range forecast (the first guess). The weights given to the observations and the first guess depend on the observation errors and on the forecast error statistics. The former depend on the instrument, while the latter are flow-dependent and are based on the most recent EDA. Thus, changes to the EDA (e.g. an increase in its spread) induce a change in the relative weight given to the observations and the first guess. They thus cause the analysis to be closer to, or further away from, the observations.

In 45r1, changes to SPPT have induced an increase in the EDA spread in the boundary layer and a slightly reduced spread in the upper troposphere. The result is that overall the analysis is drawn closer to the observations, and further away from the first guess, especially in the lower troposphere. On average this improves the EDA reliability, but it can have a negative impact on the short-range forecast error evaluated against the analysis. Thus, care must be taken in interpreting the scorecard values computed against analyses (the top half of the scorecards) versus the values computed against observations (the lower part of the scorecards).

A second change introduced in 45r1 that has an effect on verification is the fact that more observations are used. This is the case, for example, for the ocean wave analysis. Since more observations are assimilated, again the analysis is drawn further away from the first guess, and this can have a negative impact on forecast scores computed against the analysis. The combination of the changes in EDA spread and the use of more observations explains why wave forecasts have an increased error when verified against analyses.

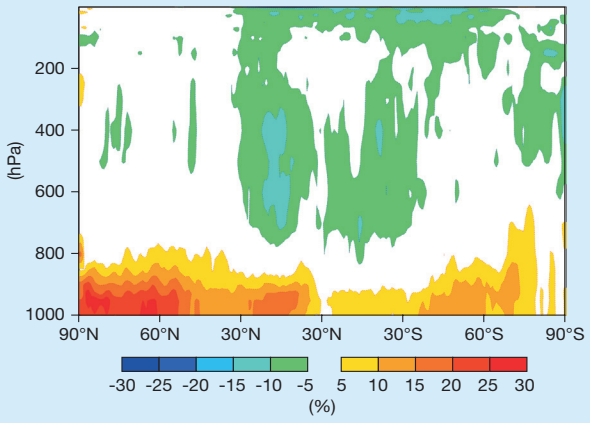

Vertical cross-section of the difference (in %) between the average EDA standard deviation of IFS Cycles 45r1 and 43r3 for temperature in January 2017. Positive values mean that the 45r1 EDA spread is bigger.

The coupling of the HRES from day zero and the full coupling in the tropics for HRES and ENS also have an impact on the verification against the analysis of near-surface fields. In the tropics, before the upgrade the high-resolution atmospheric analysis used the sea-surface temperature (SST) from OSTIA, while the coupled forecast model is initialised from the OCEAN5 SST.

Verification against observations (buoys) shows that results are neutral for both HRES and ENS.

Tropical cyclones

The implementation of the ocean–atmosphere coupling in the HRES removes the overall negative bias in tropical cyclone central pressure and thereby reduces the mean absolute intensity error by about 10% in the short range and by about 20% from day 5 onwards (Figure 3). Evaluations indicate statistically neutral results for the position error. For further details on the influence of ocean–atmosphere coupling on tropical cyclone intensity forecasts, see *Mogensen et al.* (2018).

Extended range

Changes in scores for the monthly system are generally positive across the range of parameters, with significant improvements for tropical winds. The only indication of degradation is for precipitation in the tropics with a consistent negative signal across all four weeks. There is an indication of a positive effect on skill across all parameters in Europe. Before the upgrade, there was too little spread in the MJO Index. Changes in 45r1 to the SPPT scheme have now brought the spread and error into close agreement throughout the 30-day forecast range. The underestimation of the MJO Index amplitude has been significantly reduced throughout the forecast.

Scorecard upgrades

To improve the evaluation of ENS, two major scorecard upgrades have been prepared. First, the 45r1 ENS scorecard now includes verification against observations for many more parameters, reflecting what has been done for many years for the HRES forecast. The plan is to use this upgraded ENS scorecard for all future cycle evaluations. The second upgrade is that, for some parameters, scores against observations have been computed taking into account observation errors. This allows us to measure the impact of a cycle change on ENS more correctly. It has for example emerged that, if observation errors are taken into account, then the statistical significance of certain changes can decrease. Work in this area has just started, and we will report more on the results once it is complete.

Summary

The implementation of IFS Cycle 45r1 brings us another step closer to the implementation of ECMWF's Strategy. It means that HRES, ENS and SEAS5 now use the same coupled ocean, sea-ice, land and atmosphere models, and it makes the simulation of model uncertainties identical in the EDA and ENS. It enables the use of more observations and improves their assimilation, and it includes changes to the model physics that bring an improved representation of Earth system processes. The upgrade also introduces new output parameters that can help to save lives by providing additional indications of severe weather. Overall, the changes included in IFS Cycle 45r1 have a neutral or slightly positive impact on forecast scores, with larger improvements over the tropics and for extended-range predictions. The upgrade also helps to pave the way for future progress by updating ECMWF's software infrastructure.

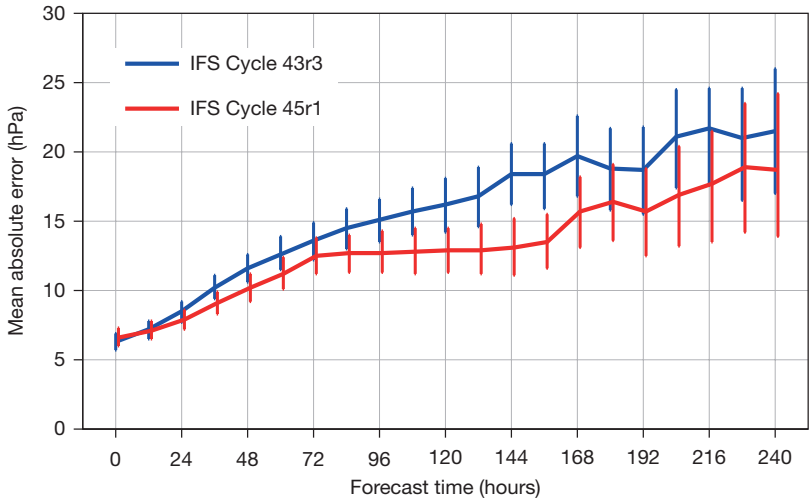

Figure 3 Mean absolute error of HRES forecasts of tropical cyclone (TC) intensity (mean sea level pressure) in IFS Cycle 45r1 (using the coupled model) and in IFS Cycle 43r3 (using the uncoupled model). The sample comprises all TCs present at the initial time of the forecast; the sample size therefore decreases as the forecast time increases, consistent with the TC life span: it includes about 750 cases at initial time, decreasing to about 200 at forecast days 5–6 and to about 50 at day 10. Bars indicate 95% confidence intervals.

FURTHER READING

Buizza, **R.**, **P. Bechtold**, **M. Bonavita**, **N. Bormann**, **A. Bozzo**, **T. Haiden**, **R. Hogan**, **E. Holm**, **G. Radnoti**, **D. Richardson**, & **M. Sleigh**, 2017a: IFS Cycle 43r3 brings model and assimilation updates. *ECMWF Newsletter* **No. 152**, 18–22.

Buizza, **R.**, **J.-R. Bidlot**, **M. Janousek**, **S. Keeley**, **K. Mogensen** & **D. Richardson**, 2017b: New IFS cycle brings sea-ice coupling and higher ocean resolution, *ECMWF Newsletter* **No. 150**, 14–17.

Forbes, **R.**, **A. Geer**, **K. Lonitz** & **M. Ahlgrimm**, 2016: Reducing systematic error in cold-air outbreaks. *ECMWF Newsletter* **No. 146**, 17–22.

Ingleby, **B.**, **L. Isaksen**, **T. Kral**, **T. Haiden** & **M. Dahoui**, 2018: Improved use of atmospheric in situ data. *ECMWF Newsletter* **No. 155**, 20–25.

Lopez, **P.**, 2018: Promising results for lightning predictions, *ECMWF Newsletter* **No. 155**, 14–19.

Mogensen, **K.**, **L. Magnusson**, **J.-R. Bidlot** & **F. Prates**, 2018: Ocean coupling in tropical cyclone forecasts. *ECMWF Newsletter* **No. 154**, 29–34.

doi:10.21957/4ska25furb

Dynamic sea ice in the IFS

SARAH KEELEY, KRISTIAN MOGENSEN

Including more Earth system components in numerical weather prediction models has the potential to improve weather forecasts because of the interactions of those components with the atmosphere and with each other. One such component is sea ice. Until a few years ago, it was assumed that sea ice fields change so slowly that it is acceptable to keep them fixed for the period covered by global medium-range forecasts. Although this may be true for the total pack ice, in regions close to the ice edge, where there is often rapid growth or melt, this assumption is not justified. The presence of sea ice influences surface fluxes, especially when the overlying atmosphere is much colder than the ocean, as is usually the case in winter. Fluxes can be several hundred W/m^2 over open water and zero over thick ice. Open water thus provides a local heat source which has the potential to alter the local and also the wider meteorological situation.

In November 2016, ECMWF included a dynamic–thermodynamic sea ice model in ensemble forecasts (ENS) as part of an upgrade of its Integrated Forecasting System (IFS Cycle 43r1). Since the implementation of IFS Cycle 45r1 in June 2018, high-resolution forecasts (HRES) have also benefitted from dynamic coupling between sea ice, the ocean and the atmosphere.

Here we show why the assumption of persistence of sea ice concentration is not suitable for medium-range forecasts; we describe the sea ice model used at ECMWF; and we present some regional case studies that illustrate how the model is able to capture relatively rapid changes in sea ice concentration. Verification results show that using the dynamic sea ice model generally improves sea ice predictions, which in turn has repercussions on local 2-metre temperature forecasts. The impact on large-scale atmospheric forecast performance is mostly neutral.

Limitations of persistence

To illustrate the need for modelling sea ice dynamically rather than using a simple model of persistence, we consider the sea ice conditions for the year April 2017 to March 2018. To assess how persistent the ice field was, we calculated the difference between the sea ice analysis field from OCEAN5 on any given day and the same field on each of the following ten days (see Box A for details on OCEAN5). For each of the following ten days, if the change in sea ice concentration at a model grid point was more than 15%, we considered that a significant change had occurred. We then calculated the total area in which a change in sea ice concentration of more than 15% occurred, as a proportion of the total sea ice field. We chose to use OCEAN5 rather than OSTIA as it is less susceptible to fluctuations due to erroneous data, which can appear from time to time in the OSTIA product (see Box A for more details on OSTIA).

Figure 1 shows the monthly mean percentage area in which significant changes occurred over periods of time ranging from one day to ten days. The first thing to note is that there are times of the year when the ice concentration is particularly active. In both hemispheres, the greatest activity is in the early autumn as the hemisphere transitions into the polar night. In those conditions sea ice can form rapidly. As shown in Figure 1, the assumption that the ice concentration remains static is a poor assumption at this time of year even for three-day periods, with significant changes in sea ice concentration in nearly 10% of the total ice field area in the southern hemisphere. The second peak in activity occurs in the summer months when the ice is melting. It is thinner at this time, so it can rapidly be removed through local heating, and wave breaking can also play a role (*Zhang*, 2012).

Sea ice modelling and coupling

The model used to represent the sea ice dynamic and thermodynamic evolution is LIM2, which has been developed at the Belgian Université catholique de Louvain (*Fichefet*, 1997) and is part of the community ocean model NEMO (version 3.4.1). The sea ice model is relatively simple in that it has a single thickness category, and it does not

OSTIA and OCEAN5

A

OSTIA (Operational Sea Surface Temperature and Sea Ice Analysis) (*Donlon*, 2012) is a daily sea-surface temperature (SST) and sea ice analysis product produced by the UK Met Office. The SST analyses are made using observations from satellite and in situ platforms. The sea ice field is a regridded version of the OSI-SAF sea ice product derived from passive microwave observations. It is not necessarily consistent with the SST at the same grid point and uses a relatively simple interpolation method to infill missing data to produce a globally complete gridded sea ice field. This means that the system is very sensitive to missing data. If large areas are missing from a day's analysis, the OSTIA system cannot provide values. Close to the coast, where the OSI-SAF microwave product is unable to distinguish between land and ice and returns missing data values, the OSTIA product interpolates to the land–sea mask. This can lead to unphysical sea ice concentrations in regions marked by complex coastlines, e.g. in the Gulf of Finland.

OCEAN5 is ECMWF's ocean and sea ice reanalysis and real-time analysis system. It estimates the state of the sea ice and 3D ocean by using a 3D variational assimilation system (NEMOVAR). The system produces initial conditions for the sea ice model by assimilating daily sea ice concentration values which come from the gridded sea ice concentration of OSTIA. By assimilating the sea ice concentration OSTIA data, there is better physical agreement between the SST and sea ice field and the system is less susceptible to missing data as there is memory in the assimilation system.

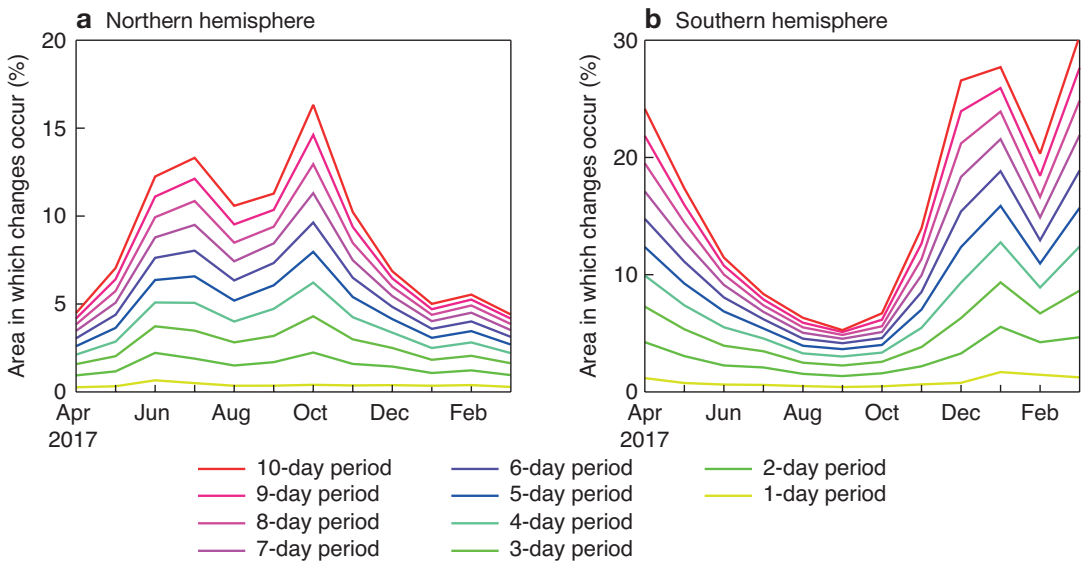

Figure 1 Monthly mean percentage of the sea ice field in which significant changes in sea ice concentration (> 15%) occur over different periods of time, based on OCEAN5 analysis fields for April 2017 to March 2018, for (a) the northern hemisphere and (b) the southern hemisphere.

model some key surface processes, such as the forming of melt ponds. However, it is computationally relatively cheap and, as we will show later, performs well at medium to sub-seasonal timescales. The sea ice model uses a rheological model to describe the internal ice dynamics, and a three-layer thermodynamic model, with two layers of ice and one of snow.

There are some limitations which have guided how we have coupled the sea ice model (LIM2) components to the atmospheric model. For example, as the parametrizations within the sea ice model are relatively simple, we cannot capture summer melt pond processes, making the albedo of the LIM2 model too high in summer. For this reason, we have continued to use the albedo climatology of the atmospheric model. Currently we only couple the sea ice concentration from LIM2. Work is ongoing to couple additional fields. Sea ice concentration is updated in the IFS every coupling step (currently every hour), but we continue to use the sea ice tile in the surface model of the IFS to adjust the surface energy balance on faster timescales.

New sea ice analysis

The sea ice model is initialised using the OCEAN5 analysis system, as is the ocean model. For sea ice observational input, OCEAN5 assimilates sea ice concentration from the OSTIA sea-surface temperature (SST) and sea ice analysis. Until June 2018, the HRES forecast was uncoupled and used the OSTIA sea ice product, which is not necessarily consistent with the OSTIA sea-surface temperature analysis and can be vulnerable to missing or spurious data in the sea ice field. Sea ice concentrations are especially hard to determine close to the coast due to contamination in the satellite retrieval caused by the effects of land. This means that determining the sea ice concentration within the Baltic region using passive microwave retrievals is incredibly challenging, and the OSTIA product does not always perform well in this region. To try to account for potentially unreliable data, the surface analysis for the uncoupled system removed ice below a 20% threshold. Figures 2a,b show the initial conditions of the sea ice field from the new coupled HRES using OCEAN5 and the uncoupled HRES using OSTIA. There are some differences between the two. OCEAN5 is able to adjust the sea ice concentration close to land, consistent with its SSTs, whereas the OSTIA product makes an extrapolation near the coast and fails to do this correctly, for example in the Gulf of Finland.

To highlight the impact of the new coupled system and the types of event it is able to reproduce, we show recent examples when the coupled and uncoupled systems were running concurrently and conclude with an example from the extended-range (monthly) forecast system.

Sea ice prediction case studies

The three case studies presented here illustrate the impact of coupling in HRES as implemented on 5 June in IFS Cycle 45r1.

Sea ice melt in the Baltic Sea

In the uncoupled configuration, the sea ice concentration is fixed for the duration of the forecast. Figure 2 illustrates the impact of having a coupled sea ice model within HRES. Figure 2c shows the state of the ice in the OCEAN5 analysis for 11 April 2018. Compared to the OCEAN5 analysis for 1 April shown in Figure 2a, over the course of ten days the ice has retreated within the Gulfs of Finland, Riga and Bothnia. This reduction in sea ice concentration is well captured by the coupled model, as can be seen in the 10-day forecast shown in Figure 2d.

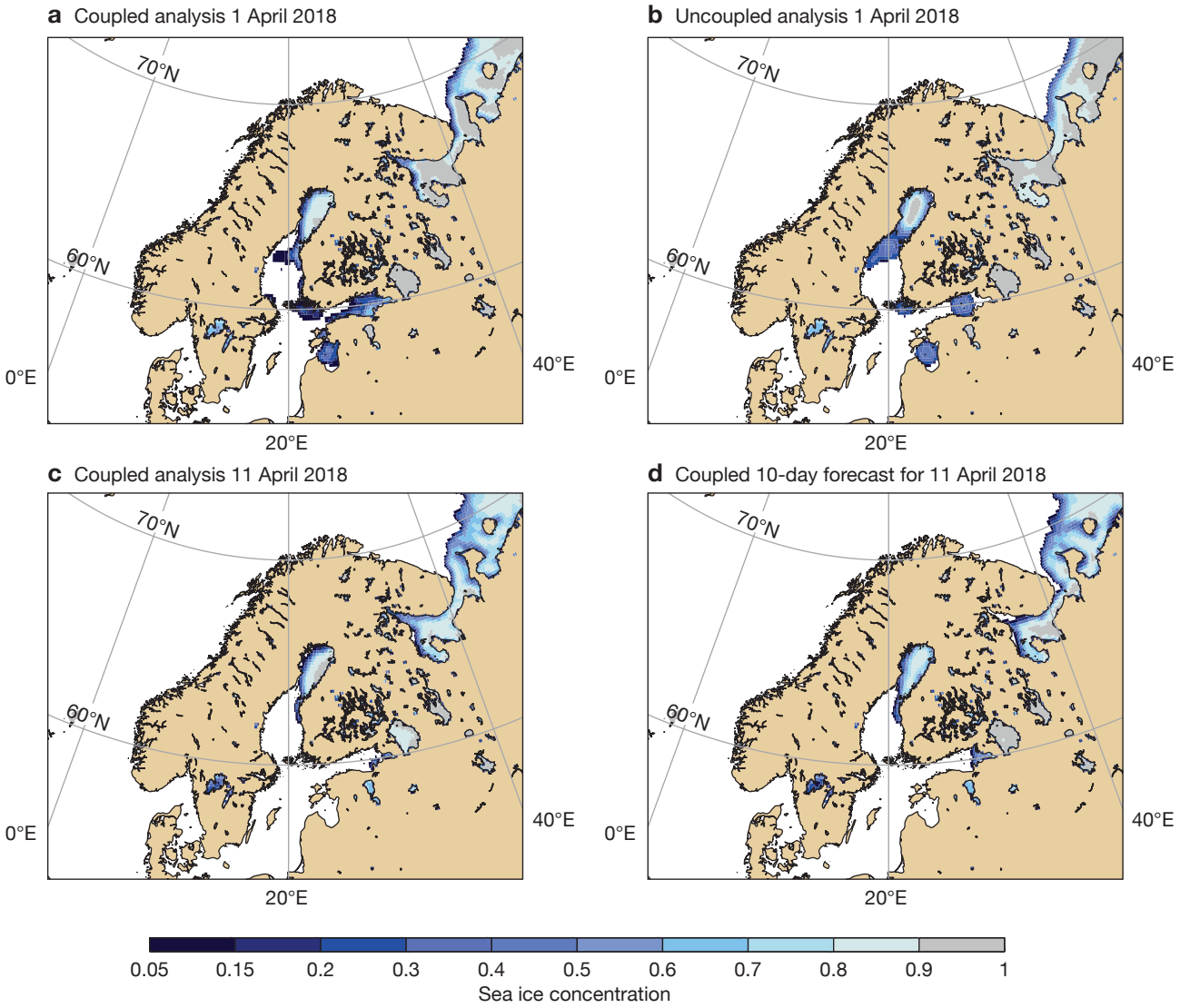

Figure 2 Performance of HRES sea ice concentration predictions with dynamic sea ice. The plots show (a) the HRES coupled analysis of sea ice concentration based on OCEAN5 for 1 April 2018, (b) the HRES uncoupled analysis of sea ice concentration based on OSTIA for 1 April 2018, (c) the HRES coupled analysis for 11 April 2018 and (d) the HRES coupled 10-day forecast for 11 April 2018.

Sea ice concentration can have a strong impact on predictions of local 2-metre temperature, although the size of the impact depends on how the surface fluxes are altered by local meteorological conditions (e.g. the overlying atmospheric temperature) and the concentration: where concentrations are high, the heat flux from the ocean to the atmosphere is significantly reduced. To illustrate this, Figure 3 shows the difference in temperature and sea ice concentration between 24-hour high-resolution forecasts with and without ocean–sea-ice–atmosphere coupling. The differences in predicted temperature in the Gulf of Bothnia of up to 6°C can largely be attributed to the differences in sea ice concentration. The size of the changes in 2-metre temperature also depends on the large-scale meteorology. For example, the temperature differences in the Gulf of Finland are not large in the forecasts shown, but they become more pronounced at longer time ranges.

Opening in Greenland ice

On 24 February 2018, there was a sizeable opening in the sea ice concentration near Cape Morris Jesup in north-east Greenland (see satellite image in Figure 4d). In winter, this can be important for local temperatures as heat can be exchanged between the relatively warm underlying ocean and the cold overlying atmosphere. The opening was established over the course of a week. The event was interesting because it was mainly driven by advection of the sea ice off the coast rather than local heating. Figure 4 shows the coupled HRES forecast with different lead times initialised on 18 February, which captured the event. In addition to predicted sea ice concentration, it shows the preceding 24-hour mean 10 m wind field. Initially sea ice concentration is high even at the coast (Figure 4a), by 21 February the predicted opening has increased slightly (Figure 4b), and

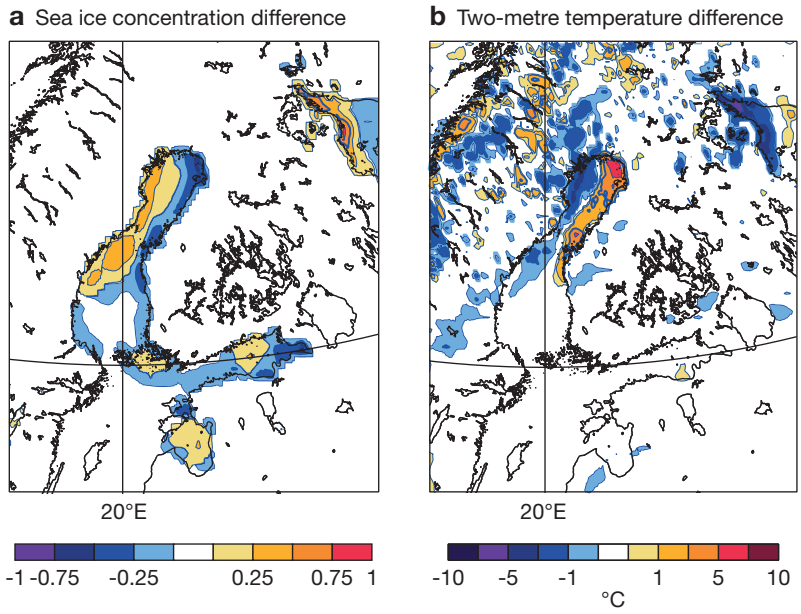

Figure 3 Difference between uncoupled and coupled 24-hour HRES forecasts for 2 April 2018 00 UTC (uncoupled minus coupled) for (a) sea ice concentration and (b) 2-metre temperature.

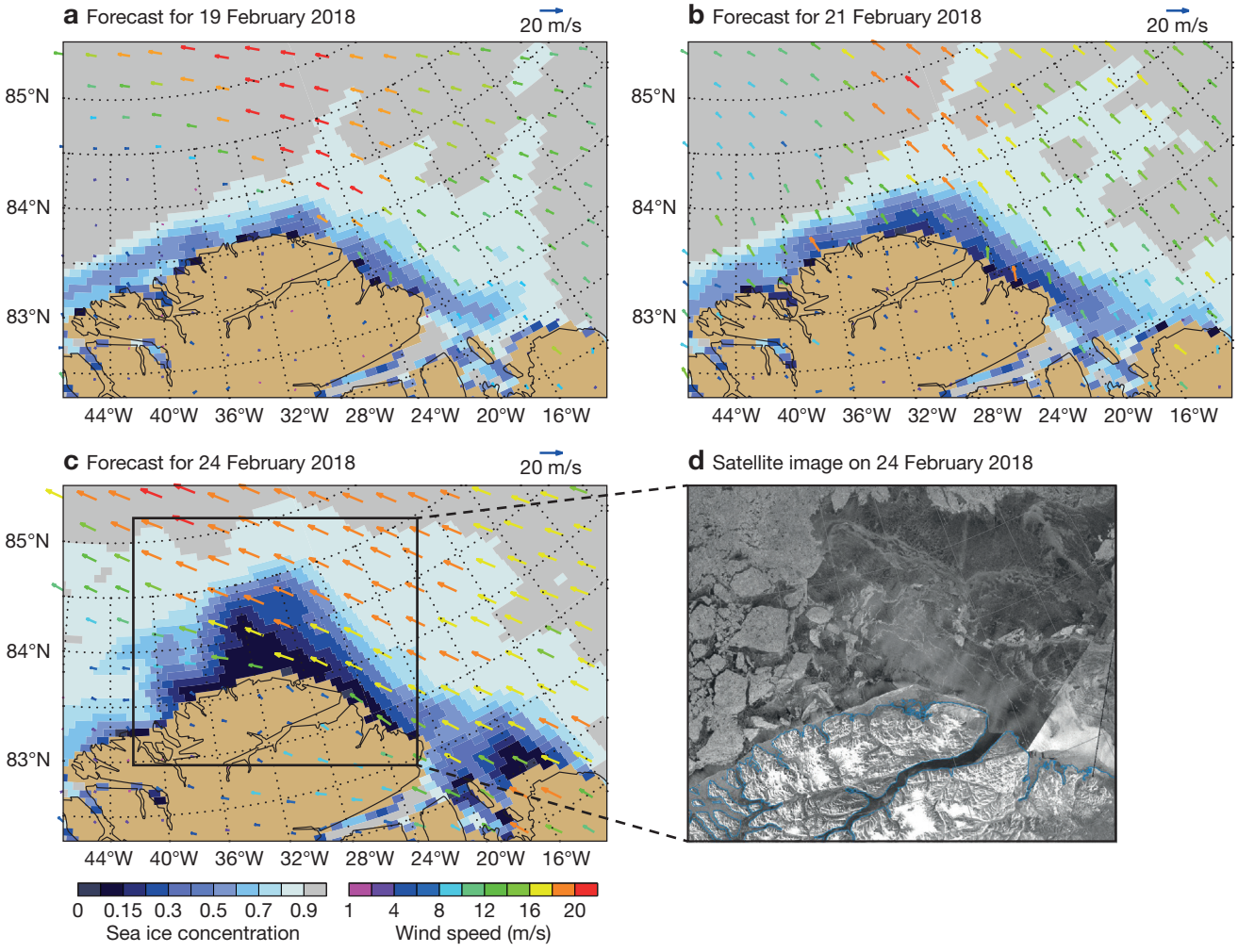

Figure 4 Evolution of sea ice concentration and the preceding 24-hour mean 10-metre wind field for forecasts initialised on 18 February 2018 and valid on (a) 19 February, (b) 21 February and (c) 24 February. Panel (d) shows the Synthetic Aperture Radar (SAR) image from the Sentinel-1B satellite for 24 February around Cape Morris Jesup. (Satellite image: European Space Agency via Danish Meteorological Institute)

it continues to grow to its maximum size on 24 February after strong winds the previous day (Figure 4c).

Sea ice loss in the Bering Sea

This year the maximum sea ice extent was marked by relatively low sea ice in the Bering Sea and relatively extensive sea ice in the Sea of Okhotsk compared to recent climatology. Here we analyse the forecast taken from the monthly forecast system initialised around the day of the maximum sea ice extent for the Arctic, 12 March 2018. Figure 5a shows the control forecast analysis of the sea ice concentration for that day. Figure 5d shows the analysis on 3 May. The Bering Sea was nearly ice free by then. The sea ice extent at that time was the lowest ever recorded in the region for this time of year. In Figure 5b we show the 45-day ensemble forecast for 3 May. We see that there is a large spread in the Bering Sea, and clearly not all members are predicting that the region would have such a large loss of ice. Figure 5c shows an example of one of the ensemble members which captured the low sea ice extent in the Bering Sea by the start of May.

Sea ice prediction performance

Differences between OSTIA and OCEAN5 analyses pose a difficulty when verifying the performance of the sea ice model. Using one or the other of the analyses will favour either the uncoupled or the coupled model. For example, low sea ice concentrations are not present in the OSTIA analysis due to the removal of low concentrations in the preprocessing of the product for use in the uncoupled HRES, whereas OCEAN5 and the coupled model contain ice concentrations from 0 to 100%. Work is ongoing to develop appropriate verification measures for sea ice. To look at broad model performance, we show comparisons between coupled and uncoupled forecasts verified against the OSTIA analysis from the uncoupled system. If anything, this penalises the coupled forecasts more. First we consider the change in bias over the course of the forecast.

Figure 6 shows the growth in sea ice concentration bias with increasing forecast lead time for the northern hemisphere for the four seasons. In all seasons, the growth in bias is slower in the coupled model than in the uncoupled model. This highlights again why persisting the ice field is not an appropriate assumption. In winter, the coupled model bias change is opposite in sign to the uncoupled model bias change, showing that the coupled model tends to form ice more rapidly than observed. The difference between the uncoupled and coupled growth in bias is greatest in summer and smallest in winter. This is consistent with the persistence measure in Figure 1.

We next consider the spatial accuracy of the sea ice model for each season using the difference in root-mean-square error (RMSE) between coupled and uncoupled high-resolution forecasts. We would hope that the use of the sea ice model reduces the RMSE. Figure 7 shows the difference in RMSE at forecast day 10, but we see the same patterns emerging early in the forecast. The dynamic sea ice model shows a general reduction in the RMSE of Arctic sea ice concentration from days 3 to 4 for all seasons.

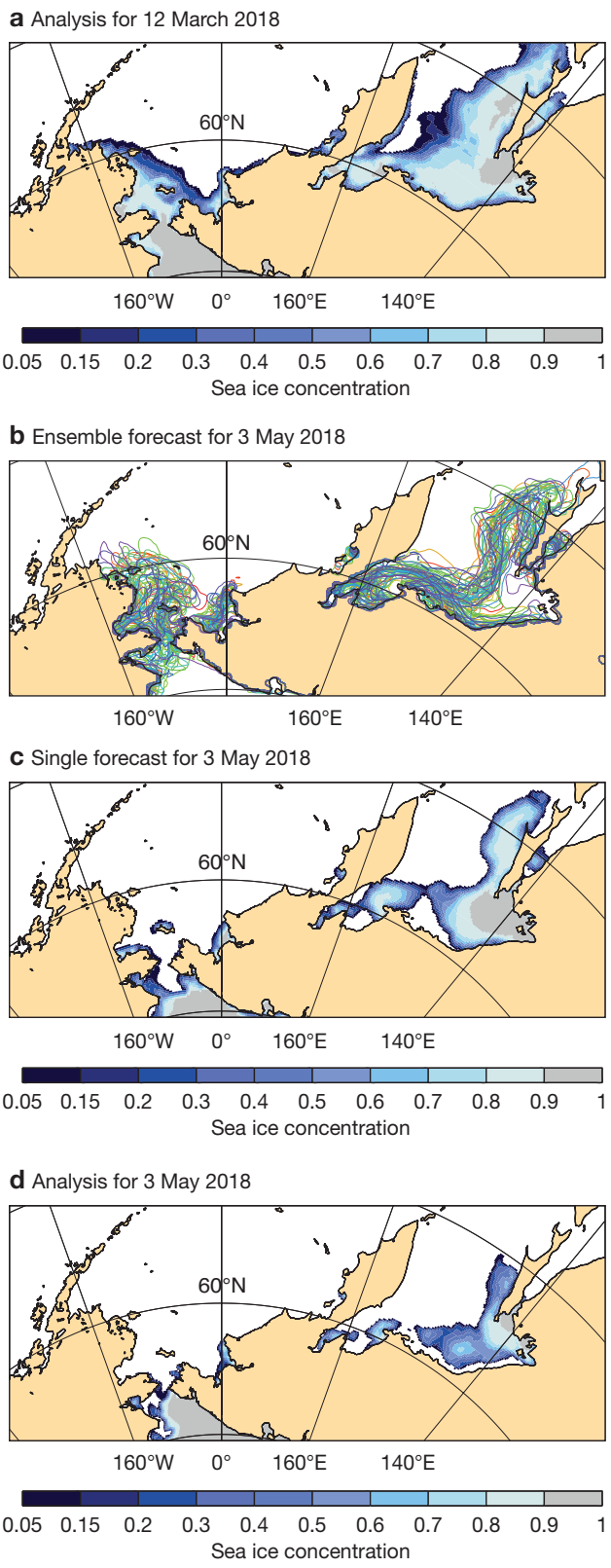

Figure 5 These maps of the Bering Sea and Sea of Okhotsk areas show (a) the analysis of sea ice concentration for 12 March 2018, (b) an ensemble spaghetti diagram for the sea ice edge from a forecast for 3 May 2018 initialised on 12 March 2018, (c) a single ensemble member prediction of sea ice concentration from the same forecast and (d) the analysis of sea ice concentration for 3 May 2018.

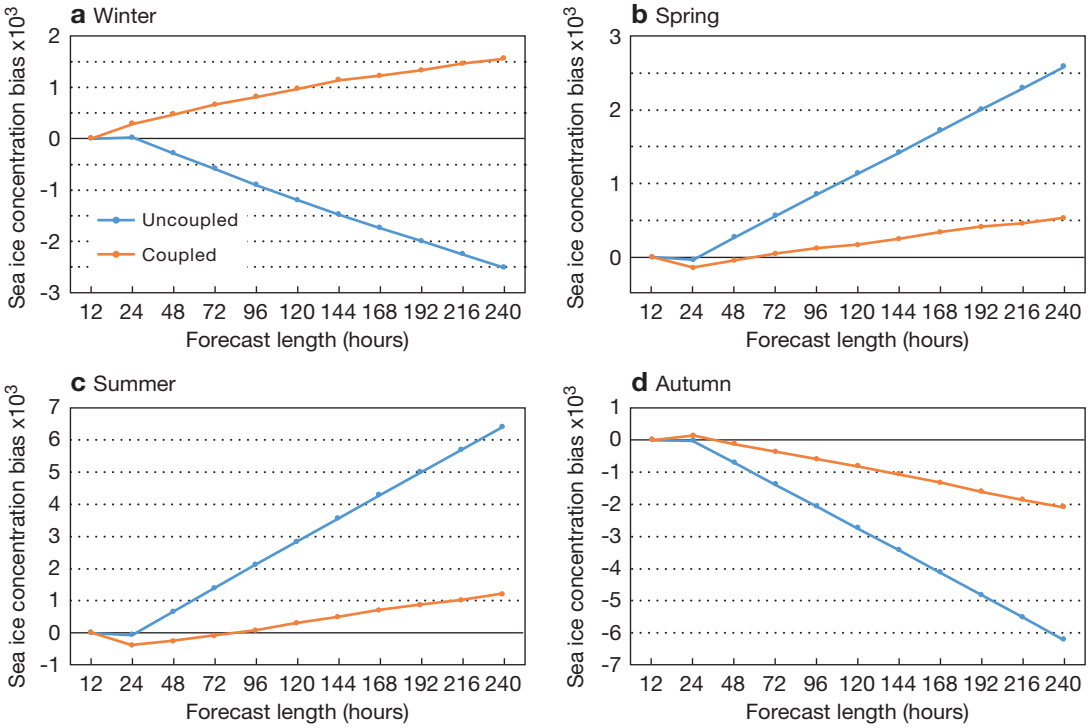

Figure 6 Sea ice concentration bias (minus initial bias) by forecast period for the northern hemisphere in (a) winter (December–January–February), (b) spring (March–April–May), (c) summer (June–July–August) and (d) autumn (September–October–November).

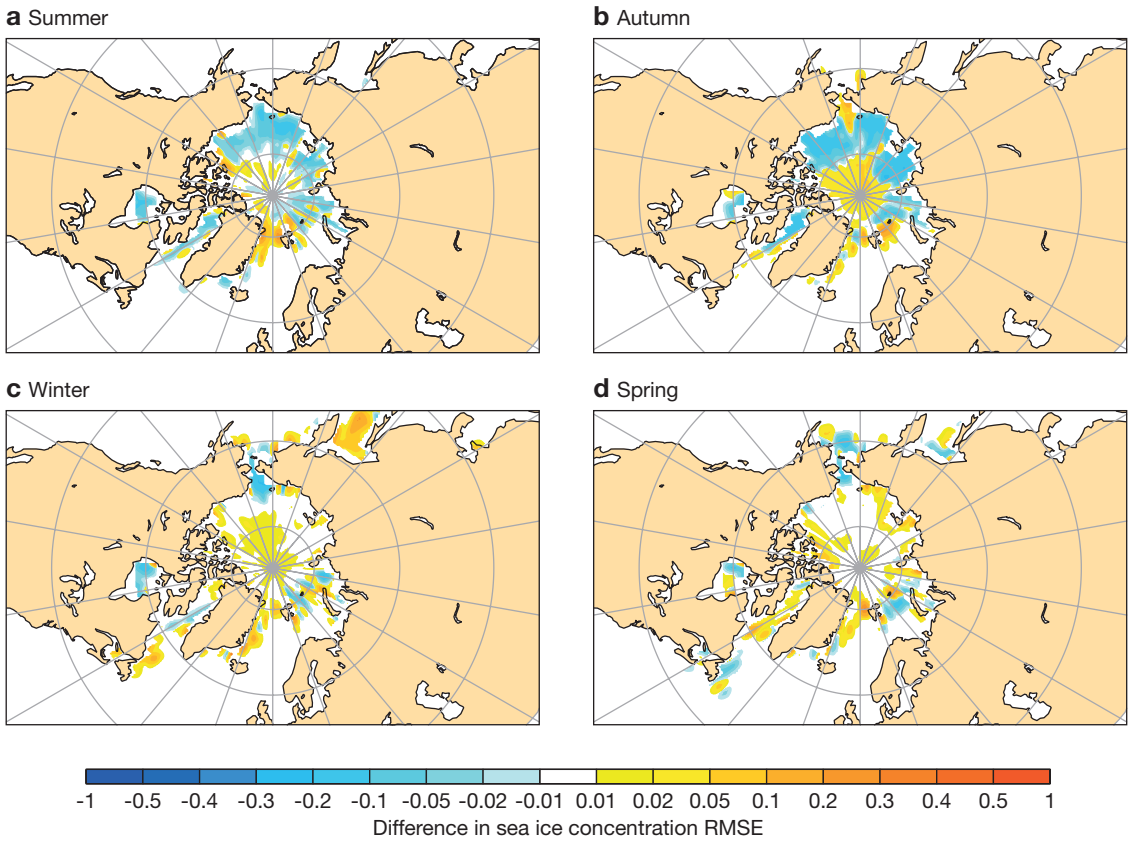

Figure 7 Difference in sea ice concentration RMSE for coupled 10-day HRES forecasts and 10-day HRES forecasts with a persisted ice field (coupled minus persisted), verified against OSTIA for (a) summer (June–July–August), (b) autumn (September–October–November), (c) winter (December–January–February) and (d) spring (March–April–May).

For summer and autumn, when the persistence assumption is particularly poor, we see improvements from day 2. There are regions where the sea ice model does not show an improvement over persistence. In the central Arctic, this is explained by the verifying analysis, which has complete concentration in the pack ice, whereas the ice model accounts for leads (narrow areas of open water or very thin ice). There are also areas sensitive to SST biases in the ocean model, in the North Atlantic. As expected, the greatest reduction in RMSE is in the summer and autumn, when the ice field changes more rapidly than in winter and spring.

Impact on atmospheric forecasts

The case studies have highlighted how the coupled system allows us to predict the evolution of the sea ice concentration itself. They have also shown that dynamic sea ice leads to local changes in 2-metre temperature forecasts. Another element of interest is the effect of using the dynamic sea ice model on global or hemispheric forecast scores. The first implementation of the sea ice model was within the ensemble system used for medium-range and monthly forecasts. For these forecasts, the effect of implementing the sea ice model on large-scale scores has been shown to be largely neutral. At weeks 3 and 4 there is an improvement in the large-scale circulation in the lower atmosphere and also in 2-metre temperature, but this is not significant. Analysis is ongoing to assess the impact of using the sea ice model on large-scale HRES forecast scores.

Next steps

We have implemented a relatively simple sea ice model which is able to capture the evolution of the sea ice concentration. Work is under way to develop the coupling of the sea ice component and implement a more sophisticated sea ice model, which should improve the prediction of the sea ice evolution, particularly on the long-range time scale.

FURTHER READING

Donlon, **C. J.**, **M. Martin**, **J. Stark**, **J. Roberts-Jones**, **E. Fiedler** & **W. Wimmer**, 2012: The Operational Sea Surface Temperature and Sea Ice Analysis (OSTIA) system. *Remote Sensing of Environment*, **116**, 140–158.

Fichefet, **T.** & **M. A. Morales Maqueda**, 1997: Sensitivity of a global sea ice model to the treatment of ice thermodynamics and dynamics. *Journal of Geophysical Research*, **102**, 12,609–12,646.

Zhang, **J. R.**, **R. Lindsay**, **A. Schweiger** & **I. Rigor**, 2012: Recent changes in the dynamic properties of declining Arctic sea ice: A model study. *Geophys. Res. Lett.*, **39**, L20503, doi:10.1029/2012GL053545.

doi:10.21957/73kl5120nb

Indian Ocean winds: changes and challenges

KATIE LEAN, NIELS BORMANN

On 2 March 2017, the geostationary satellite Meteosat-8 became the operational Indian Ocean Data Coverage (IODC) service in the ECMWF data assimilation system. With effect from that date, Atmospheric Motion Vectors (AMVs) and All Sky Radiances (ASRs) from the second-generation Meteosat-8 replaced the equivalent products from the retiring, first-generation Meteosat-7 satellite. AMVs and ASRs provide important information about wind and water vapour, respectively. Experiments have shown that assimilating the new data brings increased benefits compared to using Meteosat-7. However, they have also uncovered an area confined to the centre of the Indian Ocean at lower heights (around 850 hPa) where the benefit of the AMVs is less clear, due to a combination of model biases, suspected height assignment problems and difficulties in forecast verification.

A subsequent, more in-depth investigation of Indian Ocean AMVs considered other satellites providing good coverage. Meteosat-8 was compared with Indian National Satellite - 3D (INSAT-3D) and China's Feng-Yun - 2E (FY-2E) to consider their relative benefits or limitations. Despite different data quality characteristics, the impacts on the forecast from the different satellites were surprisingly consistent. This work also presented an opportunity to look more closely at the problematic low-level area over the ocean. The situation was revealed to be complicated with challenges for the model but also suspicious behaviour in the AMVs, in particular potentially too little variation of wind speed with height. Height assignment is a topic of great interest in the AMV community and the work presented here motivates a wider investigation and collaboration with AMV producers and other data users.

Meteosat-7 and Meteosat-8 compared

This is an active time for changes in geostationary satellites. Over the past three years, four out of the five geostationary satellites assimilated at ECMWF have been upgraded to a newer satellite. In most cases this also meant a newer generation of imaging instrument from which the AMVs are derived (see Box A for more details on the current use of AMVs). Failing to replace any of these satellites would mean a substantial gap in coverage. After a drift in orbit position to 41.5°E to focus on the Indian Ocean, Meteosat-8 was the natural choice to succeed Meteosat-7, which was at 58°E before retiring in March 2017. All Meteosat satellites are

Current AMV use at ECMWF

A

AMVs are derived by tracking cloud or water vapour features in sequences of visible or infrared imagery from geostationary or polar-orbiting satellites. The observed cloud motions are assigned to a representative height, usually an estimate of the cloud top at higher levels, which is also derived from the satellite imagery. AMVs are an important source of tropospheric wind information. At ECMWF, AMVs are currently assimilated from seven polar orbiting satellites and five geostationary satellites while five further satellites are monitored. Typical coverage of assimilated AMV data for a 12-hour assimilation cycle (12 UTC on 22 May 2018) is illustrated in the figure below.

Recently, various satellite agencies have made changes to their key operational geostationary satellites, in many cases moving to a newer generation of satellite. This has led to changes (completed or in progress) to all five geostationary satellites used at ECMWF, resulting in moving from:

- MTSAT-2 to Himawari-8 (March 2016)
- Meteosat-7 to Meteosat-8 (March 2017)
- Meteosat-10 to Meteosat-11 (February 2018)
- GOES-13 to GOES-16 (May 2018)
- And in the coming months the last remaining older generation satellite, GOES-15, will be replaced by GOES-17.

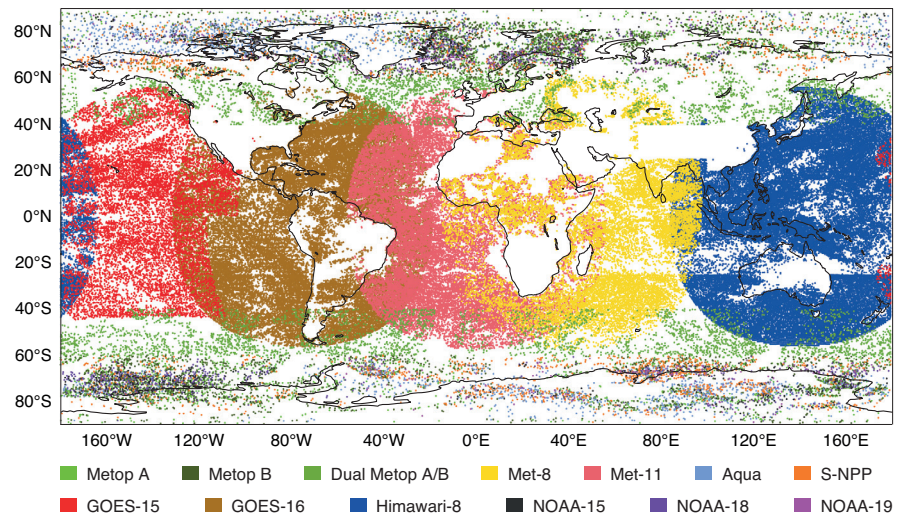

Typical AMV data coverage for a 12-hour assimilation cycle (12 UTC on 22 June 2018).

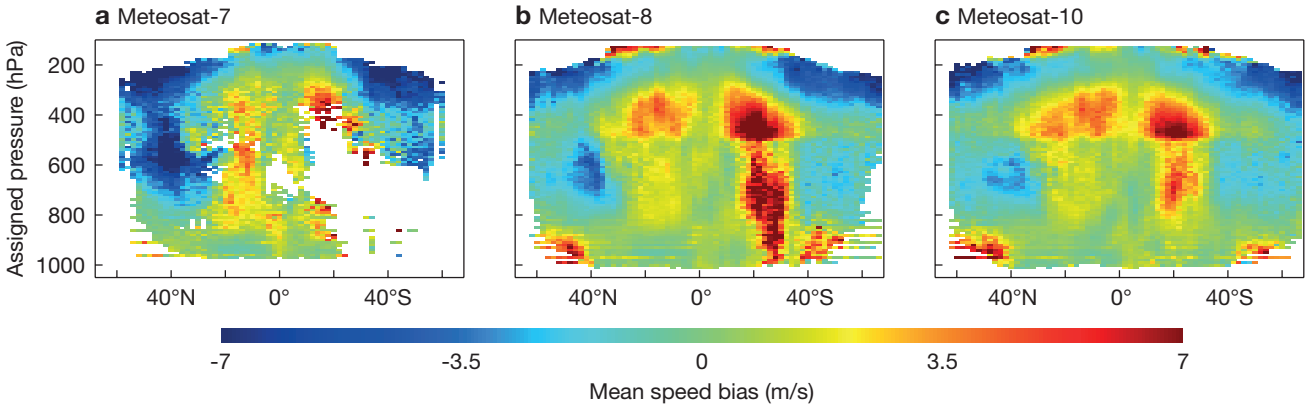

Figure 1 Distribution of speed bias by latitude and assigned pressure level for (a) Meteosat-7, (b) Meteosat-8 and (c) Meteosat-10. The Meteosat-8 statistics are improved over Meteosat-7 and reassuringly similar to Meteosat-10. Data are from the infrared channel over the period 21 October to 24 November 2016. They were passed through basic quality screening before binning (2° latitude x 10 hPa boxes). Boxes containing fewer than 20 AMVs are left blank.

operated by the European Organisation for the Exploitation of Meteorological Satellites (EUMETSAT).

The first step in assessing Meteosat-8 focused mainly on using the differences between observations and the model background (a short-range forecast) to diagnose the data quality. We refer to these differences as background departures. While looking to confirm an improvement from its predecessor, Meteosat-7, Meteosat-8 coverage also has significant overlap with the adjacent geostationary satellite at the 0° orbit position, Meteosat-10 at the time of testing. Meteosat-8 and Meteosat-10 are same-generation satellites, so similar results between the two are expected. It is also worth noting that in moving to a more advanced imaging instrument, the number of AMVs increases by around an order of magnitude from Meteosat-7 to Meteosat-8.

Statistics of background departures confirm an overall improvement when moving from Meteosat-7 to Meteosat-8. For instance, Figure 1 compares the speed bias for the AMVs derived using the infrared imager channel for Meteosat-7, -8 and -10. Between Meteosat-7 and -8 there are some clear areas of improvement. An example is the reduction of the large negative speed biases at high levels in the extratropics, where the AMVs are slower than the model equivalent. Improvement is generally expected when moving to a newer generation of satellite. There is also a strong similarity between Meteosat-8 and -10, with patterns and magnitudes of values very close despite the satellites' slightly different fields of view. At the same time, Meteosat-8 and Meteosat-10 show relatively strong positive speed biases at mid-levels in the tropics, an area that has been found challenging for AMVs in the past. Mid-level tropical AMVs are therefore blacklisted in the present

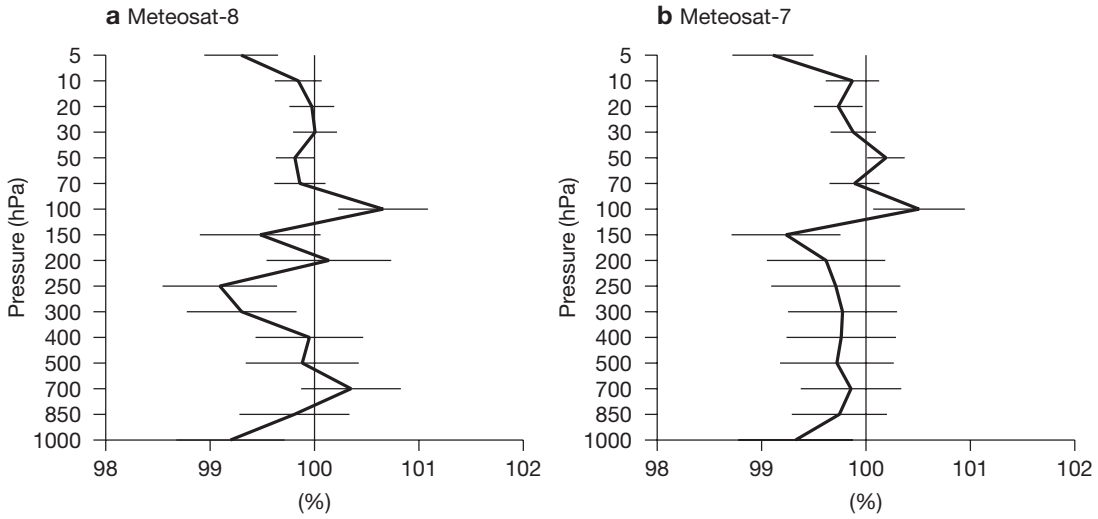

Figure 2 Normalised difference in standard deviation of radiosonde U-wind background departures between a control experiment without AMV assimilation (the 100% line) and an experiment with the assimilation of AMVs from (a) Meteosat-8 and (b) Meteosat-7. Significant reductions in standard deviation in the upper troposphere for Meteosat-8 and Meteosat-7 indicate improvements to the model background as a result of including IODC AMVs. Data are from the Indian Ocean region only for the period 1 November 2016 to 28 February 2017. Horizontal bars indicate 95% confidence intervals.

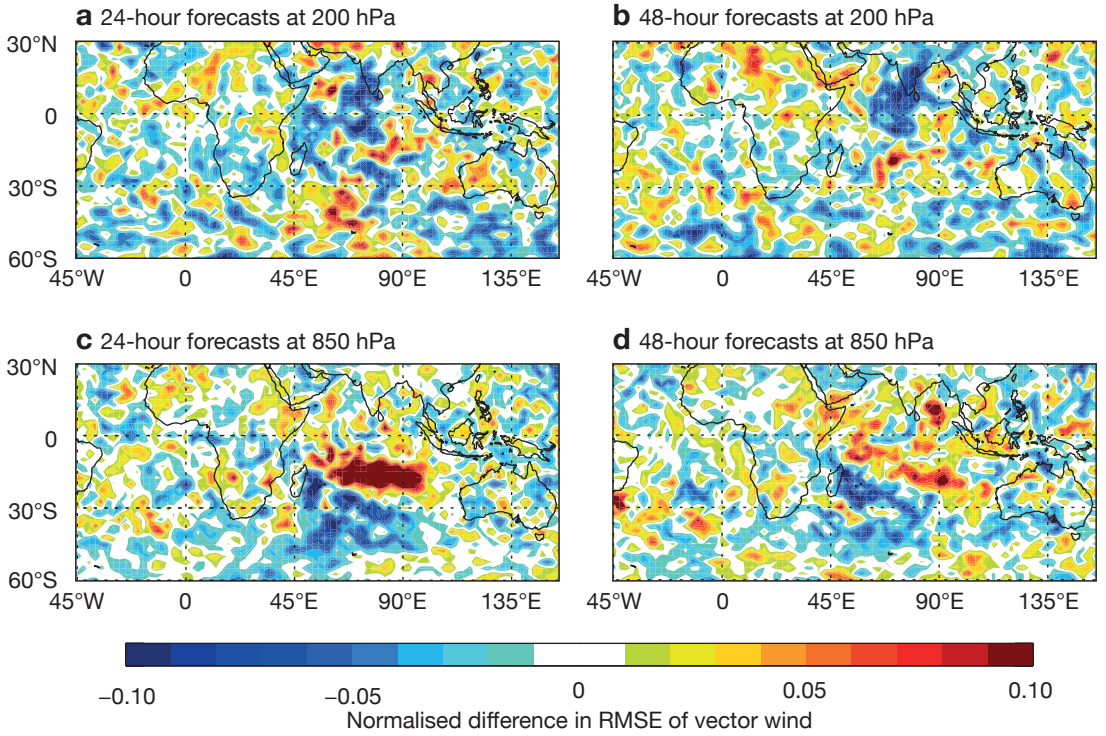

Figure 3 Normalised difference in root-mean-square error (RMSE) of the vector wind with and without Meteosat-8 AMV assimilation for vector wind forecasts (a) at 200 hPa 24 hours ahead, (b) at 200 hPa 48 hours ahead, (c) at 850 hPa 24 hours ahead and (d) at 850 hPa 48 hours ahead. Blue shading indicates a reduction in errors with AMV assimilation, red shading an increase. AMV assimilation notably reduces vector wind errors over parts of the Indian Ocean at 200 hPa but increases them in the central Indian Ocean at 850 hPa. The forecasts were verified against own analysis over the period 21 October 2016 to 7 March 2017.

assimilation of AMVs from Meteosat-10, and similar quality control appears advisable for Meteosat-8 as well.

After the initial data quality assessment, the new AMVs were tested in assimilation experiments to understand their impact on forecasts. The experiments used the 12-hour 4D-Var assimilation system at ECMWF with a reduced model resolution of TCo399 (55 km) and were run from 21 October 2016 to 7 March 2017. The control run used the same configuration but with no IODC AMVs actively used.

The large-scale hemispheric impacts for the use of IODC AMVs are relatively small and close to neutral, but there are indications of localised forecast benefits over the Indian Ocean. For instance, comparisons between short-range forecasts and radiosonde observations in the region of the IODC coverage show better agreement at higher levels when AMVs from Meteosat-7 or Meteosat-8 are included in the data assimilation (Figure 2). The reduction in standard deviation values at 250 hPa and 300 hPa is significant (using 95% confidence intervals) for Meteosat-8. These heights coincide with a layer of high-density AMVs. Consistent with this, analysis-based forecast verification also suggests a reduction in the error in the vector wind field at high levels over the Indian Ocean (Figure 3a,b). The feature is present for both Meteosat-7 and Meteosat-8 but more prominent and persisting into longer forecast lead times for Meteosat-8 (not shown). At low levels there is a localised feature showing apparent degradation at 850 hPa in the vector wind field when the

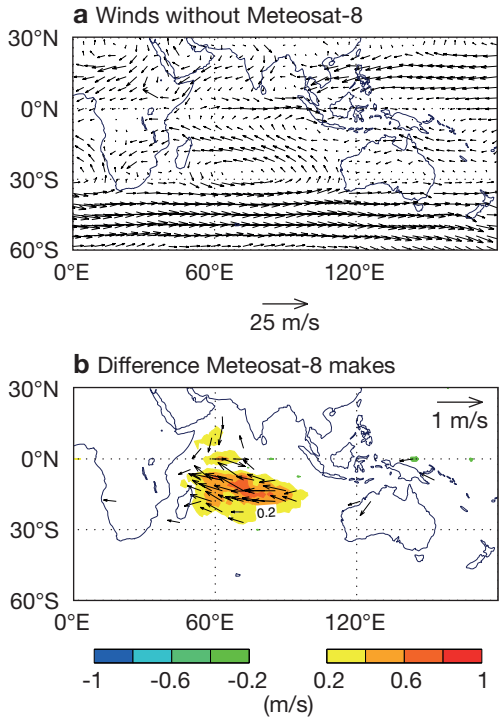

Figure 4 The charts show (a) the mean wind analysis field at 850 hPa without the assimilation of Meteosat-8 AMVs and (b) the difference in the mean wind analysis with and without Meteosat-8 AMVs. Plot (b) shows the strengthening of the westward flow when Meteosat-8 AMVs are included in the data assimilation. The experiments cover the period 21 October to 21 December 2016.

forecasts from each experiment are verified against each experiment's own analysis (Figure 3c,d). The feature is most prominent in the early weeks of the experiment and appears to weaken in the latter half (not shown). The main influence of the AMVs here is to increase the westward flow of wind in the analysis in the same area (Figure 4). The issue is further explored below following an evaluation of the data provided by other IODC satellites.

Comparison against other Indian Ocean satellites

After the successful move to Meteosat-8, the next aim was to evaluate other potential options for the IODC. At the time of the study, INSAT-3D, operated by the Indian Meteorology Department (IMD), and FY-2E, operated by the China Meteorological Administration (CMA), also had good coverage extending over the Indian Ocean. Refinements in the AMV derivation algorithms used at IMD and CMA have led to improved data quality in recent years, as seen in the Satellite Application Facility for Numerical Weather Prediction (NWP SAF) satellite data monitoring, so these two data sources may be viable providers of geostationary data coverage in this area.

Differences in the imaging instruments, in addition to each AMV production centre having a different technique for deriving the AMVs, lead to large variation in the number of AMVs. For example, for the infrared channel available on all three satellites, the number of AMVs derived on FY-2E and INSAT-3D is around half the number from Meteosat-8. In addition, the distribution of the AMVs and their data quality characteristics are also affected. For instance, Meteosat-8 and FY-2E show more similarity in the patterns of root-mean-square vector difference (RMSVD) values, whereas INSAT-3D generally shows similar or in many cases better agreement with the model background (Figure 5). However, the height assignment and quality control process used at IMD is more strongly dependent on model forecast information, so this result may reflect the extent to which the global US model (GFS) short-range forecast used in this process and ECMWF model data agree.

To test the impact of using data from the respective satellites on the forecast, experiments were run in which each satellite was assimilated individually against a control experiment without any IODC satellite AMV assimilation for the period 1 December 2016 to 30 June 2017. Data selection criteria were broadly similar for the three satellites, although specific data characteristics motivated some modifications. For instance, more mid-level water vapour winds were excluded for INSAT-3D AMVs, as these do not distinguish between clear and cloudy scenes.

Despite the differences in AMV numbers and data characteristics, the impacts of the three satellites are surprisingly similar. For all three satellites, comparisons against conventional data suggest small improvements for short-range forecasts in the IODC area, similar to those shown for Meteosat-8 in Figure 2. In verification against own analysis, the high levels show positive impacts, more significant for INSAT-3D and FY-2E than for Meteosat-8, localised over the tropical Indian Ocean (Figure 6). At lower levels, there are also some reductions in error, particularly for INSAT-3D to the south of the equator. The degradation feature in Meteosat-8 at 850 hPa is not apparent in the other satellites.

The positive results for INSAT-3D and FY-2E are encouraging. They suggest that these satellites are viable sources for operational AMV coverage over the Indian Ocean, provided data provision is reliable. For now, however, we continue to use Meteosat-8 in the operational system. This is partly motivated by the additional availability of an All-Sky Radiance (ASR) product for NWP from Meteosat-8. This provides further significant benefit, as summarised in Box B. For any potential future IODC satellite, the valuable added positive impact of the ASR product should not be overlooked.

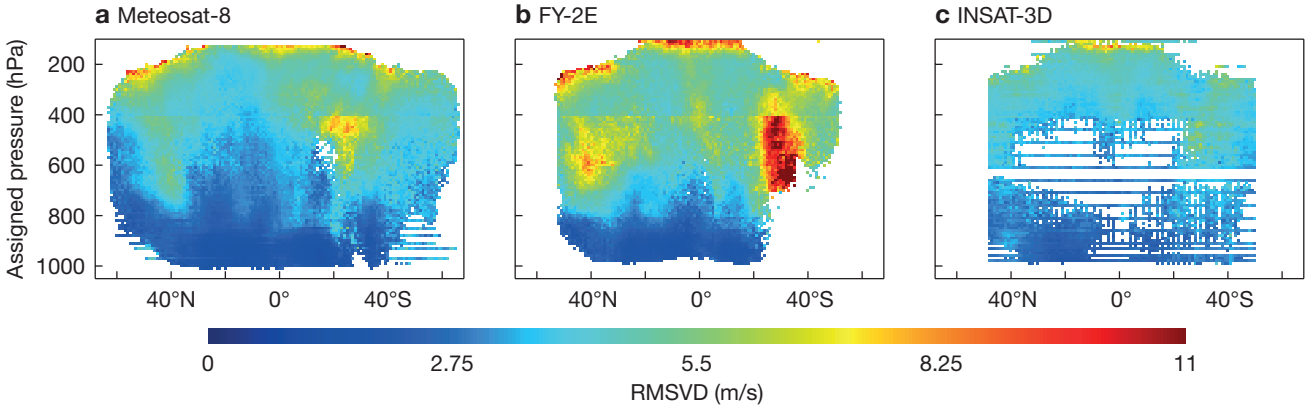

Figure 5 Distribution of the root-mean-square vector difference (RMSVD) between AMV-derived wind vectors and the model background by latitude and assigned pressure level for (a) Meteosat-8, (b) FY-2E and (c) INSAT-3D. The plots show similar patterns for Meteosat-8 and FY-2E while INSAT-3D shows better agreement with the model background. Data are from the infrared channel over the period 1 December 2016 to 15 January 2017. They were passed through basic quality screening before binning (1° latitude x 10 hPa), with boxes containing fewer than 20 AMVs left blank. Striping in INSAT-3D is due to a particular step in the height assignment that favours a set of regularly spaced pressure levels.

In the future, it would be interesting to consider the new Chinese FY-4A satellite as an additional or alternative source of Indian Ocean coverage. It carries a more advanced imaging instrument than FY-2E and the first infrared hyperspectral sounding instrument on a geostationary satellite. The availability of hyperspectral instruments represents an exciting development in the direct assimilation of radiances from geostationary orbit.

Challenges for low-level winds

As noted earlier, there is an area of apparent short-range forecast degradation at lower levels over the Indian Ocean when Meteosat-8 AMVs are assimilated. The area is associated with a westward wind which is made faster in the analysis by the addition of the Meteosat-8 AMVs. The experiments with INSAT-3D and FY-2E reveal that all three satellites have the same effect of increasing the zonal (east–west) wind in the tropics. This may indicate the presence of a model bias. However, for Meteosat-8 the change is larger (around 0.5 m/s compared to 0.2 m/s for INSAT-3D).

To investigate this aspect further, the mean forecast error (difference between forecast and analysis) in the wind field for different lead times was evaluated (not shown). This revealed an area coinciding with the degradation feature in which the mean forecast error of the U component increases with forecast lead time, indicating that the forecast winds become progressively slower compared to the analysis. This slow bias in the forecast approximately doubles over the ten-day period, suggesting a model bias in the area in question. When verifying against own analyses, the assimilation of the Meteosat-8 AMVs therefore results in a larger forecast error, as the slow model bias is in disagreement with the faster analysis. The evidence here points to model bias being at least partly responsible for the signal. However, while this feature is strong in the early part of the experiment period, from February/March the signs of model bias are no longer present. Nevertheless, the degradation feature persists and the Meteosat-8 AMVs continue to effect a relatively large change to the mean wind analysis (not shown).

The next step was therefore to try to determine whether the increase in the analysis wind speed is correct by investigating the possibility of AMV biases. To better understand the structure of the low-level AMVs, vertical profiles of the wind speed and number density were studied using data taken only from a box covering the affected area (50–100°E, 5–25°S). Figure 7 shows that the shape of the profile of the U component is very similar between Meteosat-8 and FY-2E. In both cases there is very little variation in height while the model background wind, sampled at the AMV locations of the respective satellites, suggests more wind shear. Although there is good agreement with Meteosat-8, FY-2E has relatively few winds in the region, which may result in any signal being too weak to show in the verification. INSAT-3D agrees more with the model winds, but this may be due to the higher dependence on forecast model data in the derivation process.

Additional benefit from ASRs

B

The All-Sky Radiance (ASR) product uses radiances from channels particularly sensitive to water vapour at around 300–500 hPa in a combination of clear-sky and overcast conditions. Typically the assimilation of water vapour channel radiances has greatest impact on humidity and related fields. ASRs often also indirectly impact wind fields: physical parametrizations and model equations within 4D-Var are used to generate changes in the wind in order to advect observed features in humidity. These are broader-scale motions with changes limited mostly to clear sky situations and the mid-troposphere. In contrast, AMVs are capable of capturing small-scale motions, are located in cloudy regions and are generally restricted to layers in the high (200 hPa) and low (850 hPa) troposphere. For the IODC satellites, the AMVs show little influence on the humidity fields. The inclusion of ASRs from Meteosat-8 gives clear added benefit in the fit of independent humidity-sensitive observations to the model background compared to AMVs alone on INSAT-3D or FY-2E. This is illustrated in the example below showing the reduction in the standard deviation of the brightness temperature background departures for the humidity sounding channels (18–22) of the Advanced Technology Microwave Sounder (ATMS) when including Meteosat-8 ASRs. Here, the effects are large enough for the reduction in standard deviation to be significant even when verifying over much larger areas than just the region covered by the IODC satellites.

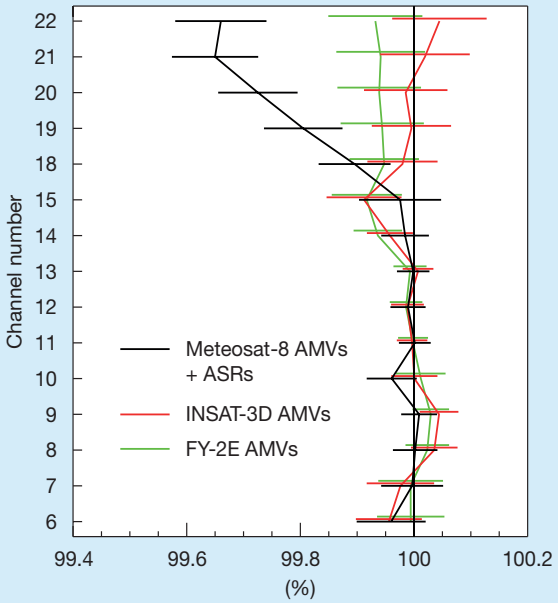

Normalised difference in global standard deviation of brightness temperature background departures between an experiment without the assimilation of AMVs or ASRs (the 100% line) and experiments in which AMVs are assimilated from INSAT-3D and FY-2E, and AMVs and ASRs are assimilated from Meteosat-8.

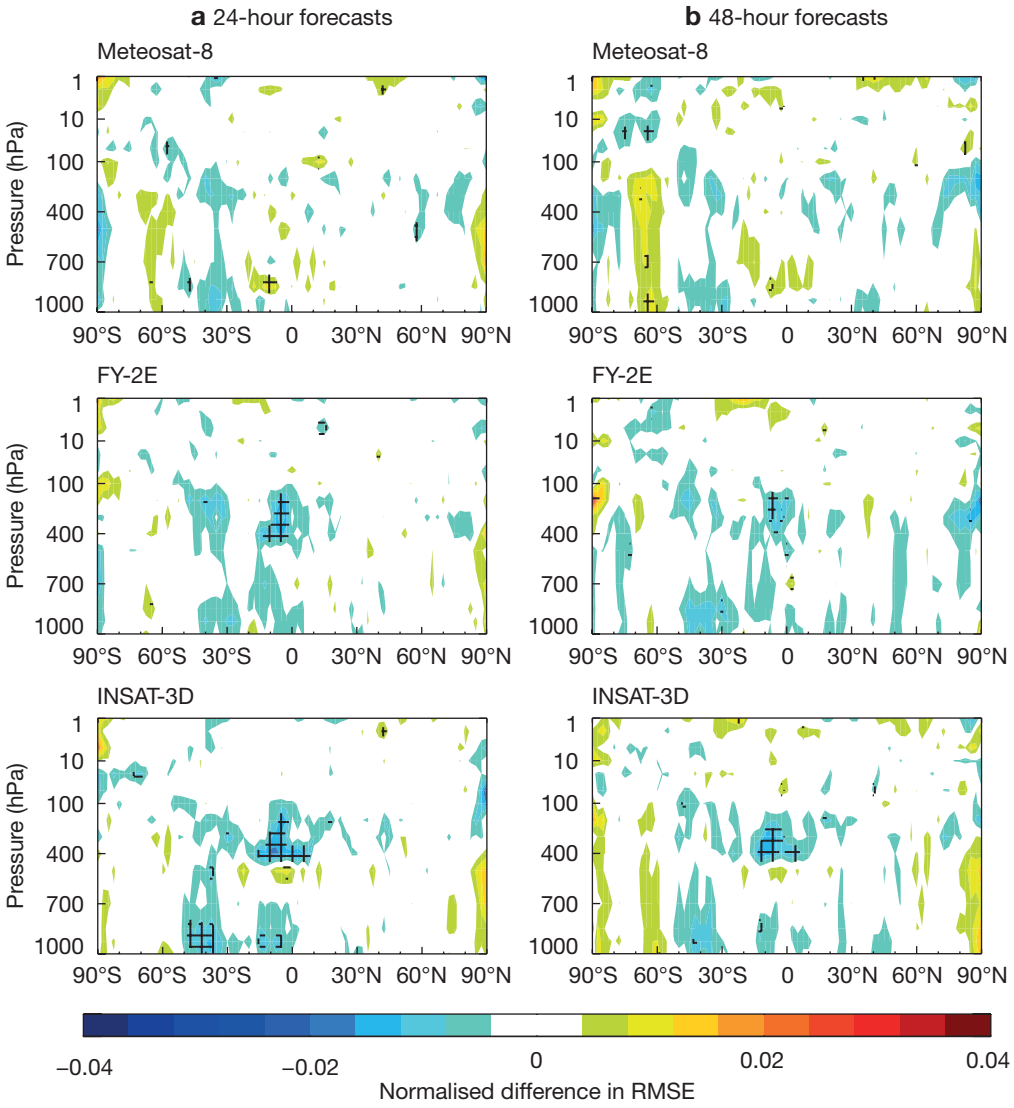

Figure 6 Distribution of differences in vector wind RMSE verified against own analysis between forecasts with and without the assimilation of AMVs, normalised by the RMSE of forecasts without AMV assimilation, for (a) 24-hour forecasts and (b) 48-hour forecasts. Cyan and blue colours in the tropics show reductions in error as a result of including IODC AMVs. Data are from the period 1 December 2016 to 30 June 2017 and hatching indicates significance at the 95% level.

Unfortunately, this area of the ocean is very sparsely covered by conventional wind observations, which would allow an independent assessment. Nevertheless, profiles from two radiosonde sites (Cocos Island and Réunion Island) on the periphery of the affected area both support similar variation with height as exhibited by the model. This suggests that the AMVs might have a height assignment error where the faster winds are being placed too high, or that the height assignment cannot reliably distinguish different levels between 700 and 950 hPa. While the discussion here on the low-level winds has focused on the Indian Ocean, profiles of winds from Meteosat-10 in the tropical Atlantic Ocean show similar characteristics, indicating that it is potentially a wider problem.

Our analysis therefore suggests that the apparent degradation in the short-range forecasts of low-level wind over the Indian Ocean is the result of a combination of model bias for at least some parts of the experiments and deficiencies in the height assignment of the low-level AMVs in the area. The feature of apparent degradation is confined to short-range forecasts, which are difficult to verify in this area, and it does not appear to negatively affect medium-range forecasts. We therefore consider that it is still beneficial to continue the assimilation of these low-level AMVs in an otherwise poorly constrained area for wind.

Future work on low-level height assignment

Subsequent to the investigation presented here, the issue with the low-level height assignment has been added to the features requiring study in the latest AMV monitoring report compiled for the NWP SAF (*Warrick & Cotton*, 2018). There has so far been interest from EUMETSAT, the UK Met Office and the German national meteorological service (DWD) to work together with ECMWF to understand the issue.

In the near-absence of conventional observations, other routes to gaining information about the AMVs could include comparing the height assignment of the winds, which typically uses the cloud top height, with cloud heights from Cloud-Aerosol Lidar and Infrared Pathfinder Satellite Observation (CALIPSO). The Multiangle Imaging SpectroRadiometer (MISR), which uses a stereoscopic

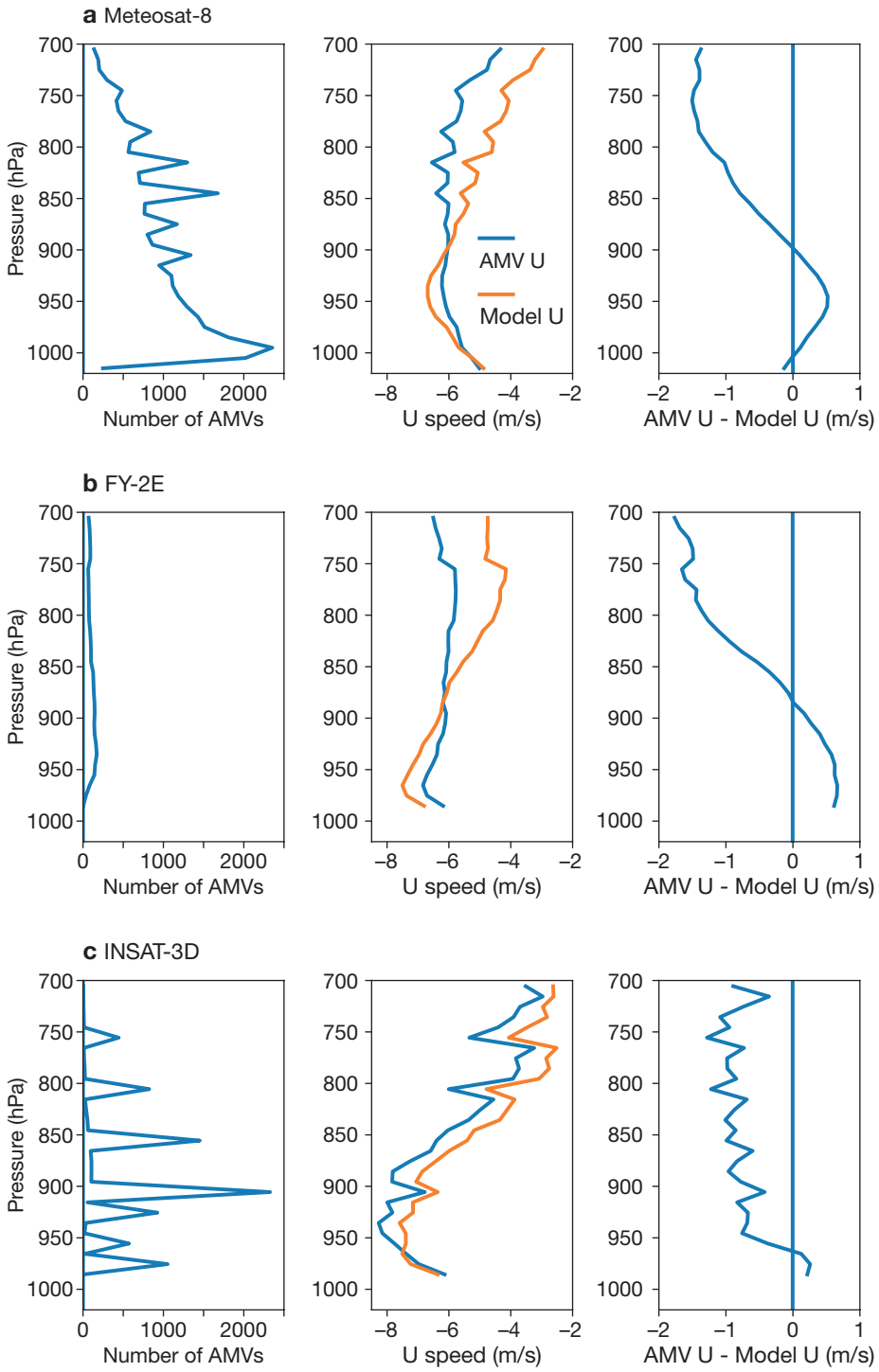

Figure 7 Mean of the daily vertical profiles of the number of observations, the U component of wind for AMV and model background wind sampled at the AMV locations, and the difference between AMV and model wind for (a) Meteosat-8, (b) FY-2E and (c) INSAT-3D. Here the model background is generated without assimilating any IODC AMVs. Data are from both infrared and visible channels over the period 1 to 31 December 2016 within the box 50–100°E and 5–25°S. Basic quality screening has been applied. Spikes in the profiles of Meteosat-8 correspond to inversion levels, where many more AMVs are assigned.

method to derive winds, may also give some insight into the heights and provide further information about the typical wind shear. In the future, the Aeolus satellite, capable of high-resolution vertical profiles of the wind, will allow an independent assessment. Looking into relationships between the AMV and model cloud parameters could also reveal more about any systematic differences.

Katie Lean's work is funded by the EUMETSAT Fellowship Programme.

FURTHER READING

Lean, **K.** & **N. Bormann**, 2018: Indian Ocean AMVs: Moving to Meteosat-8 and assessing alternative options. *EUMETSAT/ECMWF Fellowship Programme Research Report*, **No. 46**.

Warrick, **F.** & **J. Cotton**, 2018: NWP SAF AMV monitoring: the 8th Analysis Report (AR8). Available online at: *https://www.nwpsaf.eu/site/monitoring/winds-quality-evaluation/amv/amv-analysis-reports/*

doi:10.21957/83cs60nb21

Using ECMWF's new ensemble vertical profiles

CIHAN SAHIN, TIM HEWSON, SYLVIE LAMY-THÉPAUT, IVAN TSONEVSKY, UMBERTO MODIGLIANI, DAVID RICHARDSON

ECMWF has developed a new product to show the vertical structure of the atmosphere at a point in ensemble forecasts (ENS). In June 2018, the new product was incorporated into ECMWF's web-based chart-viewing applications, which include ecCharts, clickable web charts and the Dashboard, to use and assess. Users can now examine vertical profiles of the atmosphere anywhere across the globe, at 6-hour intervals, up to a lead time of 120 hours. These can provide considerable assistance with many forecasting challenges, such as predicting cloud layers, layers of instability, precipitation type, wind gust penetration to the surface, propensity for supercells to develop, etc.

The history of this initiative is that ECMWF forecast users have for many years been asking to see vertical profiles of the atmosphere at points, in various different formats. *Ihász & Tajti* (2011) demonstrated ways of doing this for the ENS over Hungary, but for ECMWF, whose products cover the globe, 'big data' challenges had precluded progress until now. The new products are designed to address the various user requirements, and they were demonstrated for the first time at ECMWF's user meeting (UEF) in June 2018. Initial feedback was very positive, and monitoring statistics collated since then have shown substantial uptake, but ECMWF would very much welcome further feedback and requests for changes from users. These will be used to shape future improvements.

Data choices

For ECMWF, the production and visualisation of vertical profiles from the ensemble posed many technical challenges. The first was dealing with the huge data volumes involved while at the same time providing a responsive interactive service. This required careful preparation of the raw ensemble data:

- deriving required parameters on carefully selected model levels from ensemble and deterministic model outputs for all selected lead times
- preparing suitable point databases that would provide retrieval and plotting of a vertical profile for any given point in an acceptable time frame (2 to 5 seconds).

To plot, say, a 10-day meteogram for a point is relatively straightforward: one only needs about 1,400 data values. To plot vertical profiles for the same time window potentially requires about 800 times more data! Coupled with the need to reference the whole globe at 18 km resolution, access can become very slow, and indeed the problem becomes intractable. This is a good example of a big data challenge where the derivation and presentation of information present in the raw data requires careful thinking. Our approach has been to ensure good performance by cutting down the amount of data used while preserving the most important aspects of the forecast. One option was to use only pressure level data. For winds this is acceptable. However, for thermodynamic variables we would have distorted the picture of the atmosphere as represented by the model. For example, critical information such as the presence of thin cloud layers beneath inversions would have disappeared, whilst unrealistic instabilities would have been created where the atmosphere in the model is actually stable. Instead we chose to show all available model levels up to about 700 hPa in order to retain everything in the all-important lower troposphere, then every other level from about 700 to 100 hPa, where structure is less critical, and to discard anything above about 150 hPa, which is of little relevance to surface weather. We have also limited lead times to 5 days. This is because there is less benefit in overlaying profiles from the increasingly disparate synoptic patterns one sees at longer lead times: the plots would just become confusing. Together these measures enabled an 80% reduction in data volume. This makes it possible to deliver a new set of ensemble profiles to the computer screens of users in around 3 seconds.

Visualisation

The second challenge was to show multiple profiles from ENS together in a meaningful way. We wanted to show the key variables measured by radiosondes (temperature, dewpoint, wind speed and wind direction) and also the critical relationships between those variables, such as dewpoint depression and vertical wind shear. Meanwhile ECMWF's Strategy calls for continued improvements in the prediction of severe weather. Whilst some convective hazards cannot yet be explicitly represented by the Integrated Forecasting System (IFS), ensemble vertical profiles can give very useful pointers on whether there is a risk of such hazards. In particular, CAPE (convective available potential energy) and CIN (convective inhibition) and their juxtaposition are of fundamental importance. The vertical profile chart layout has been designed with these considerations in mind. The charts now include four key components. These are illustrated in Figure 1, which shows a winter time case at day 5 near the Antarctic Peninsula:

- A thermodynamic diagram, in the current implementation a tephigram (top left), is used to show temperature and dewpoint ranges at different levels within ENS. Specifically we delineate, with differently shaded bands, the minimum, median and maximum, and the 25th and 75th percentiles of the temperature and dewpoint distributions at each level, in a way that mirrors the use of box-and-whisker plots on meteograms.
- A similarly styled panel (top right) is used to show the range of dewpoint depression values found on different model levels. In the same panel we also show wind flags from HRES at standard pressure levels. Showing them in this panel is not because winds relate directly to dewpoint depression but for plotting convenience.

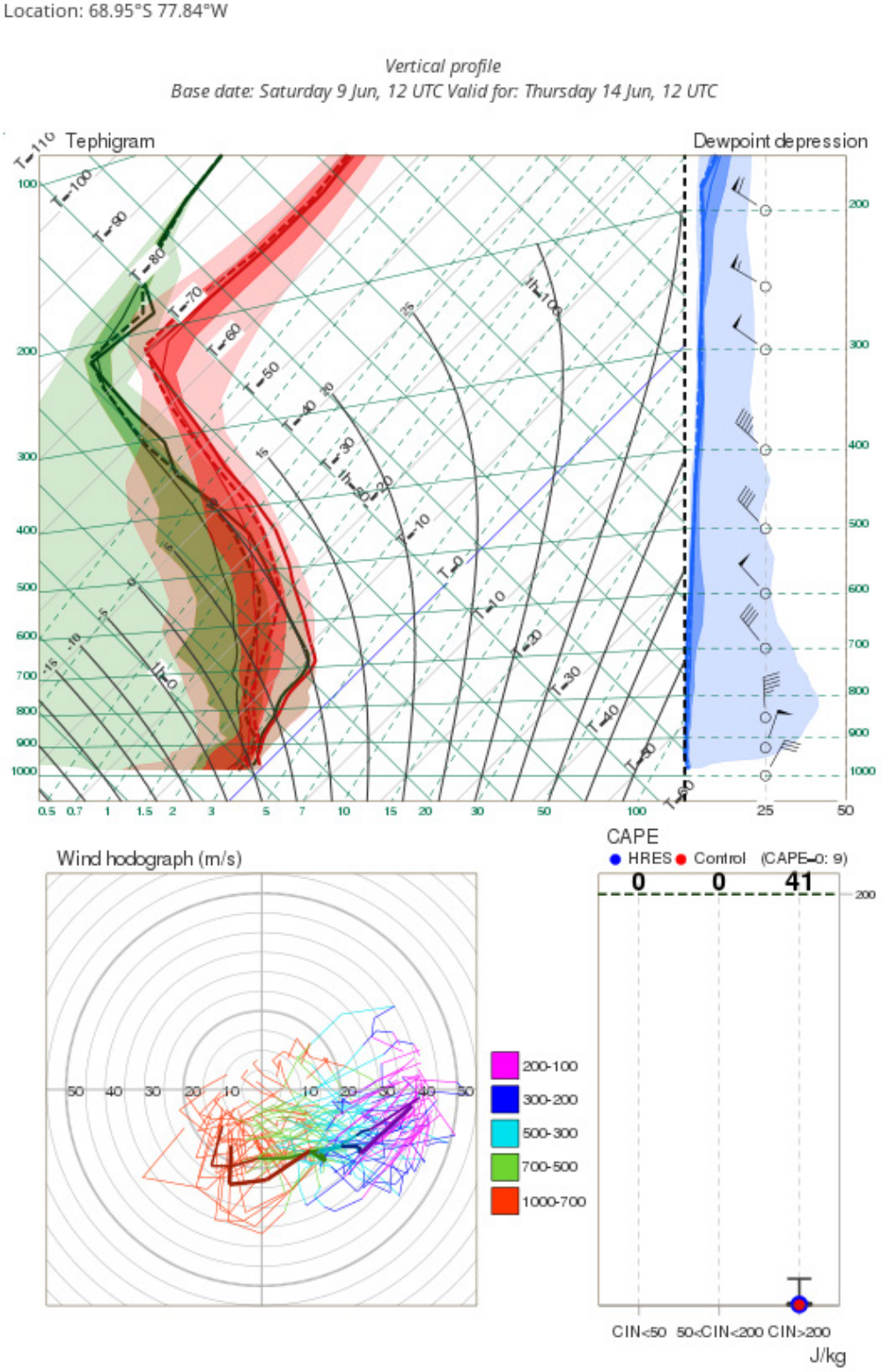

Figure 1 Example vertical profile chart for T+120h from the southern hemisphere winter. Some interesting features of this product are: (i) marked vertical wind shear in HRES and ENS, on the hodograph, implying thermal gradients and a front in the vicinity. Using standard techniques, one can visualise the frontal orientation and the approximate frontal speed of movement. (ii) HRES is something of an outlier solution, having more of an incursion of warmer air than virtually all ENS members at 700 hPa. (iii) Whilst most members are close to saturation through deep layers, which probably relates to the presence of a strong front, some have a very dry low to mid troposphere, probably because of the incursion of dry, cold Antarctic air poleward of any front. (iv) In this case most members (82% + HRES + Control) show very small, non-zero values of CAPE. It looks, based in part on the HRES and Control profiles, that this is elevated rather than surface-based instability, within the frontal cloud. Relatively high convective inhibition (CIN) would have to be overcome for this to be released, but forced dynamical uplift, commonly associated with fronts, may be able to do this.

- In part because showing wind barbs from 52 runs is not viable, the vertical vector wind distribution from ENS is plotted as a hodograph (bottom left), using one line for each ENS member and one colour for each of a range of levels, with warmer colours denoting low levels and colder ones denoting upper levels. Only data from standard pressure levels are shown. The radial wind speed scale varies to span the value range represented, with certain values (20, 50, 100 m/s) highlighted to aid quick interpretation.
- Simple box-and-whisker plots (bottom right) are used to show distributions of most unstable CAPE for three different categories of CIN. These three categories were selected to denote, respectively, when CAPE is likely to be released (CIN < 50 J/kg), when CAPE may be released (50 J/kg ≤ CIN < 200 J/kg), and when CAPE release is not expected (CIN ≥ 200 J/kg). This addresses difficulties that often occur when viewing CAPE fields in isolation; for example, very high values can sometimes be seen where convection is not really possible, and thus false alarms can arise. Scaling for CAPE varies according to the full range of values present, with 200, 500, 1000, 2000 and 5000 J/kg highlighted. The user should note that ECMWF provides most unstable CAPE in the lowest 350 hPa of the atmosphere, whilst CIN is the minimum found in the same atmospheric layer. Therefore, CAPE and CIN provided as a model output are not necessarily computed for the same departure levels. Nevertheless, CIN can be used qualitatively as an indicator of the likelihood of convective initiation. Thus, the CAPE diagram provided within this product should be used for a rough estimate of how easily CAPE might be released.

In each of the panels described above, we also show the high-resolution forecast (HRES thick solid line) and Control forecast (dashed line) as on meteogram products. At present, as with meteograms, it is not possible to link data from one particular ENS member across the four panels. Nevertheless, we believe that the new product will prove extremely valuable for assessing many different aspects of atmospheric structure as modelled by the IFS.

Surface pressure assumption

A third challenge arising when combining data from different model runs is variations in surface pressure. Potentially the greatest impact would be seen on thermodynamic diagrams which use pressure as a vertical co-ordinate. The 1,000 hPa level could be at the surface in one ENS member, well below for another and well above for a third. This makes percentile computation and display extremely challenging. We have taken a pragmatic approach by assuming, for the purposes of plotting, that the ENS mean surface pressure at a given lead time is representative for all members, which means that the data stored for a given model level, for each ENS member, will always be mapped to the same pressure level. The fact that we only make lead times up to T+120h available renders this assumption quite reasonable, because spread in mean sea level pressure is mostly small compared to the vertical scale gradations on a tephigram. Figure 2 shows that, in winter over Europe, the difference between the minimum and the maximum surface pressure at day 5 within ENS is on average between about 10 and 20 hPa.

Case study

A vigorous supercell produced large hail, very strong winds and heavy rain that caused a lot of damage along the storm's path over north-western Bulgaria in the afternoon hours on 15 May 2018. The affected region was on the eastern flank of an upper low centred over Italy (Figure 3a).

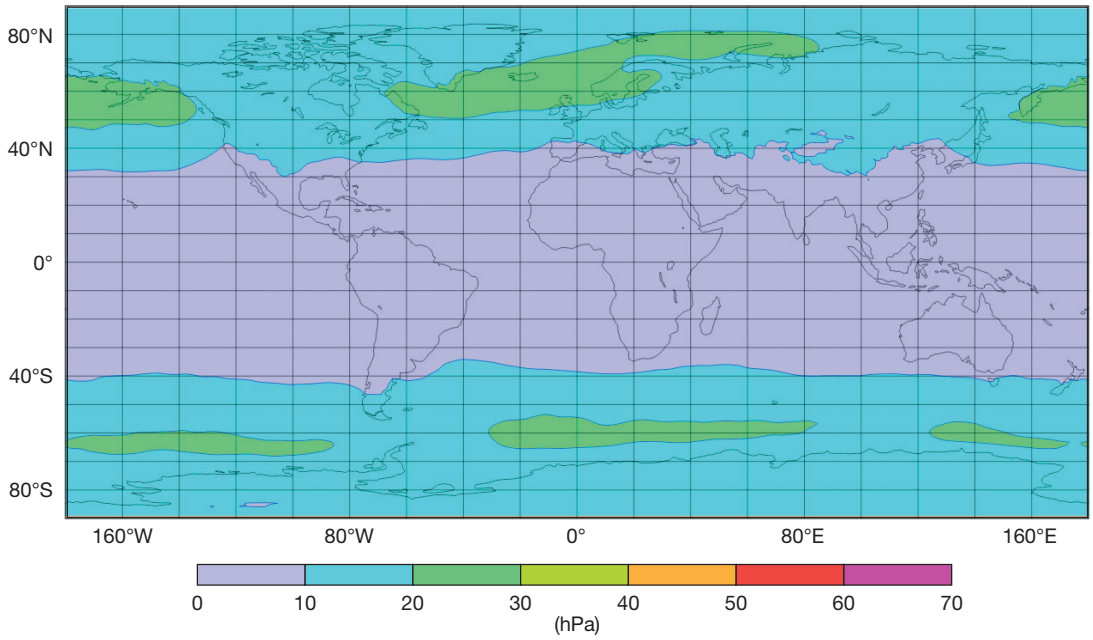

Figure 2 Approximate average difference in mean sea level pressure between extreme ENS members during the 2017/2018 northern hemisphere winter, at T+120h.

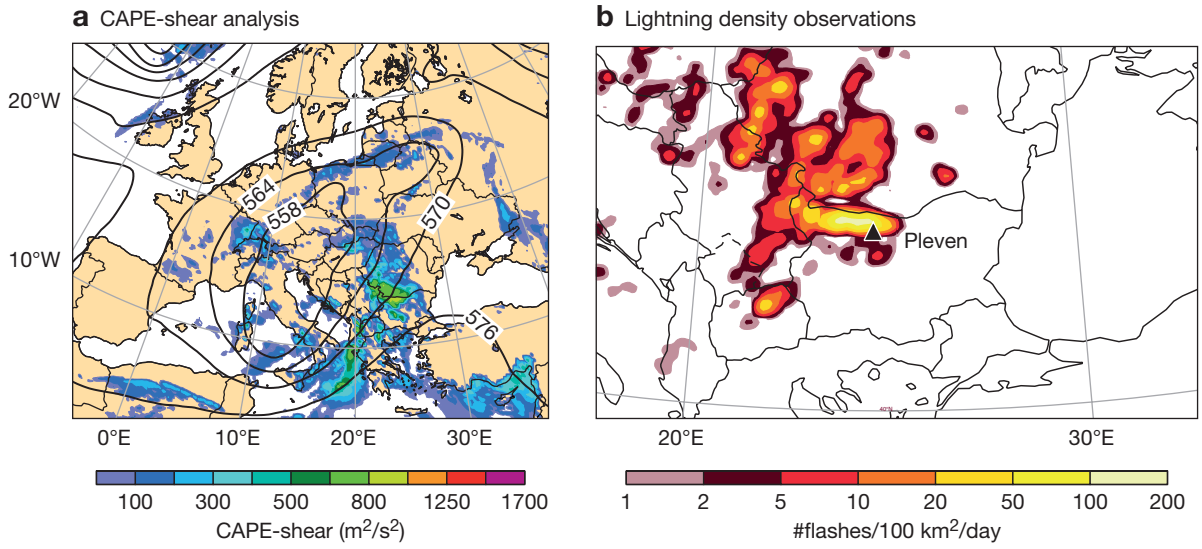

Figure 3 The plots show (a) the ECMWF analysis of 500 hPa geopotential height (contours, in decametres) and CAPE-shear (shading) valid for 12 UTC on 15 May 2018 and (b) ATDnet lightning density observations on 15 May 2018. Bright colours represent high values of lightning density associated with the supercell. The city of Pleven is marked on the map.

The co-location of high instability and significant deep-layer wind shear (also Figure 3a) favoured well-organised deep moist convection. The severe thunderstorm was initiated over the far north-west of Bulgaria and travelled eastwards producing a swathe of intense lightning activity (Figure 3b) and other convective hazards.

Figure 4 shows the new ensemble vertical profile forecast product for a lead time of 108 hours, valid for 12 UTC on May 15, for the city of Pleven, where the supercell caused havoc in the late afternoon. At this lead time, 14 members have CAPE=0 (top right on the panel), so in those members' representations deep moist convection is not possible and they are not shown within the CAPE/CIN plot. Meanwhile 9 members predict moderate to high CAPE from a few hundred to about 1000 J/kg, with CIN less than 50 J/kg. In all these 9 members, it would be relatively easy for the CAPE to be released and convection initiated, e.g. due to diurnal heating. The member with the most CAPE, almost 1200 J/kg, is also in this category. The second CIN category is populated with 14 members and CAPE values are of the order of a few hundred J/kg. As CIN is higher, between 50 and 200 J/kg, more substantial uplift would be required for convection to be triggered. Thirteen members belong to the third CIN category, and these have quite low CAPE (less than 400 J/kg). For these ENS representations convection would be very unlikely even if CAPE values were larger. HRES and Control forecasts, represented by blue and red dots respectively, also belong to this category, and show just a tiny amount of CAPE. In this forecast the risk of deep moist convection is arguably about 46% ((9+14)/50), although HRES and control runs do not support that outcome.

The hodograph plot allows us to assess how the wind changes with height in the 52 IFS runs, and how much uncertainty in the wind speed and direction there is in all these layers. In this example, near surface winds (red colour lines) are weak, with an easterly component in some members including HRES, which is shown with the wind flags on the dewpoint depression plot. In the mid- to high troposphere the uncertainty in the wind speed and direction increases but overall a westerly component is dominant. Thus deep-layer wind shear could be quite substantial (above 20 m/s). This means that, if convection is initiated, it could readily become well organised. The ensemble tephigram also shows the moisture content in the boundary layer and its uncertainty.

Access to plots and data

The new vertical profile product is available in ecCharts (Figure 5), clickable web charts and the Dashboard. In the ecCharts application, it can be accessed through the menu item 'Views/Vertical profiles window', which opens a separate, movable window on top that displays ensemble vertical profiles for any point selected on the background map. Vertical profiles are displayed for a given forecast valid time, hence changing the valid time for the background map triggers a new profile request for the selected time. Note that ecCharts maps have 3-hourly time steps whilst vertical profiles are only available on 6-hourly time steps. The vertical profile window displays a message if there is no vertical profile available for the selected lead time.

The Dashboard facility can provide access to all available forecast base times and lead times in a convenient way. To display them on the Dashboard, one needs to create a 'New Vertical profile' widget by using the 'Add new widget' menu item. Once a widget is created, it can be configured to any co-ordinate. Hovering over the widget will display time controls at the bottom left of the widget panel, as in meteograms and EFI/CDF plots, where users can easily navigate through available forecast base times and lead times. Users could, for example, create many widgets displayed side by side for data points that they are often interested in (Figure 6).

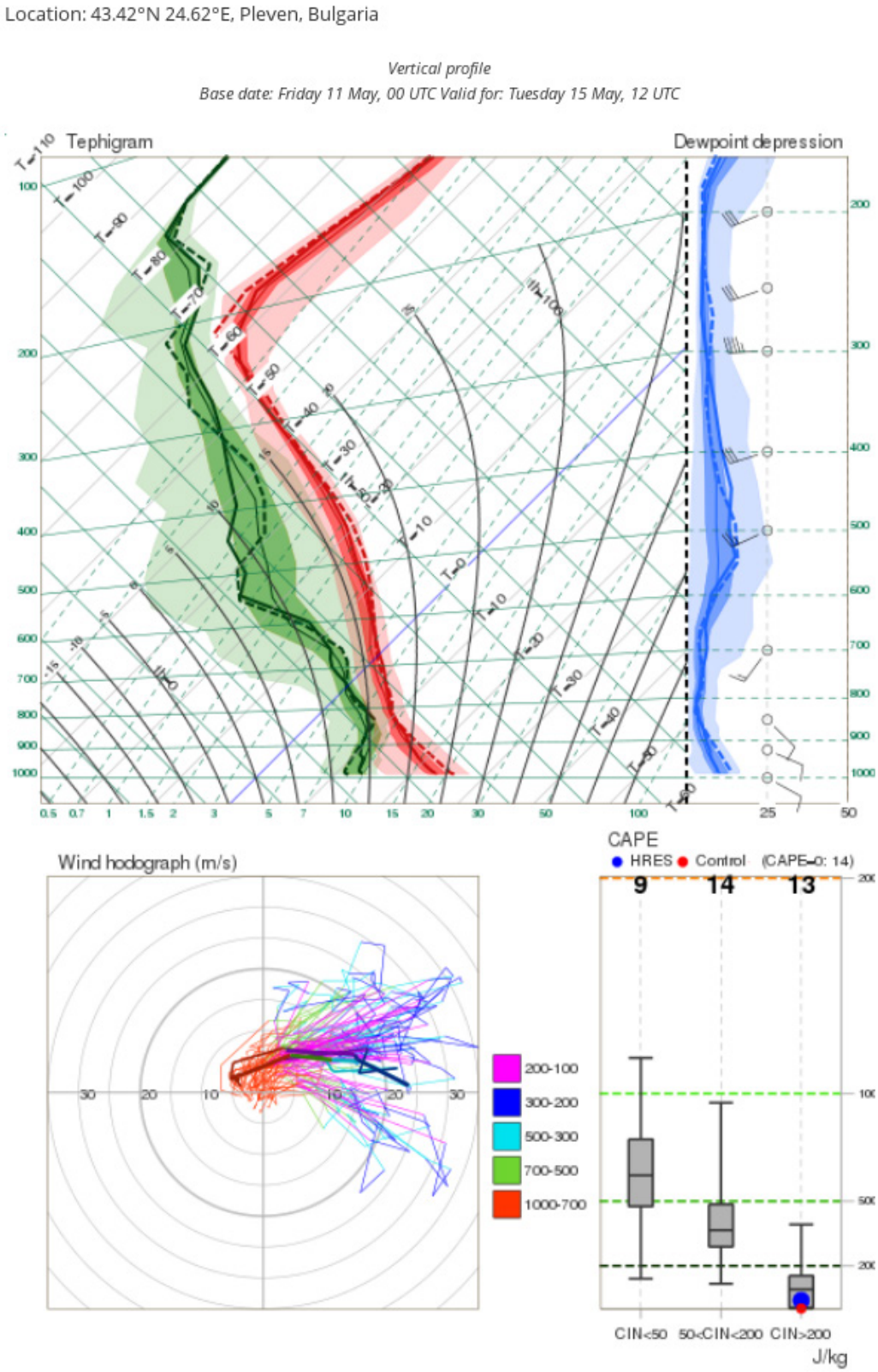

Figure 4 Vertical profile chart for the city of Pleven in northern Bulgaria affected by the severe thunderstorm on 15 May 2018. The forecast lead time is 108 hours, the valid time is 12 UTC on 15 May.

In addition to ecCharts and Dashboard access, vertical profile plots are also now included as an option on the standard clickable web charts, alongside the classical meteogram and EFI/CDF plot options that have been available for some time. Some users may be interested in accessing data files directly, to incorporate ECMWF vertical profiles into their own applications. To enable this, the data files for a given point will be provided via an ECMWF Web

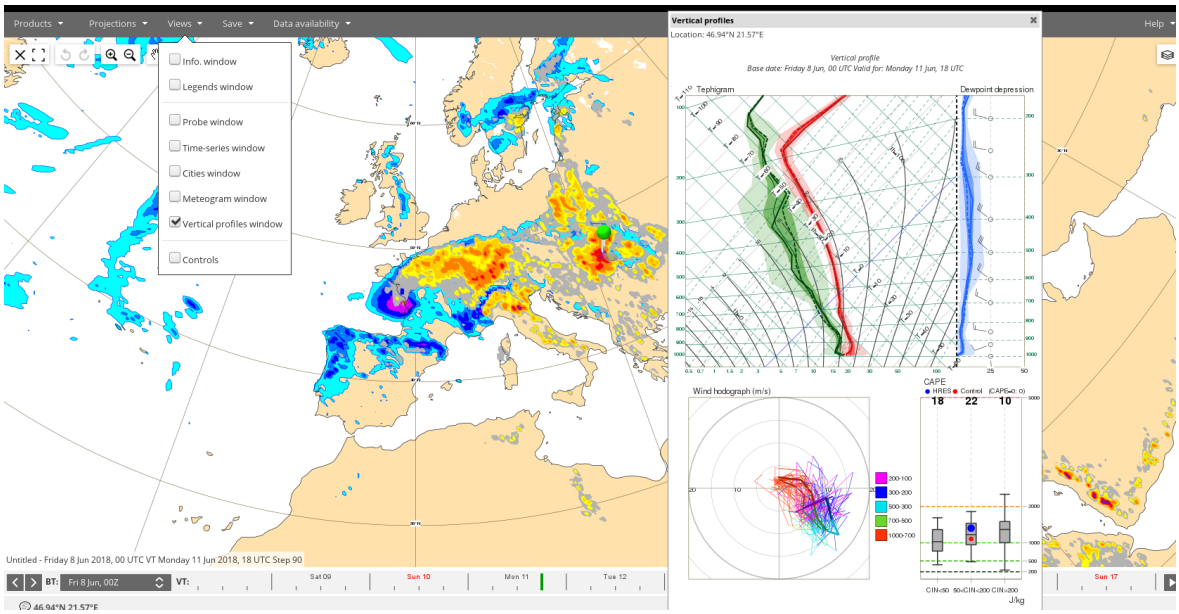

Figure 5 ecCharts interface showing a vertical profile for a selected point. The vertical profile window is added from the menu by clicking on 'Views' - 'Vertical profiles window'. Clicking on the background chart thereafter will generate vertical profile plots for the new selected location.

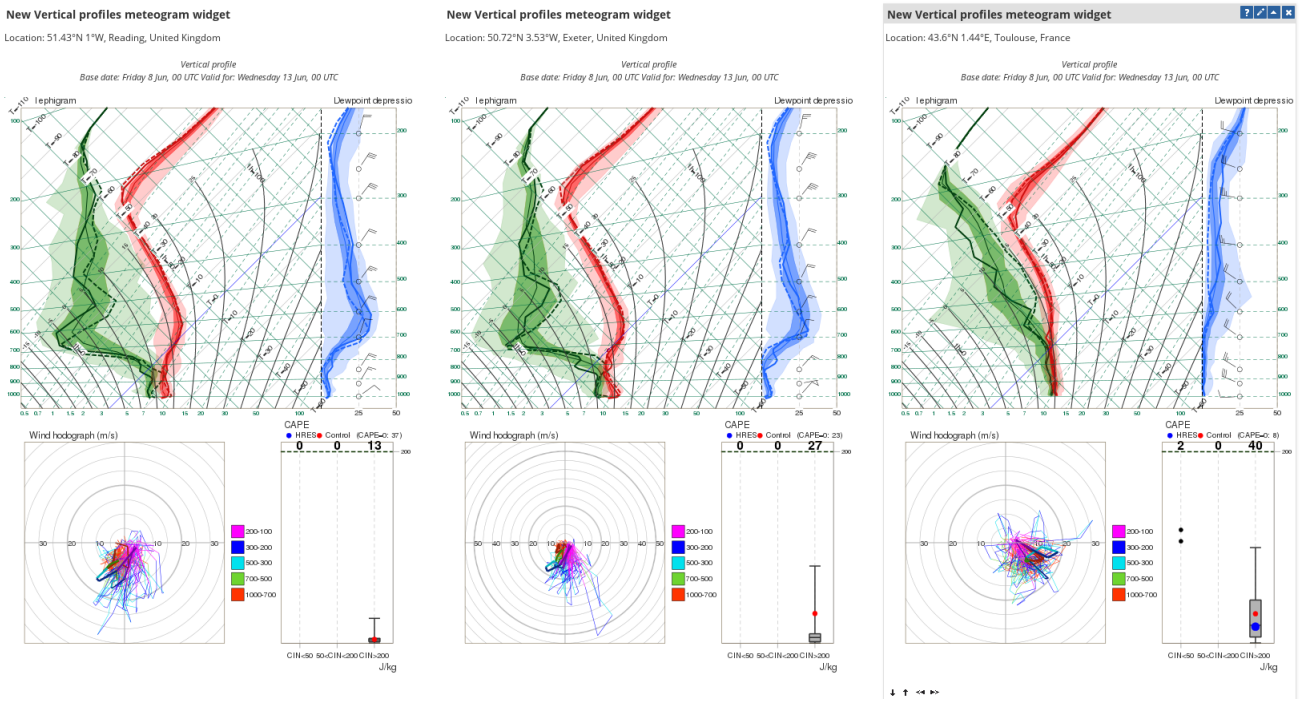

Figure 6 Dashboard interface showing three vertical profile plots side by side. Hovering over a vertical profile window calls up control buttons in the bottom left corner (visible in the third panel), where the user can control the base times and lead times available for this specific plot. Note also that a 'control widget', added through the Dashboard menu, could be used to change base times and lead times of all vertical profile plots on the page simultaneously. This interface provides the user with side-by-side comparisons, as well as allowing them to quickly scan through different lead times.

API that functions in a similar way to meteograms and that delivers output in JSON format. Note that vertical profile databases are kept online for 7 days (14 cycles), which is similar to meteograms.

For more information on ecCharts, visit: *https://confluence.ecmwf.int/display/ECCHARTS*

FURTHER READING

Ihász, I. & **D. Tajti**, 2011: Use of ECMWF's ensemble vertical profiles at the Hungarian Meteorological Service, *ECMWF Newsletter* **No. 129**, 25–29.

doi:10.21957/pdm369wj41

Using NWP ensembles in nuclear test verification

PIETER DE MEUTTER (RMI, SCK•CEN, Ghent University – Belgium), **ANDY DELCLOO** (RMI), **JOHAN CAMPS** (SCK•CEN), **PIET TERMONIA** (RMI, Ghent University)

Atmospheric transport and dispersion models are used as part of the verification regime of the Comprehensive Nuclear-Test-Ban Treaty. Nuclear weapon tests result in a radionuclide signature that is transported and dispersed in the atmosphere. Eighty stations equipped with very sensitive detectors are or will be monitoring these radionuclides globally.

If radionuclides are detected, atmospheric transport and dispersion models are used to locate possible source regions and the associated release period. This process is called inverse atmospheric transport modelling. Radionuclides measured by the monitoring stations may also come from certain civilian nuclear facilities. To estimate the contribution from these civilian sources to the measurements made at detection stations, once again atmospheric transport and dispersion models can be used. This process is called direct atmospheric transport modelling.

In order to have more confidence in the analysis of the signatures of nuclear weapon tests, it is useful to be able to quantify uncertainties. To quantify the uncertainty arising from the use of meteorological data, the ensemble method can be used. The Belgian Nuclear Research Centre (SCK•CEN) is currently collaborating with the Royal Meteorological Institute of Belgium (RMI) and Ghent University to use ECMWF's Ensemble of Data Assimilations to tackle this problem.

Solving the inverse modelling problem

Solving the source localisation problem following the detection of suspicious levels of radionuclides comprises three steps. First, numerical weather prediction (NWP) data is extracted or created. We have extracted (i) ECMWF forecasts and analyses from the MARS archive, and (ii) data from our own experiments set up in collaboration with ECMWF.

The second step is to run an atmospheric transport and dispersion model. We have used the Lagrangian particle model Flexpart. Lagrangian particle models are state-of-the-art atmospheric transport and dispersion models that track the movement of many individual particles. These particles constitute the plume of the tracer of interest. There is no numerical diffusion since the positions of individual particles are being tracked, independent of any grid.

Flexpart is coupled offline to data from NWP models. Particles are advected following the wind fields provided by the NWP model. Dispersion is parametrized by adding a random turbulent and mesoscale wind fluctuation to each particle's velocity. These wind fluctuations are obtained using a Langevin equation. The turbulent diffusivities are parametrized in the boundary layer and set to a constant value above. Flexpart can also take into account convection based on the convective scheme of Emanuel and Živković-Rothman; dry and wet deposition; and radioactive decay.

Flexpart relates a source term for all geo-temporal points in the simulation to a simulated observation. The third step in the inverse modelling is to find a source term which minimises the difference between simulated observations and actual observations. This is done using a cost function. For details, see Box A.

A real-world example

In January 2016, the Democratic People's Republic of Korea announced that it had conducted its fourth nuclear test. The seismic component of the International Monitoring System to verify compliance with the Comprehensive Nuclear-Test-Ban Treaty had picked up the signals of an underground human-made explosion. To discriminate conventional explosions from nuclear explosions, radionuclides (and in particular radioactive xenon) are monitored. However, since

Inverse modelling using Flexpart

A

Flexpart is a state-of-the-art atmospheric transport and dispersion model that tracks the movement of many individual particles. For the source localisation problem, it is more efficient to run Flexpart in backward mode. The result is the source-receptor-sensitivity M_{ij} that relates an observation y_i to a source term x_j (the index i goes over all selected observations, the index j over all geotemporal points in the simulation; ε is the combined model and observation error):

$$y_i = M_{ij}\, x_j + \varepsilon \quad (1)$$

The next step is to find a source term x_j so that (1) holds. To quantify the disagreement between the simulated concentrations $M_{ij}\, x_j$ and observed concentrations, a cost function is defined. Different cost functions can be chosen depending on the problem at hand. It is assumed that possible source locations and their associated source terms have low cost functions. A simple square error cost function is shown in (2):

$$cost\,function(x_j) = (y_i - M_{ij}\, x_j)^2 \quad (2)$$

For the current applications, we are interested in single grid box sources. Therefore, the inverse modelling is applied and repeated for each grid box, so that a cost function value and associated best grid box source term is obtained for each grid box in the domain. The most likely source regions are those grid boxes that have the lowest cost function.

The advantage of using Flexpart in backward mode to calculate source-receptor-sensitivities is that there is then no need to rerun the model while searching for an optimal set of source parameters.

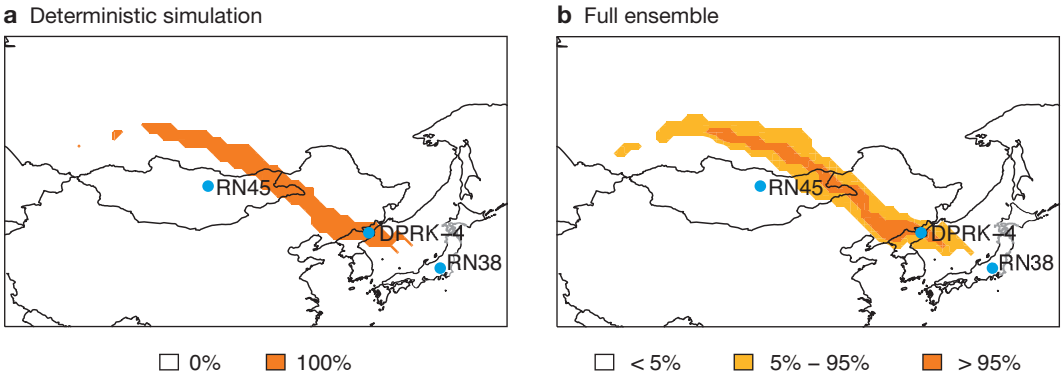

Figure 1 Possible source regions of the ^{133}Xe detections made after the Democratic People's Republic of Korea announced that it had carried out a fourth nuclear test, showing (a) results from the control (deterministic) simulation and (b) results from the full ensemble. The location of the monitored human-made explosion is labelled DPRK-4. Two monitoring stations (RN38 and RN45) are also shown.

the explosion took place underground, it was not clear how many radionuclides would have been released into the atmosphere nor when exactly this would have happened.

Seven weeks after the announced nuclear test, elevated concentrations of radioactive xenon were measured at a noble gas monitoring station in Takasaki (Japan). We applied inverse modelling to the detected values. We also selected non-detections at that station before and after the elevated radioactive xenon measurements, and non-detections at other stations; in total, 50 detections and non-detections were used. A threshold cost function was defined to discriminate possible source regions with low cost function values from other regions. The result is shown in Figure 1a.

To quantify uncertainty from the meteorology, ECMWF's Ensemble of Data Assimilations (EDA) was used (see Box B). This ensemble consists of 25 perturbed members and one unperturbed member. For each perturbed EDA member, its perturbations were calculated with respect to the ensemble mean, and these were then added to and subtracted from the unperturbed member, resulting in 50 perturbed members and one unperturbed member. For each of the resulting 51 members, a set of Flexpart simulations was performed, followed by the inverse modelling. The result was a set of 51 cost function maps. We then counted for each grid box how many ensemble members had a cost function value below the cost function threshold. This allowed us to construct grid-point probability maps as shown in Figure 1b.

Adjusting for civilian nuclear facilities

The verification of the Comprehensive Nuclear-Test-Ban Treaty is complicated by the existence of a background of radioactive xenon emitted by civilian nuclear facilities. Indeed, nuclear power plants and medical isotope production facilities routinely emit radioactive xenon, which can be measured by the very sensitive global noble gas monitoring network. One way to deal with this issue is to explicitly model the contribution from these civilian nuclear facilities to the measurements made at the noble gas monitoring stations. We have assessed how well we can simulate the radioactive xenon background at two noble gas stations in Europe for the year 2014. Since xenon is a noble gas, there is no deposition, which is beneficial from both an observational point of view and a modelling point of view. To estimate the uncertainty associated with simulations based on meteorological data, we used an 11-member subset of the 51 ensemble members that make up ECMWF's ensemble forecasts (ENS) (10 perturbed members and the control forecast - see Box B). The observed and simulated ^{133}Xe activity concentration can be seen in Figure 2 (note that there were no observations available in October or the first half of November 2014).

Extraction and creation of ENS/EDA data

B

The 11-member subset of ECMWF's ensemble (ENS) was created with a lead time of 7 days for all of 2014 at a horizontal resolution of 50 km with 91 vertical levels (TL399/L91). The computational cost was about 15k system billing units (SBU) for one day, and the total computational cost was 5.5M SBU.

We have also run ECMWF's 26-member Ensemble of Data Assimilations (EDA) for two periods of interest in 2013. The first period (14 March 2013 – 19 April 2013) was chosen to assess the Democratic People's Republic of Korea's announcement of a third nuclear test. The second period (6 May 2013 – 11 June 2013) was chosen to repeat an international atmospheric transport modelling exercise that was set up to test which level of agreement could be obtained between simulated ^{133}Xe concentrations and observed ^{133}Xe concentrations released by a nuclear facility in Australia. The analysis of the data is being finalised. Since the EDA experiments are rather expensive (~160k SBU per run, two runs per day), we ran these experiments with two inner-loop minimisations at 210 km/125 km horizontal resolution (TL95/TL159), keeping the outer-loop resolution at 80 km (TL255). The total computational cost was 26M SBU.

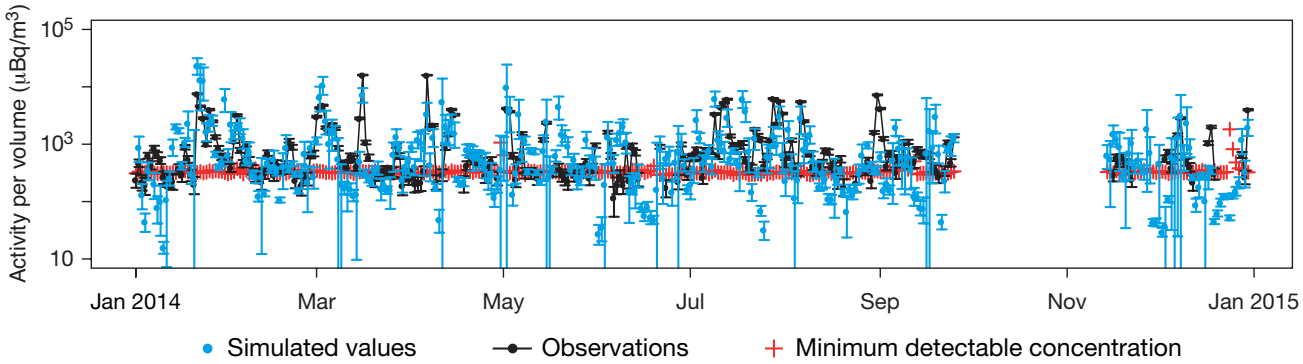

Figure 2 Activity concentration of ^{133}Xe at the monitoring station RN33 for the Comprehensive Nuclear-Test-Ban Treaty near Freiburg (Germany) as observed and as simulated, from known civilian sources. The minimum detectable concentration (MDC) is shown in red. If an observation is just below the MDC, it is still accepted, otherwise it is set to zero. The black vertical bars show the standard deviation of the observation and the blue vertical bars show the standard deviation among the ensemble members. (Source: *De Meutter et al.*, 2016)

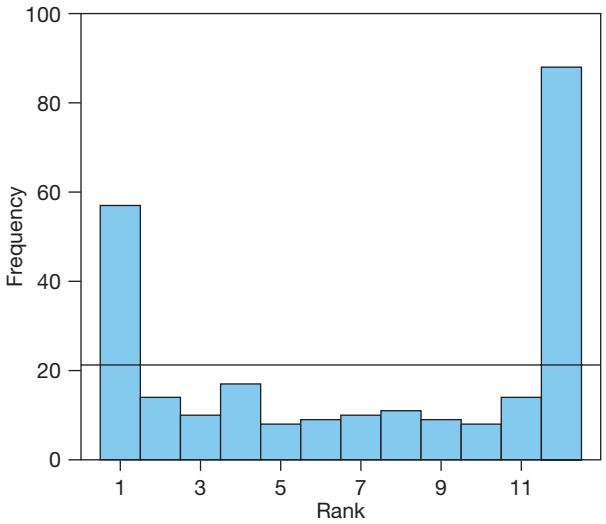

Figure 3 Rank histogram for the ensemble data shown in Figure 2. The horizontal line shows the ideal height of all the bins. The shape of the histogram suggests that the ensemble is underdispersive. (Source: *De Meutter et al.*, 2016)

The ensemble makes it possible to capture part of the uncertainty, as can be seen in the rank histogram (Figure 3). Rank histograms show how often observations match different parts of an ensemble member distribution. The outermost bars show the number of times the observed values are smaller/bigger than the smallest/biggest ensemble member values. In Figure 3, the U-shape of the rank histogram suggests that the ensemble is underdispersive. This could be explained by the fact that we took into account only meteorological uncertainty and not, for example, uncertainty in the emissions from civilian nuclear facilities. We note, however, that rank histograms need to be interpreted with care as reasons other than underdispersiveness can result in the same features on a rank histogram.

The added value of the ensemble approach when simulating the observed activity concentration was quantified by calculating the Brier score, shown in Figure 4a. For each activity concentration threshold, the full ensemble

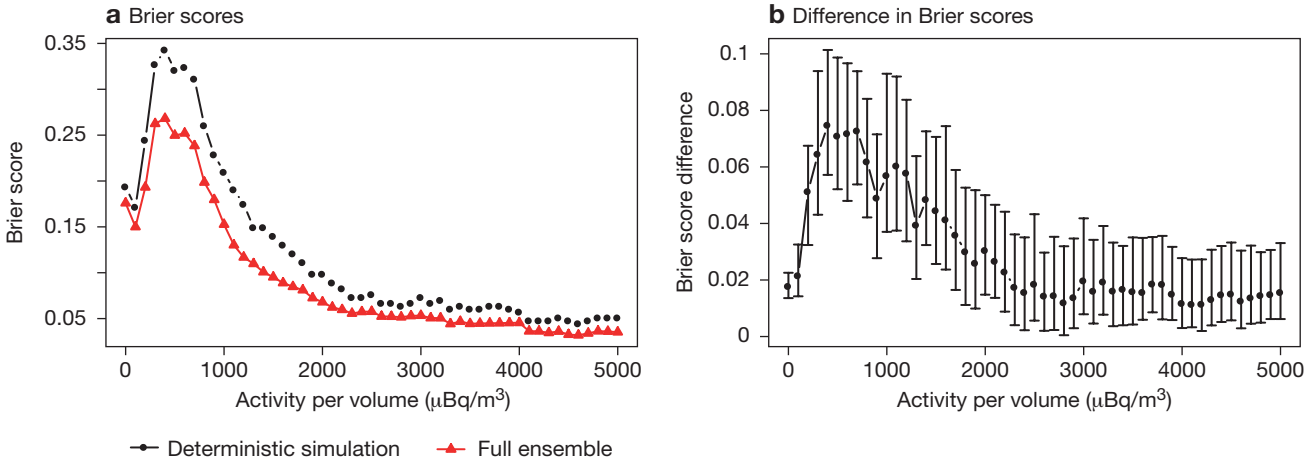

Figure 4 The plots show (a) the Brier score for the noble gas monitoring station DEX33 for the deterministic simulation and the full ensemble and (b) the difference between the Brier scores of the deterministic simulation and the full ensemble. The error bars in (b) represent 95% confidence intervals obtained using the bootstrap method. They show that the improvement when using the ensemble is significant. (Source: *De Meutter et al.*, 2016)

has a lower Brier score than the deterministic simulation. The statistical significance was tested with the bootstrap method (Figure 4b). We note that the ensemble mean and median did not outperform the deterministic simulation for other scores, such as the correlation and the normalised root-mean-square error.

Summary

The work described here shows that NWP data, and in particular ensemble data, can be put to good use in the verification of possible violations of the Comprehensive Nuclear-Test-Ban Treaty. They play a role both in inverse atmospheric transport modelling, which is used to trace possible radionuclide source locations, and in direct atmospheric transport modelling, which serves to estimate the contribution of civilian nuclear facilities to the radionuclide activity concentrations measured at monitoring stations. More work is needed to fully understand the apparent underdispersion of the ensembles used in our 2014 experiment to simulate that contribution.

FURTHER READING

De Meutter, **P.**, **J. Camps**, **A. Delcloo**, **B. Deconninck** & **P. Termonia**, 2016: On the capability to model the background and its uncertainty of CTBT-relevant radioxenon isotopes in Europe by using ensemble dispersion modeling. *J. Environ. Radioact.*, **164**, 280–290.

De Meutter, **P.**, **J. Camps**, **A. Delcloo** & **P. Termonia**, 2017: Assessment of the announced North Korean nuclear test using long-range atmospheric transport and dispersion modelling. *Sci. Reports.*, **7(1)**, 8762.

Seibert, **P.** & **A. Frank**, 2004: Source-receptor matrix calculation with a Lagrangian particle dispersion model in backward mode. *Atmospheric Chem. Phys.*, **4**, 51–63.

Stohl, **A.**, **C. Forster**, **A. Frank**, **P. Seibert** & **G. Wotawa**, 2005: Technical note: The Lagrangian particle dispersion model FLEXPART version 6.2. *Atmospheric Chem. Phys.*, **5**, 2461–2474.

ECMWF Calendar 2018/2019

Sep 10–13	Annual Seminar
Sep 13–14	Workshop on Radio-Frequency Interference (RFI)
Sep 24–28	Workshop on high-performance computing in meteorology
Oct 1–3	Training course: Use and interpretation of ECMWF products
Oct 8–10	Scientific Advisory Committee
Oct 11–12	Technical Advisory Committee
Oct 22–23	Finance Committee
Oct 24	Policy Advisory Committee
Oct 29	Advisory Committee of Co-operating States (in Estonia)
Oct 30–31	Workshop on developing Python frameworks for Earth system sciences
Dec 4–5	Council
Jan 30 – Feb 1	Training course: ecFlow
Feb 4–8	Training course: ecCodes
Feb 11–14	Training course: Use and interpretation of ECMWF products
Feb 25 – Mar 1	NWP training course: Predictability and ensemble forecast systems
Mar 4–8	NWP training course: Parametrization of subgrid physical processes
Mar 11–15	NWP training course: Data assimilation
Mar 18–22	EUMETSAT/ECMWF NWP-SAF training course: Satellite data assimilation
Mar 29–25	Training course: Advanced numerical methods for Earth system modelling
Apr 2–5	Workshop on predictability, dynamics and applications research using the TIGGE and S2S ensembles
Apr 3	Policy Advisory Committee (PAC)
Apr 9–11	ACDP and data policy meetings of ECOMET and EUMETSAT
Apr 29 – May 1	Technical workshop for software development
May 2–3	Finance Committee
Jun 3–6	Using ECMWF's Forecasts (UEF)
Jun 27–28	Council
Sep 2–6	Annual Seminar
Oct 7–9	Scientific Advisory Committee
Oct 7–9	Training course: Use and interpretation of ECMWF products
Oct 10–11	Technical Advisory Committee
Oct 28–29	Finance Committee
Oct 29	Advisory Committee of Co-operating States (in Estonia)
Oct 29	Policy Advisory Committee
Nov 4–8	Workshop on the use and diagnostics of ECMWF forecasts during meteorological campaigns
Dec 10-11	Council

ECMWF publications

(see *http://www.ecmwf.int/en/research/publications*)

Technical Memoranda

824 **Shepherd**, **T.G.**, **I. Polichtchouk**, **R.J. Hogan** & **A.J. Simmons**: Report on Stratosphere Task Force. *June 2018*

821 **Largeron**, **C.**, **H.L. Cloke**, **A. Verhoef**, **A. Martinez-de-la-Torre** & **A. Mueller**: Impact of the representation of the infiltration on the river flow during intense rainfall events in JULES. *January 2018*

ESA Contract Reports

Rodriguez-Fernandez, **N.-J.**, **P. de Rosnay**, **C. Albergel** & **F. Aires**: SMOS Neural Network Soil Moisture Data Assimilation. *January 2017*

Contract Report for Vaisala Oyj

Ingleby, **B.**: Radiosonde assimilation experiments for Vaisala. *June 2018*

Contact information

ECMWF, Shinfield Park, Reading, Berkshire RG2 9AX, UK

Telephone National	0118 949 9000
Telephone International	+44 118 949 9000
Fax	+44 118 986 9450

ECMWF's public website http://www.ecmwf.int/

E-mail: The e-mail address of an individual at the Centre is firstinitial.lastname@ecmwf.int. For double-barrelled names use a hyphen (e.g. j-n.name-name@ecmwf.int).

For any query, issue or feedback, please contact ECMWF's Service Desk at *servicedesk@ecmwf.int*.

Please specify whether your query is related to forecast products, computing and archiving services, the installation of a software package, access to ECMWF data, or any other issue. The more precise you are, the more quickly we will be able to deal with your query.

Index of Newsletter articles

This is a selection of articles published in the *ECMWF Newsletter* series during recent years.
Articles are arranged in date order within each subject category.
Articles can be accessed on ECMWF's public website – http://www.ecmwf.int/en/research/publications

ECMWF
Newsletter | Number 156 – Summer 2018
European Centre for Medium-Range Weather Forecasts
www.ecmwf.int